TU Delft Delft University of Technology

Faculty of Technology, Policy and Management

Engineering and Policy Analysis
Master Thesis

Assessing future flood resilience of the Mumbai Metropolitan Region: A land-use modelling case study

---

First supervisor:
Prof. Dr. T.Comes

Second supervisor:
Dr. N.Y. Aydin

Advisor:
MSc. S. Krishnan

Student:
Q. Lafleur

November 7, 2022

An electronic version of this thesis is available at:
http://repository.tudelft.nl/

The codes used by this thesis is available at:
https://github.com/QuintLafleur97/Thesis_MMR_Resilience.git

Acknowledgements

Hereby I express my genuine gratitude towards Supriya Krishnan, Nazli Aydin, and Tina Comes for guiding me through the process of writing this master thesis.

Furthermore, I want to thank Marya El Malki for the data processing on which this thesis was built and Gautami Kushwaha for spending her free time contributing to this project.

Also, I would like to thank my housemates Mark Loopstra, Johan Poort and Barend Bootsma for enduring my permanent presence in the living room.

Contents

Executive Summary

Climate change results in sea-level rise and increases the frequency and intensity of heavy precipitation events and storm surges. Concurrently, the Global South is urbanising at an unprecedented pace, often characterised by unstructured patterns resulting in urban growth in flood-prone areas. Jointly, these developments will result in increased flood risk for large parts of the world population. In light of these developments, cities in the Global South need to adapt and transform to become more flood resilient.

Urban flood resilience is traditionally acquired through flood control structures, such as dams, pump stations and others. However, for various reasons, flood control structures have not been adequate in establishing sufficient urban flood resilience since cities around the world have remained vulnerable to flood hazards. This has led to increased interest in approaches that acknowledge periodic floods as inherent environmental dynamics of an urban environment and focus on adaptation to floods instead of control. Adapting the physical landscape through urban planning is one of the key ways in which flood adaptation can be applied. Through urban planning, one can transform the urban environment in the face of urban floods, without attempting to change the flood regime but by guiding the structure of the city in such a way that flood-vulnerable land use is mainly located away from flood-prone areas, with the aim of reducing flood risk.

Various studies for cities in the Global North have researched this flood-risk-land-use interaction by coupling land-use models and flood hazard maps. However, a research gap is present concerning such modelling case studies on cities in the Global South. This thesis aims to contribute to the body of knowledge concerning the interaction between flood risk and land use and how they impact the long-term flood resilience of cities in the Global South by executing a modelling case study for a city in the Global South. In this modelling case study, a flood-risk-land-use interaction is modelled that allows the assessment of acquired resilience by various urban planning policies. Furthermore, an in-depth flood risk assessment is executed. In this thesis, resilience was directly assessed by assuming a negative correlation between flood risk and urban flood resilience; hence low flood risk is associated with high resilience and the other way round.

Consequently, the main research question is:

[RQ] How will the interaction of flood risk and land use impact the long-term flood resilience of cities in the Global South?

The modelling case study is executed for the Mumbai Metropolitan Region (MMR).

In this thesis is derived that, in case no governmental intervention occurs, riverine floods will result in more affected people and more monetary damage. Furthermore, the most vulnerable communities will relatively suffer the most. In addition, the future increase in flood risk can mainly be attributed to urban growth in flood-prone areas, not climate change-induced increased flood hazards. Unstructured growth frequently occurs in cities in the Global South; hence it was

deemed likely that urban growth in flood-prone areas will significantly contribute to the increase in flood risk for various cities in the Global South.

On a more positive note, population growth in flood-prone areas, contrary to climate change, can be handled locally. According to our case study, local handling of the problem through urban planning can significantly contribute to the flood resilience of an urban environment if applied effectively.

The effectiveness of urban planning policies varied significantly per land-use class and largely depended on the strictness with which these policies were implemented and enforced. Logically, the urban environment was deemed more resilient if stricter urban planning policies were implemented and enforced since stricter urban planning leads to more movement away from flood-prone areas, subsequently resulting in a reduction of flood risk. Problematic was that the most vulnerable land-use classes, consisting of informal settlements, were least obedient to urban planning policies. Therefore, land-use-specific treatment is required to increase the system's overall resilience.

Contrarily, the effectiveness of urban planning policies was largely independent of the perceived climate future. This was due to two reasons. Firstly, in the case study, the flood-prone areas were largely equal for an optimistic and a worst-case climate scenario. Secondly, uncertainty associated with future climate was present in the inundation depths that these flood-prone areas will endure; however, this does not affect the effectiveness of urban planning policies.

Future climate projections, of course, cannot be generalised for the Global South. However, the case study does indicate that significant flood-prone regions are possibly uncontested and that the application of urban planning policies for these uncontested regions can be promising for constructing more resilient urban environments.

Introduction

Currently, more than 1.81 billion people, or 23% of the world population, are estimated to be located in flood-prone areas (Rentschler et al., 2022). Climate change is resulting in sea-level rise and increasing the frequency and intensity of heavy precipitation events and storm surges, subsequently worsening the situation significantly. In case of no adaptation, total direct monetary flood damage is estimated to increase by a factor [1.4, 3.9], depending on the climate scenario. Also, increased flood hazard is expected to result in increased indirect monetary damage, human mortality and trauma, loss of livelihood and culture, diarrheal diseases, and risks relating to flood security, among other indirect and unpredictable impacts (IPCC, 2022b). To make matters worse, world population is expected to increase from 7.6 to 9.8 billion over the period [2017, 2050] (United Nations, 2018); leading to an increase in population in flood-prone areas if no action is taken (Kim and Newman, 2020).

Since 68% of the world population is projected to reside in urban areas in 2050 (United Nations, 2018), urban areas can be considered essential to adapt and transform in light of current and future flood risk. Building urban flood resilience can be done through flood control infrastructures, such as dams, pump stations, and stormwater drainage systems, and non-structural measures, such as early warning systems and land-use planning (IPCC, 2022b). The feasibility and effectiveness of these various approaches highly depend on what is financially, technologically, and institutionally possible at a particular location. Traditionally, the focus has been on constructing flood-control infrastructure for a specific design capacity to increase flood resilience (Zevenbergen et al., 2020; Liao, 2012). However, several problems are associated with this approach. Firstly, the construction and maintenance of flood-control infrastructure require immense capital funds, for which both political momentum and government budgets are often lacking (Nakamura et al., 2020; Jongman, 2018). Furthermore, absolute failure and subsequent catastrophic consequences occur in case of exceedance of the design capacity (Zevenbergen and Gersonius, 2007; Liao, 2012; Nakamura et al., 2020), a problem exacerbated by the uncertainty associated with climate change and future increased climate variability. At the same time, taking such uncertain factors into account by designing for several possible climatic scenarios results in a further increase in cost and complexity (Hallegatte, 2009). Moreover, flood control infrastructure can result in a false sense of security, resulting in urban development in protected flood-prone regions (Jongman, 2018). Besides, flood control infrastructure can negatively affect ecosystems' biodiversity and climate resilience through maladaptation (Opperman et al., 2009; IPCC, 2022b). Lastly, and maybe most importantly, flood control structures have proven to be insufficient in establishing sufficient urban flood resilience since cities around the world remain vulnerable to flood hazard (Liao et al., 2016).

The flaws associated with flood control structures have led to increased interest by various authors in approaches that focus on adaptation to floods instead of approaches that try to prevent the occurrence of floods. Generally, flood adaptation approaches do not result in absolute failure when the design capacity is reached (Liao, 2012). Also, they are often less costly and more

desirable in terms of biodiversity and ecosystem climate resilience (Jongman, 2018; Opperman et al., 2009).

Adapting the physical landscape through urban planning is one of the key ways in which flood adaptation can be applied. The design of such urban planning approaches that effectively increase flood resilience, requires in-depth knowledge on land-use and flood risk and how they interact. This study aims to contribute to the body of knowledge concerning this field of research. This is done through land-use change modelling of a city over time, the coupling of the land-use model and flood hazard maps, and the inclusion of various urban planning scenarios.

This study aims to result in (i) case-study-specific knowledge, relevant to local policymakers, on what form of urban planning implementation leads to resilient land-use scenarios for the city under study, (ii) general knowledge concerning the interaction between flood risk and land use and how policymakers can use this interaction to construct a more resilient urban environment, and (iii) general knowledge on the execution of a land-use modelling case-study incorporating flood risk-land use interactions and the assessment of resilience for cities in the Global South. In this manner, this thesis hopes to benefit both the city understudy and science as a whole. Due to the relevance of this research topic to both society and science and its relation with the grand challenges of establishing secure and inclusive societies, this research topic can be regarded as a relevant MSc thesis topic for the Engineering and Policy Analysis (EPA) MSc of the TU Delft.

Chapter 1

Research Design

In this chapter, in Section 1.1 a literature review is conducted to derive a knowledge gap. Thereafter, the main research question is defined based on the delineated knowledge gap. Furthermore, in Section 1.2 the research approach, and sub-questions are discussed. Lastly, the research flow is visualised.

1.1 Literature Review

A literature review was carried out to gain further insight into how land-use models and flood hazard maps have been coupled and the subsequent knowledge gaps present in literature to which a contribution can be made.

This literature review is divided into three parts. To begin with, in Section 1.1.1, the applied process is talked through. Secondly, the reviewed literature is discussed in Section 1.1.2. Lastly, in Section 1.1.3, the resulting knowledge gap and main research question are mentioned.

1.1.1 Process

To arrive at relevant literature, a literature search was executed in reference databases *Scopus* and *Google Scholar*, based on the search terms of Table 1.1. These search terms can be grouped under two categories: (i) land-use change modelling and (ii) flood hazard.

	Combine the concepts with AND	
Combine the synonyms with OR	**Land-use change modelling**	**Flood hazard**
	land?use?change?model*	flood*
	land?change?model*	
	land?use?model*	
	land?use*	
	LUCM	
	LCM	
	LUM	
	urban?growth*	

Table 1.1: *A table of the search terms that were used to arrive at relevant literature.*

The initial search based on the search terms of table 1.1 resulted in over 60 scientific sources. After that, the sources that linked land use models with flood hazard maps were selected, resulting in a total of 11 sources selected for review. An overview of the analysed literature can be found in Appendix A.

1.1.2 Literature review

In this section, the selected papers are discussed based on key characteristics used as column headers in the tables of Appendix A.

Approach

We distinguish between two approaches of linking land-use models and flood hazard maps. Firstly, land-use maps can be overlaid with flood hazard maps, leading to knowledge concerning the spatial distribution and quantity of flood risk. In this case, a certain land-use configuration leads to a certain flood risk. Consequently, this approach is coherent with *arrow:1* in Figure 1.1 and is denoted as 'approach 1'.

Secondly, flood risk leads to land-use change if policies are based on flood hazard maps. By incorporating this part of the flood risk-land-use interaction, knowledge can be derived on the spatial distribution of land use in case such policies are implemented. In this case, perceived flood risk leads to a certain land-use configuration. Consequently, this approach is coherent with *arrow:2* in Figure 1.1 and is denoted as 'approach 2'.

In case both approach 1 and 2 are applied, interaction occurs between land use and flood risk as visualised in Figure 1.1. In such cases, policies are implemented based on certain perceived flood risk that alters the land use configuration and subsequently changes flood risk. On the other hand, in case only approach 1 or approach 2 is applied, no interaction takes place.

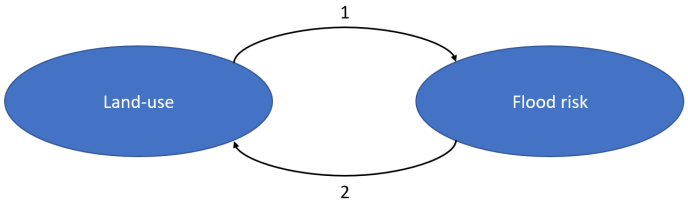

Figure 1.1: *A figure on the interaction between land use and flood risk.*

Most relevant literature only applied approach 1, indicating that land-use planning as a policy measure is rarely modelled. Furthermore, only one paper solely applied approach 2, and three papers applied both approach 1 and 2.

Time period

Almost all literature considered at least two timesteps to enable the analysis of a time-varying characteristic. Also, almost all literature applied extrapolation to the future to explore future scenarios. The furthest that someone has looked ahead is 50 years. However, more often, extrapolations of shorter duration are applied. On average, the latest timestep is approximately 32 years later than the second-to-last timestep. Furthermore, most of the analysed literature only evaluated up to 2040, which is problematic since, according to Masson-Delmotte et al. (2021), climate change uncertainties significantly increase beyond this point.

Scale and location

Almost all of the literature only considered one scale: regional. The logic behind the applied scale is often not communicated explicitly and regularly follows from arbitrary, subjective reasons or scientific tradition (Gibson et al., 2000).

Concerning location, most literature focused on the Global North instead of the Global South. The Global South generally refers to regions within Latin America, Asia, Africa, and Oceania that are less wealthy, technologically advanced, and politically stable (Odeh et al., 2010; Hollington et al., 2015). The fact that the Global North is more frequently modelled than the Global South

is problematic for three reasons. Firstly, in general, more development is associated with less monetary flood risk since more development enables better risk control through vulnerability reduction, even though the potential monetary damage associated with floods is greater in case of more development (Kovacs et al., 2017). I.e. the Global South is expected to experience more monetary flood risk. Secondly, more development is generally associated with fewer people exposed to floods, as confirmed by Rentschler et al. (2022), who estimated that 89% of the world's flood-exposed population resides in low- and middle-income countries. I.e. the Global South is expected to contain a larger population exposed to floods. Thirdly, approximately 90% of worldwide urbanisation is occurring in the Global South (Yazdani and Dola, 2013). I.e. significantly more land-use change is occurring in the Global South, increasing the relevance of a land-use modelling case study.

Type of flooding

Depending on the area under study, different flood types were evaluated. Most of the studies evaluated coastal flooding, three evaluated riverine flooding, one evaluated glacier lake flooding, while only Hoymann and Goetzke (2016) evaluated multiple types of flooding.

Modelling method

The majority of the literature applied cellular automata and GIS-based modelling. General advantages of these approaches originate from their flexibility, simpleness and ease of use (Gharaibeh et al., 2020; Koomen and Stillwell, 2007; Aburas et al., 2016). Also, they consist of explicit transition rules (Roodposhti et al., 2019) and include both spatial and temporal dimensions (Liu et al., 2014).

Scenarios

Depending on the research topic, other scenarios were considered. Concerning land use, the number of scenarios varied between 1 and 3. Concerning flood hazard maps, papers generally varied either the return period or the climate scenario and generally included [1, 7] flood hazard maps. Only te Linde et al. (2011) included clusters of flood hazard maps for various return periods for several climate scenarios. Studies including planning policies generally included one to four of them.

Planning policies

By definition, only the four papers that applied approach 2 have included planning policies. These included restrictive spatial planning by governmental authorities in flood-prone areas in their evaluated policies, while only Hansen (2010) included additional insurance costs for flood-prone areas.

Furthermore, no studies that included spatial planning policies were executed on cities in the Global South. This is a shame since building resilience through urban planning poses a valid alternative to the more expensive flood control infrastructure, which can be unaffordable for the generally less wealthy cities of the Global South (Nakamura et al., 2020; Jongman, 2018). I.e. the relevance of research on resilience building through urban planning is arguably more significant for environments in the Global South.

Flood impact assessment

By definition, only the ten papers that applied approach 1 have included some form of flood impact assessment. In most studies, only the flooded built-up area was assessed. However, three studies differentiated between various land-use classes and assessed monetary damage per land-use class. While te Linde et al. (2011); Adnan et al. (2020) went one step further by assessing flood risk in terms of expected annual damage through the conceptualisation $Flood\ risk = probability \cdot consequence$. No papers considered intangible impacts, such as the number of people affected, or relative monetary impact, such as the percentage of income lost.

1.1.3 Knowledge gap and research question

Many modelling case studies have linked land-use models and flood hazard maps to acquire knowledge on flood-resilient land-use patterns. However, a knowledge gap still exists.

To begin with, only a few studies focused on the Global South. This is problematic because the Global South generally experiences more monetary flood damage, and contains more people exposed to floods than the Global North. Furthermore, the Global South is undergoing unprecedented urbanisation, compared to the Global North.

Also, modelling the interaction between flood risk and land use, which enables the assessment of the effectiveness of policies, has not yet been executed for a location in the Global South. This is problematic since resilience building through urban planning is generally less expensive than the construction of flood control infrastructure. Hence, such research is highly relevant for the generally less wealthy countries of the Global South.

Furthermore, only one study executed a flood risk assessment. However, it did not consider relative monetary impact or intangible impact. This is problematic since vulnerable communities that require prioritisation might be forgotten when only expected annual damage is considered.

Last but not least, most analysed literature did not evaluate beyond 2040, from which climate change uncertainties significantly increase. Exploring this highly uncertain future is needed to prepare humanity for the perils ahead.

Based on the formulated knowledge gap, the following main research question was defined:

How will the interaction of flood risk and land use impact the long-term flood resilience of cities in the Global South?

"Long term" indicates that time scales beyond 2040 are considered. More precisely, a time horizon of 2050 is applied for this land-use modelling case study.

1.2 Research Approach and Design

This section is broken up into three parts. To begin with, in Section 1.2.1, the chosen research approach is discussed. After that, the sub-questions are formulated in Section 1.2.2. Lastly, in Section 1.2.3 the sub-questions are connected to form one research flow.

1.2.1 Research approach

A land-use modelling case study was executed to research the described research question. This allowed us to (i) evaluate the interaction between flood risk and land use, (ii) evaluate time scales beyond 2040, (iii) focus on a city in the Global South, and (iv) incorporate multiple flood risk indicators. The execution of such a modelling case study is done to gain (i) case-study-specific knowledge, relevant to local policymakers, on how urban planning implementations can lead to resilient land-use scenarios for the city under study, (ii) general knowledge concerning the interaction between flood risk and land-use and how policymakers can use this interaction to construct more resilient urban environments, and (iii) general knowledge on the execution of a land-use modelling case-study incorporating flood-risk-land use interactions and the assessment of resilience for cities in the Global South.

Mumbai Metropolitan Region (MMR) will be the city under study for multiple reasons. To begin with, the MMR is one of the cities most severely threatened by both coastal and riverine floods (Murali et al., 2020). During the monsoon period, the city's western side is threatened by tidal variations, the eastern side by runoff from steep hills, and the city's northern side by high river discharge. Together these can result in catastrophic events similar to the one on July 26, 2005, when rainfall of approximately 190 mm/h coincided with high tides resulting in tremendous human, economic and infrastructural loss (Pathak et al., 2020). To make things worse, floods are projected to increase due to climate change (Strauss et al., 2021; Ward et al., 2020). Nonetheless, the migration to the city is projected to continue for the coming years, resulting in an estimated population of approximately 29 million in 2031 and 32 million in 2041 (MMR, 2016). This population growth will inevitably be accompanied by significant land-use change (Bhanage et al., 2021). A land-use change modelling case study thus seems beneficial for the MMR due to the various changing factors and associated uncertainties. However, one has, to our knowledge, not been constructed yet. Consequently, the MMR is expected to benefit from a case study like this significantly.

1.2.2 Sub-questions

To structure scientific research, the main research question is broken up into the following sub-questions (SQs). These sub-questions logically lead to an answer to the main research question, and all address a subsection of the earlier derived knowledge gap present in literature.

First, SQ1 results in essential knowledge for establishing a land-use model for the MMR. After that, SQ2 results in knowledge concerning how resilient urban planning is defined and measured for the MMR. Furthermore, SQ3 results in how the flood-risk-land-use interaction is conceptualised for the MMR. Lastly, SQ4 discusses the potential pathways to resilience that can be derived from integrating the land-use model with flood hazard maps and the defined scenarios.

SQ1 What drivers of land-use change and flood hazards are essential to the MMR?

SQ2 How can resilient urban planning be conceptualised and assessed for the MMR?

SQ3 How can the flood-risk–land use interaction be conceptualised for the MMR?

SQ4 What are the potential pathways of land-use change towards resilience considering flood-risk-land-use interaction for MMR that can be derived from the results of the land-use simulations?

1.2.3 Research flow

In general, this modelling case study consists of the sub-components *land-use modelling*, *resilient urban planning*, and *flood-risk-land-use interaction* that require literary research, conceptualisation and operationalisation. In Chapter 2, the relevant literature to the three sub-components is discussed. In Chapter 3, the conceptualisation of the three sub-components takes place, i.e. the general concepts and applied procedures are introduced and discussed. In Chapter 4, operationalisation, i.e. in-depth technical discussions, take place where necessary. Concerning resilient urban planning and flood-risk-land-use interaction, this is jointly done in the flood-risk assessment section. In Chapter 5, the generated land-use model, the applied flood hazard maps and the analysis of their interaction in relation to flood risk and urban flood resilience are discussed. Moreover, in Chapter 6, the answers to the sub-questions and main research question, the scientific and societal impact of the conducted research, a reflection on the impact on the Global South and limitations and future work are addressed. An overview of the various steps, chapters, and sub-questions is given in Figure 1.2.

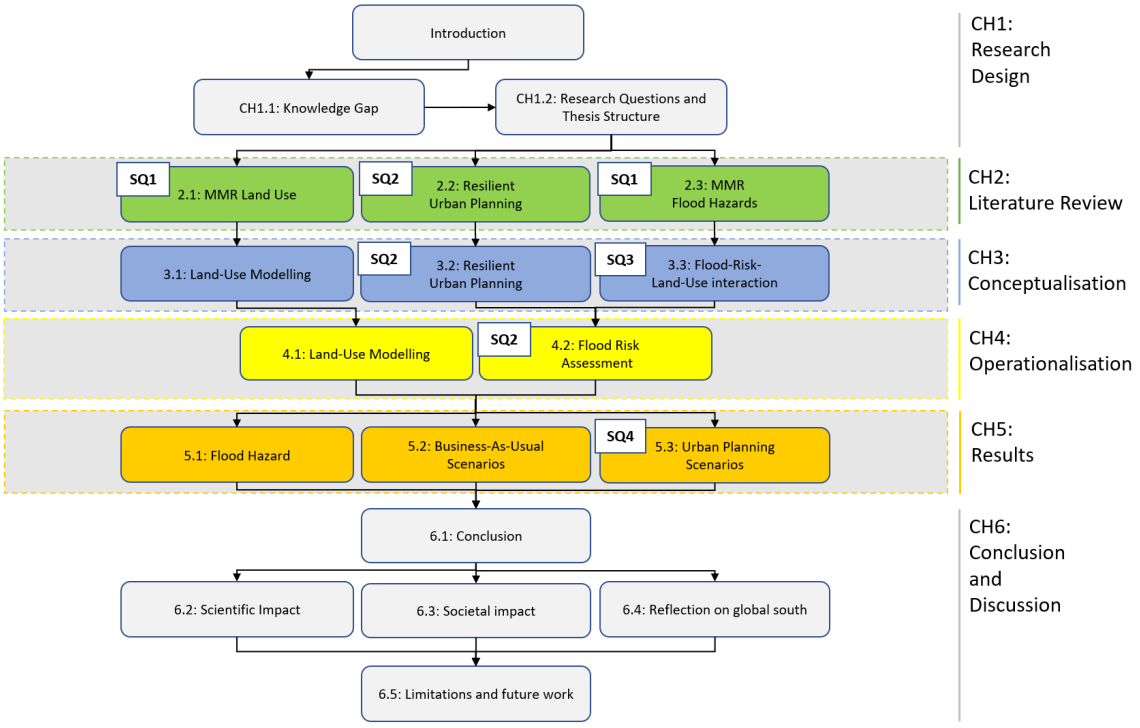

Figure 1.2: *A figure that visualises a research flow that will lead to the answering of the main research question.*

Chapter 2

Literature Review

As discussed in Section 1.2.1, the MMR is one of the cities most severely threatened by coastal and riverine floods worldwide, which are projected to increase due to climate change. To make things worse, the city will experience significant urban expansion due to population growth in the 21st century. Consequently, the MMR's current and future urbanised areas need to become more flood resilient. In this chapter, the required literature reviews are discussed. First, Section 2.1 discusses the essential driving forces of land-use change and past and future growth of the MMR. Thereafter, Section 2.2 discusses urban resilience, resilient urban planning, and assessment of resilience. Lastly, Section 2.3 discusses the essential flood hazards of the MMR.

2.1 MMR Land-Use

This chapter will answer the first part of SQ1 based on an extensive literature review.

What drivers of land-use change and flood hazards are essential to the MMR?

To answer this question, first, in section 2.1.1, a general overview is given of the MMR. After that, in section 2.1.2, MMR's stage of urbanisation is discussed. Subsequently, in section 2.1.3, the estimated past, present, and future behaviour of land-use classes and the land-use driving forces are discussed. Lastly, in section 2.1.4, urban policies essential to the development of the MMR are discussed.

2.1.1 General overview

The Mumbai Metropolitan Region (MMR) is an urban region of 4312 km^2 situated in the western part of Maharashtra province, India. Its elevation above sea level varies from 0 to approximately 900 m. Based on the Koppen-Geiger classification, its climate can be categorised as a tropical wet-dry climate (Aw), indicating that it is moderately hot with a high humidity level and that most precipitation occurs in the high-sun season (summer). In the case of MMR, this occurs between June and September due to the southwest monsoon. The total annual rainfall varies between 1800 mm and 2500 mm, and the summer temperature of the region ranges typically between 21 °C and 36 °C (Vinayak et al., 2021). Economically, the region is India's "capital" (MMR, 2016). It is responsible for 40 % of Maharashtra's economy, more than 6% of India's economy and facilitates more than 10 % of India's industrial jobs (Ghorpade, 2017). Also, it houses the country's largest stock market, various financial firms, and many domestic and international banks (MMR, 2016). Furthermore, foreign companies present in India are frequently managing their business from offices in the MMR. Additionally, the MMR is one of the main hubs connecting India with the rest of the world through air networks. All of this results in the region creating employment opportunities for people of all skill levels, with population migration from neighbouring and distant regions as a consequence (Das and Bhusan, 2014). Hence, the population of the MMR is expected to increase from approximately 27 million people in 2021 to approximately 29 million in 2031 and approximately 32 million in 2041 (MMR, 2016).

2.1.2 Urbanisation of MMR

van den Berg et al. (1982) proposed a model describing the rate and direction of population changes in urban regions that are typical for the various stages of urban development. This model describes how population growth will first occur at the core (urbanisation) and subsequently shift to the periphery (exurbanisation). Das and Bhusan (2014) deems it valid, even though this model was constructed 40 years ago and was developed with cities of developed nations in mind, to categorise Mumbai as an urban region in the exurbanisation stage of urban development, and more specifically in the absolute centralisation stage. This absolute centralisation stage is characterised by (i) a decreasing population at the core and (ii) an increasing population at the periphery. In line with this, Chakraborty et al. (2015); Chatterjee and Chattopadhyay (2020); Vinayak et al. (2021) all analysed the growth of Mumbai and concluded that the region's spatial change and population growth mainly takes place in the suburbs and satellite towns. In contrast, growth in Mumbai has stagnated.[1] Various reasons for this geographical shift in growth are discussed in the following sections.

[1] We refer to B.1, for the delineation of these administrative boundaries.

Transport networks

India's first railway passenger train service was established between Mumbai and Thane in 1853, resulting in the dispersal of people and the establishment of the suburb Thane (Chatterjee and Chattopadhyay, 2020). The transport network of the MMR has thenceforth further increased in size and progressed in efficiency, allowing the further dispersal of people towards the periphery (Das and Bhusan, 2014). Ever since, urban growth in the MMR has often taken place around transportation networks (Vinayak et al., 2021), and particularly around transportation hubs (Makandar, Suhel M and Naik, Saharsha A., 2020).

Industrial development and job availability

The first industrial estate of the state of Maharashtra was established in Thane in 1961. This resulted, similarly to the railway passenger service, in dispersal; dispersal of first, industries and jobs and thereafter of people from Mumbai city towards Thane (Sangameswaran, 2021). Ever since, several SEZs, IT clusters and CBDs have been developed on the east of Greater Mumbai, generating jobs and subsequently pulling the population to the periphery. In line with this, the fraction of jobs generated by Greater Mumbai with respect to the MMR, decreased from 62% in 2001 to 55% in 2011 (MMR, 2016).

Overfull Mumbai

MMR is one of the most densely populated cities in the world (Murali et al., 2020). According to Hu et al. (2021), Mumbai and its suburbs have an approximated density of 37.000 people/km^2. Unsurprisingly this has the undesirable side effect of exorbitant housing prices. Consequently, in 2016, half of the MMR's population could not afford a house in Greater Mumbai (Chatterjee and Chattopadhyay, 2020). Subsequently, MMR (2016) concluded that the city's core is full, which creates an outwardly directed force that results in growth at the periphery instead of in the core.

Enforcement of urban planning regulations

Another factor that results in increased growth at the periphery is the enforcement of urban planning regulations. Urban planning policy is relatively strict on paper. However, in practice, these regulations are less strictly enforced at the periphery than at the core. Resulting in more urban sprawl at the edges (Chatterjee and Chattopadhyay, 2020).

2.1.3 Land-use classes and driving forces

This section discusses a literature review on the past, current and future prevalence of various land-use classes in the MMR and what driving forces impact their presence. To arrive at relevant literature, a preliminary literature search was executed in reference database *Scopus*, based on the search terms of Table 2.1. These search terms can be grouped under two categories: (i) land-use-change modelling and (ii) MMR.

	Combine the concepts with AND	
	land-use-change modelling	**MMR**
Combine the synonyms with OR	land?use?change?model*	MMR
	land?change?model*	Mumbai?Metropolitan?Region
	land?use*	Mumbai
	LUCM	
	LCM	
	LUM	
	urban?growth*	

Table 2.1: *A table of the search terms that were used to arrive at relevant literature.*

First, in section 2.1.3, the past and current surface area of various land-use classes are discussed. Second, in section 2.1.3, the past, current, and future growth or decline and movement of growth are discussed per land-use class. After that, in section 2.1.3, the tendency of various land-use classes to change to other land-use classes and the other way round is discussed. Lastly, in section 2.1.3, various driving forces of land-use change to specific land-use classes are mentioned.

After doing a preliminary literature search, which resulted in over 27 scientific sources, a number were selected based on if they contained (i) quantitative estimates of past, current, and future growth or decline, (ii) information on the movement of growth, (iii) information on the tendency of various land-use classes to change to other land-use classes and the other way round, and (iv) land-use specific information on the various driving forces of land-use change. Subsequently, these were combined with available planning documents to arrive at the final literature list of six sources. These six sources are visualised in various Tables in the following sections.

The selection of land-use classes considered in this literature review was based on the land-use classes evaluated in most considered studies. In the evaluated literature, the aggregation level of the evaluated land-use classes was relatively high. Therefore, this literature review also considered high aggregation level land-use classes.

Past and current land-use

In this section, an overview is given of the prevalence of the various land-use classes in (i) the city of Mumbai, (ii) Greater Mumbai, or (iii) the MMR for both the past [1990, 2010] and the present [2010, 2022]. We refer to B.1, for the delineation of these administrative boundaries.

land-use class	Past amount [1990,2010](km^2 or %)	Current amount [2010,2022](km^2 and %)
Built-up	Greater Mumbai (875 km^2, 1990): 185 km^2 (21%) (Shafizadeh Moghadam and Helbich, 2013). Greater Mumbai (875 km^2, 2001): 255 km^2 (29%) (Shafizadeh Moghadam and Helbich, 2013).	MMR(4311 km^2, 2016): 700 km^2 (16%)(MMR, 2016). Greater Mumbai (875 km^2, 2010): 356 km^2 (41%) (Shafizadeh Moghadam and Helbich, 2013).
Informal residential	X	X
Industrial and quarries	X	MMR(4311 km^2, 2016): 93 km^2 (2%)[2] (MMR, 2016).
Green space	City of Mumbai(630 km^2, 1998): 205 km^2 (32%) (Rahaman et al., 2021). City of Mumbai(630 km^2, 2008): 173 km^2 (27%) (Rahaman et al., 2021).	City of Mumbai(630 km^2, 2018): 168 km^2 (27%) (Rahaman et al., 2021). Greater Mumbai (905 km^2, 2019): 289 km^2 (32%) (Ranagalage et al., 2021).
Forest	MMR(2834 km^2, 1992): 874 km^2 (31%) (Vinayak et al., 2021). MMR(2834 km^2, 2002): 829 km^2 (29%) (Vinayak et al., 2021).	MMR(2834 km^2, 2011): 598 km^2 (21%) (Vinayak et al., 2021). MMR(4311 km^2, 2016): 833 km^2 (19%)(MMR, 2016).
Agriculture	MMR(2834 km^2, 1992): 1090 km^2 (38%)[3] (Vinayak et al., 2021). MMR(2834 km^2, 2002): 999 km^2 (35%)[4] (Vinayak et al., 2021). Greater Mumbai (875 km^2, 1990): 397 km^2 (45%) (Shafizadeh Moghadam and Helbich, 2013).[5] Greater Mumbai (875 km^2, 2001): 341 km^2 (39%) (Shafizadeh Moghadam and Helbich, 2013).[6]	MMR(4311 km^2, 2016): 1307 km^2 (30%)[7] (MMR, 2016). MMR(2834 km^2, 2011): 981 km^2 (35%)[8] (Vinayak et al., 2021). Greater Mumbai (905 km^2, 2019): 25 km^2 (3%) (Ranagalage et al., 2021).
Wetlands and Coastal land	Greater Mumbai (875 km^2, 1990): 97 km^2 (11%) (Shafizadeh Moghadam and Helbich, 2013). Greater Mumbai (875 km^2, 2001): 91 km^2 (10%) (Shafizadeh Moghadam and Helbich, 2013).	Greater Mumbai (875 km^2, 2010): 82 km^2 (9%) (Shafizadeh Moghadam and Helbich, 2013). MMR(4311 km^2, 2016): 304 km^2 (7%)(MMR, 2016).
Water bodies	Greater Mumbai (875 km^2, 1990): 83 km^2 (9%) (Shafizadeh Moghadam and Helbich, 2013). Greater Mumbai (875 km^2, 2001): 78 km^2 (9%) (Shafizadeh Moghadam and Helbich, 2013).	Greater Mumbai (875 km^2, 2010): 71 km^2 (8%) (Shafizadeh Moghadam and Helbich, 2013). MMR(4311 km^2, 2016): 180 km^2 (4%)(MMR, 2016).

Table 2.2: *In this Table, information derived from various scientific sources on the past and current amount of the various land-use classes in the MMR is summarised. Take into account that all numbers in this Table are rounded on whole numbers and that X's indicate that no information could be found.*

Growth and movement

The current growth or decline of the various land-use classes was estimated based on the statistics in Table 2.2. This was subsequently visualised in Table 2.3, with projections of future growth or decline and movement of the centroid of the land-use class.

land-use class	Growth or decline	Movement of centroid
Built-up	Previous growth projected to continue; planned to increase from 697 km^2 (16%) in 2016 to 992 km^2 (23%) in 2036 for the MMR (4311 km^2) (MMR, 2016).	Movement to the periphery; more growth in the satellite towns than infill development in Greater Mumbai (MMR, 2016; Shafizadeh Moghadam and Helbich, 2013).
Informal residential	Currently stable in Greater Mumbai (Nijman, 2012), however governmental ambition to create a decline by increasing the availability of low-cost urban-formal (MMR, 2016).	Movement to the periphery due to forced relocation and redevelopment in the centre and new growth in suburbs and satellite towns (Nijman, 2012).
Industrial and quarries	Planned growth; planned to more than double in size by 2036 due to development of new industrial areas in various areas and the promotion of the primary sector (MMR, 2016).	Planned dispersal across the region; shift to the satellite towns with Planned new industrial zones in Vasai Virar, Bhiwandi, Taloja, Khalapur, Khopta and both sides of Amba river (MMR, 2016).
Green space	Reducing decline for centre of Mumbai, steeper decline for MMR (Rahaman et al., 2021; Shafizadeh Moghadam and Helbich, 2013).	Movement to Greater Mumbai due to more removal at the periphery than in Greater Mumbai (Shafizadeh Moghadam and Helbich, 2013), however envisioned establishment of new regional parks[9].
Forest	Previous decline is projected to change into growth; planned to increase from 833 km^2 (19%) in 2016 to 1071 km^2 (25%) in 2036 for the MMR (4311 km^2) (MMR, 2016).	Movement to Greater Mumbai due to more removal at the periphery of the MMR than in Greater Mumbai (Shafizadeh Moghadam and Helbich, 2013; Vinayak et al., 2021).
Agriculture	Previous decline is projected to accelerate in the future; estimated to decline from 981 km^2 (35%) in 2011 to 503 km^2 (18%) in 2050 for the MMR(2834 km^2) (Vinayak et al., 2021).[10]	Further movement to the periphery (Vinayak et al., 2021; Shafizadeh Moghadam and Helbich, 2013).

[2] 88 km^2 industry + 5 km^2 quarry = 93 km^2
[3] Also sparsely vegetated and barren land are incorporated here.
[4] Also sparsely vegetated and barren land are incorporated here.
[5] Also open land is incorporated here.
[6] Also open land is incorporated here.
[7] Also other primary activities are incorporated here, such as quarries.
[8] Also sparsely vegetated and barren land are incorporated here.
[9] The new envisioned parks are Kharbav Regional Park, Lonad Regional Park and Regional Park near Matheran.
[10] Also sparsely vegetated and barren land are incorporated here.

Wetlands and Coastal land	Previous decline is projected to change into slight growth; estimated to grow from 194 km^2 (7%) in 2011 to 210 km^2 (7%) in 2050 for the MMR(2834 km^2) (Vinayak et al., 2021).	Little movement of centroid (Vinayak et al., 2021; Shafizadeh Moghadam and Helbich, 2013).
Water bodies	Previous very slight decrease is projected to continue; projected to decrease from 180 km^2 (4%) in 2016 to 147 km^2 (3%) in 2036 for the MMR (4311 km^2) (MMR, 2016).	Little movement of centroid (MMR, 2016).

Table 2.3: *In this Table, various land-use classes, their growth or decline, and centroid movement are summarised. Take into account that all numbers in this Table are rounded on whole numbers.*

Alternation over time

The various land-use classes change into the other land-use classes and thus alternate one another over time. Per land-use class one can specify if it has a tendency to *change towards others* and if others have a tendency to change towards it. This dichotomy has been expressed in Table 2.4. This Table is, to a large extent, based on the outcomes of Markov Chain models.

land-use class	**Change to other land-use classes**	**Change to this land-use class**
Built-up	High inertia; little tendency to change to other land-use classes (Vinayak et al., 2021; Shafizadeh Moghadam and Helbich, 2013).	• Strong tendency of agriculture to change to built-up (Shafizadeh Moghadam and Helbich, 2013; Vinayak et al., 2021). • Weak tendency of forests to change to built-up (Shafizadeh Moghadam and Helbich, 2013; Vinayak et al., 2021). • Weak tendency of coastal lands and wetlands to change to built-up (Shafizadeh Moghadam and Helbich, 2013; Vinayak et al., 2021). • Tendency of industrial lands to change to built-up (MMR, 2016).
Informal residential	X	X

Industrial and quarries	• Tendency of industrial lands to change to built-up (MMR, 2016). • Potential tendency of quarries to change to green space (MMR, 2016).	X
Green space	Debated tendency to change to built-up (Rahaman et al., 2021; Vinayak et al., 2021).	Potential tendency of quarries to change to green space (MMR, 2016).
Forest	Small tendency to change to built-up (Shafizadeh Moghadam and Helbich, 2013; Vinayak et al., 2021).	No specific land-use classes with a tendency to change into forests (Shafizadeh Moghadam and Helbich, 2013; Vinayak et al., 2021).
Agriculture	Strong tendency to change to built-up (Shafizadeh Moghadam and Helbich, 2013; Vinayak et al., 2021).	No specific land-use classes with a tendency to change into forests (Shafizadeh Moghadam and Helbich, 2013; Vinayak et al., 2021).
Wetlands and Coastal land	Weak tendency to change to built-up (Vinayak et al., 2021; Shafizadeh Moghadam and Helbich, 2013).	No specific land-use classes with a tendency to change into agriculture (Shafizadeh Moghadam and Helbich, 2013; Vinayak et al., 2021).
Water bodies	High inertia; little tendency to change to other land-use classes (Shafizadeh Moghadam and Helbich, 2013; Vinayak et al., 2021).	No specific land-use classes with a a likely tendency to change into water bodies (Shafizadeh Moghadam and Helbich, 2013; Vinayak et al., 2021).

Table 2.4: *In this Table, the tendency of land-use classes to change towards each other is summarised. Take into account that X's indicate that no information could be found.*

Driving forces

The appearance of land-use classes throughout space and their resulting alteration over time is determined by site and surrounding specific forces that lead to attraction and repulsion. These attracting and repelling forces are called the driving forces of land-use change. The various forces that, according to literature, attract and repel the emergence of land-use classes in the MMR are mentioned in Table 2.5. Attracting, in this case, indicates a positive correlation (if the force increases, the potential emergence of a land-use class also increases), while repelling indicates a negative correlation (if the force increases or decreases, the potential emergence decreases or increases, respectively).

land-use class	Attracting forces	Repelling forces
Built-up	• The density of open and arable land (Shafizadeh-Moghadam and Helbich, 2015).	• The distance to SEZs (Vinayak et al., 2021). • The distance to a business district (debated) (Shafizadeh-Moghadam and Helbich, 2015). • The density of built-up land (Shafizadeh Moghadam and Helbich, 2013). • The distance to other built-up areas (Shafizadeh-Moghadam and Helbich, 2015). • The distance to a transportation network (roads, railway, rivers) or hub (airport, harbour, railway station) (Vinayak et al., 2021; Shafizadeh Moghadam and Helbich, 2013; Chatterjee and Chattopadhyay, 2020). • Altitude of the location (Shafizadeh Moghadam and Helbich, 2013). • Slope of the location (Shafizadeh Moghadam and Helbich, 2013).
Informal residential	X	X
Industrial and quarries	the presence of an SEZ (MMR, 2016).	• MMR's development authority stated that "quarrying at the edges and foothills of forests, protected areas and steep slopes are leading to degradation of forested areas and lead to erosion" (MMR, 2016). Hence, it seems likely that this will lead in the near future to zoning policies that prevent quarrying next to these areas. • 44% of factory employment (2009) in the MMR took place in MIDC industrial areas, indicating an attracting force of these areas (MMR, 2016).
Green space	X	X
Forest	The steepness of a slope (MMR, 2016).	X
Agriculture	X	X
Wetlands and Coastal land	X	X
Water bodies	X	X

Table 2.5: *In this Table, the driving forces of land-use change for the various land-use classes of the MMR are summarised. Take into account that X's indicate that no information could be found.*

2.1.4 Urban planning policies

Several governmental policies dictate how land is used in the MMR. In this section the various relevant urban planning policies are discussed.

Industrial location policy 1992

The industrial location policy for Mumbai was implemented in 1992. This policy is discussed in MMR (1995). A summary is given in this section.

The region is divided up into three zones:

Zone-I: Greater Mumbai and areas of Thane Municipal Corporation and Mira- Bhayander Municipal Council.

Zone-II: areas of Kalyan and Navi Mumbai Municipal Corporation, Ulhasnagar, Ambernath, Kulgaon-Badlapur Municipal Councils and Bhiwandi, Uran and Vasai-Virar Sub-Regions.

Zone-III: the rest of the MMR.

The industries are subsequently classified into three categories in the following manner.

Category-I: non polluting, high-tech or high-value-added industrial units.

Category-II: highly polluting, hazardous or obnoxious industrial units.

Category-III: other industries than in categories I and II.

Per zone, urban policies are subsequently implemented in the following manner.

Zone-I policy: Category-I industrial units can be constructed or expanded. New category-II industrial units are not allowed to be constructed or expanded. Expansion of category-III industrial units is allowed on 25% of the connected land.

Zone-II policy: Construction of category-I and III industrial units is allowed freely. Category-II industrial units are only allowed in the MIDC areas.

Zone-III policy: All industries are permitted.

MIDC areas

MIDC areas are delineated by the Maharashtra Industrial Development Corporation (MIDC), and promoted for industrial development through low-cost land, development of transport networks, and development of water networks (Shaw, 2004). A list of the various MIDC areas located in the MMR can be found in (MIDC, 2020).

MIDC also delineates various IT-development areas, also known as IT parks. MIDC offers low-rent offices and high-speed internet in these parks to attract development. A list of the various MIDC IT-parks can be found in (MIDC, 2020).

Bhiwandhi industrial areas

The Institute for Spatial Planning and Environment Research has delineated several areas for industrial development in their draft development plan 2008-2028 for the Bhiwandi Surrounding Notified Area (MMRDA, 2008). Industrial development is allowed in the delineated regions while prohibited in other areas.

Special economic zones

Santacruz Electronics Export Processing Zone (SEEPZ) was the MMR's first Special Economic Zone (SEZ). It was established by the federal government in 1973 and is located in central Mumbai (Andheri East), with a focus on, at first, electronics and, after that, gems and jewellery (MCGM, 2016). Apart from SEEPZ, there are six other operational SEZs in the MMR; one in the city of Mumbai, two in Navi Mumbai and three in Thane. All of these have been set up by private parties and are focused on information technology and associated services (Shira, 2019). The promotion and subsequent creation of SEZs have contributed to the current polycentric growth pattern for the MMR, according to MCGM (2016).

Business districts

Business districts are famous for attracting urban development. MMR's business districts can be divided into three major classes: (i) the primary business districts (PBDs) located in the city of Mumbai, (ii) the secondary business district (SBDs) located in the western and eastern suburbs [11] and Thane and (iii) the emerging business district located in Navi Mumbai (Verma et al., 2020). The first business market was established in the 1950s in Ballard Estate in the southern part of the city centre, which, combined with Nariman Point and Cuffe Parade, grew to become the central business (CBD). In the 1970s, the Branda-Kurla Complex (BKC) was established, which has grown so significantly that it is considered the modern CBD of the MMR. Together with other zones in central Mumbai, these are considered the PBDs. SBDs arose along the two main traffic arteries (The Western and Eastern Express Highways) from the city of Mumbai to the periphery in the western and eastern suburbs and at the end of the Eastern Express Highway in the satellite town of Thane. Lastly, a business district has emerged in the satellite town of Navi Mumbai since the 1990s (Verma et al., 2020). For an overview of the business districts present in Mumbai, we refer to Verma et al. (2020).

The impact of the BKC on urban development is doubted by Shafizadeh-Moghadam and Helbich (2015), who argue that the distance to the modern CBD was insignificant in their analysis. The significance of other business districts was not evaluated in their analysis.

Coastal regulation zones

Ministry of Environment, Forest and Climate Change (2019) discusses the different coastal regulation zones (CRZs) that apply to the MMR. The following section summarises what areas they encompass and what land-use classes are allowed in the various types of zones.

CRZ-I covers the most environmentally critical areas and is subdivided into CRZ-I A, and CRZ-I B. CRZ-I A encompasses Ecologically Sensitive Areas (ESAs), such as mangroves, corals, national parks, among others, and other protected areas under the provision of Wild Life Protection Act (1972), Forest Conservation Act (1980), or Environment Protection Act (1986). CRZ-I B encompasses the intertidal zone, i.e. the area between the low tide line (LTL) and high tide line (HTL).

CRZ-II covers developed land areas close to the shoreline that are substantially built-up (50% of the plots are built-up), which have been provided with drainage, approach roads, and other infrastructural facilities, such as water supply and sewerage.

CRZ-III covers relatively undisturbed land areas close to the shoreline (< 500 m) and is subdivided into CRZ-III A, and CRZ-III B. CRZ-III A encompasses areas with a population density larger than 2161 people/km^2, while CRZ-III B encompasses areas with a population density

[11] These suburbs are part of Greater Mumbai.

smaller than 2161 people/km^2. In CRZ-III A and CRZ-III B, the areas up to 50 and 200 meters from the HTL are designated as No Development Zones (NDZs).

CRZ-IV covers the various water bodies and is subdivided into CRZ-IV A, and CRZ-IV B. CRZ-IV A encompasses the water and sea bed area between the LTL and the twelve nautical miles line on the seaward side. CRZ-IV B encompasses the water and sea bed area in tidal areas.

Several *special* areas are governed differently from CRZ-I up to CRZ-IV. Among these are (i) the Critically Vulnerable Coastal Areas (CVCAs), such as the Sundarban region of West Bengal, Gulf of Khambat, Gulf of Kutch in Gujarat, Malvan, Achra-Ratnagiri in Maharashtra, Karwar and Coondapur in Karnataka, Vembanad in Kerala, Gulf of Mannar in Tamil Nadu, Bhaitarkanika in Odisha, Coringa, East Godavari and Krishna in Andhra Pradesh, (ii) the CRZs for inland Backwater islands and islands along the mainland coast, and (iii) the CRZs that fall within municipal limits of Greater Mumbai.

Cessed buildings

In the MMR, cessed buildings are dilapidated buildings that are governed by the Maharashtra Housing and Area Development Authority (MHADA). These buildings can be over a hundred years old and must be restored or redeveloped. Homeowners pay a tax (cess) to the MHADA that subsequently tries to ensure the safe habitation of these buildings. The local government also raised the maximally allowed FSI in various areas with many cessed buildings to promote high-density redevelopment. There were approximately 16 thousand cessed buildings in the MMR in 2008, most of which are located in the island city of Mumbai (MCGM, 2016).

Heritage

Mumbai's heritage list comprises heritage buildings and precincts and is subject to periodic revisions. A large majority of the list is located in Greater Mumbai, and some structures date back as far as the year 100 CE. Regulations state that no development is allowed in the region 100 meters around a monument and that only regulated development is allowed until 300 meters from a monument (MCGM, 2016). Besides Mumbai's heritage designation, some sites are also defined as cultural, natural or mixed heritage by UNESCO. These sites should contain one or more of the ten 'outstanding universal value' criteria. Once on the UNESCO world heritage list, protecting the site's 'outstanding universal value' becomes the state's responsibility. Hardly never[12] it happens that a site is affected and subsequently 'delisted' (Alsalloum, 2018). Hence we assume that, concerning UNESCO world heritage sites in the MMR, this will not occur and that no development will occur at these sites.

[12]Only on two occasions this happened(Alsalloum, 2018).

2.2 Resilient Urban Planning

In this Chapter, we discuss in Section 2.2.1 what is generally considered to be a suitable definition of urban resilience in light of climate change, in Section 2.2.2 how urban planning fits in the body of knowledge concerning resilience, and in Section 3.2.2 how resilience has been quantitatively assessed in previous studies.

This literature review provides a stepping stone for answering SQ2:

How can resilient urban planning be conceptualised and operationalised for the MMR?

2.2.1 Urban resilience

The concept of resilience has a long history in fields such as sociology, engineering, psychology, ecology and disaster management. These fields all attributed different definitions to it with conceptual fuzziness as a consequence (Meerow et al., 2016). According to Sharifi and Yamagata (2016); Liao (2012); Zevenbergen et al. (2020), the socio-ecological framework should be applied to acquire urban resilience in the face of climate change. The socio-ecological framework acknowledges that the stability domain of man-made and ecological systems changes over time due to external shocks and drivers (Zevenbergen et al., 2020). Consequently, in this framework, systems have various equilibria that change over time and the emphasis is on transformation and adaptation to the inherent variability and uncertainty of the system while maintaining functionality (Sharifi and Yamagata, 2016; Olazabal et al., 2012; Folke, 2003). Hence, socio-ecological resilience is often defined as "the capacity of a system to absorb disturbance and reorganise while undergoing change so as to still retain essentially the same function, structure, identity, and feedbacks" (Meerow et al., 2016).

2.2.2 Urban planning and a flood resilient urban environment

Traditionally the approach to establishing urban flood resilience is based on an engineering approach to resilience, focusing on establishing stability by constructing flood control infrastructure for a specific design capacity (Zevenbergen et al., 2020; Liao, 2012). Although this approach has been applied extensively through the construction of dams, pump stations, stormwater drainage systems and others, it has proven to be insufficient in establishing sufficient urban flood resilience since cities around the world remain vulnerable to flood hazards (Liao et al., 2016). This is fundamentally connected with flood control systems being based on engineering resilience, where the focus is on a single equilibrium state to which the city should return after a disruption. This focus on 'stability' becomes problematic when one applies it to inherently dynamic systems and for which returning to the predisaster state can be far from optimal (Cumming et al., 2006). Also, in the face of climate change uncertainty and resulting increased flood hazards, relying solely on flood control infrastructure designed for a specific design capacity cannot be considered reliable, due to their absolute failure when an event exceeds the design capacity (Zevenbergen and Gersonius, 2007; Liao, 2012; Nakamura et al., 2020). Attempts are made to design flood control infrastructure that can cope with a large range of climate scenarios. However, the design of such infrastructure is more complex, and construction is more expensive (Hallegatte, 2009). Furthermore, according to socio-hydrological research, flood control infrastructure can result in a false sense of security, resulting in a boost of development in protected flood-prone regions (Jongman, 2018). In addition, flood control infrastructure negatively affects the biodiversity and climate resilience of ecosystems through maladaptation (Opperman et al., 2009; IPCC, 2022b). Flood control infrastructure can also leave a lot to be desired in terms of feasibility. They can

take years to construct, by which the capacity for which they were designed may no longer be sufficient and they can requires immense capital funds, for which both political momentum and government budgets are often lacking (Nakamura et al., 2020; Jongman, 2018). An example of this is the, in Section 2.3.3 and 2.3.4 discussed, improved stormwater drainage system for the MMR that has still not been finalised and is being constructed for rainfalls that are yearly exceeded. To make things worse, costs have turned out at least three times higher than expected (Chatterjee, 2019).

The inability of flood control structures to supply cities with sufficient flood resilience has lead to various authors, such as (Zevenbergen et al., 2020; Liao et al., 2016), promoting a paradigm shift from the 'flood control paradigm', which states that flooding should be prevented in the first place, to the 'flood adaptation paradigm', which focuses on preventing damage when flooding occurs. This paradigm shift can be seen as a transition from engineering resilience to the, in light of climate change uncertainty, more suitable socio-ecological resilience. Flood adaptation based on socio-ecological resilience begins with acknowledging periodic floods as inherent environmental dynamics of an urban environment. And coherently with the earlier mentioned definition of socio-ecological resilience, the emphasis in the 'flood adaptation paradigm' is on transformation and adaptation to the inherent variability and uncertainty of the system while maintaining functionality (Liao, 2012).

Hence, according to the adaptation paradigm, urban environments should be adapted and transformed in the face of recurring floods and inherent flood variability and uncertainty. Not to prevent floods but to prevent damage and ensure citizens' flood safety, resulting subsequently in flood-resilient urban environments (Liao, 2012; Liao et al., 2016). Consequently, the adaptation of the urban environment in light of future flood risk (i) corresponds with the socio-ecological perspective on resilience, which is the suitable resilience paradigm to apply for urban environments facing climate change, and (ii) can contribute to the urban flood resilience of urban environments by reducing flood risk.

2.2.3 Resilience indicators

Concerning measuring flood resilience there are, according to (Hammond et al., 2015), two mayor approaches applied in literature. The first approach tries to assess flood resilience by measuring characteristics of a system that are correlated with the system being resilient. This approach has been applied by, for example, Sun et al. (2016); Xu et al. (2021); Cutter et al. (2008), who used surrogates such as 'GDP density', 'rescue capabilities' and 'percentage of non-elderly' to asses flood resilience. The second approach tries to assess flood resilience more directly by quantifying the response of a system to floods. This approach depends on the, generally accepted, notion of resilience as a desirable attribute (Meerow et al., 2016), and that flood resilient cities experience little flood impacts (Hammond et al., 2015). Consequently, by estimating flood risk, a city's flood resilience can be assessed. I.e. low risk is associated with high resilience and high risk is associated with low resilience. This approach has been applied to various types of natural hazards (Bruneau et al., 2003; De Bruijn, 2004; Su et al., 2018; Hazbavi et al., 2018).

The first approach is not considered in this literature review since the first approach requires high-detailed spatial data that is to our knowledge unavailable for the area under study. Hence, only the second approach is considered in this literature review. An overview of the the resilience indicators applied in the relevant literature, and elaboration on how they are calculated, can be found in Table 2.6.

Source	Resilience indicators	Explanation
De Bruijn (2004)	1. the amplitude of the reaction 2. the graduality of the increase of reaction with increasing discharges 3. the recovery rate	1. The amplitude of the reaction indicates the expected damage short after a flood has occurred. Primary direct tangible damage is estimated using the unit loss method and communicated using the concept of expected annual damage. Indirect tangible damage is estimated using the indicator method and the assumption that intangible damage is correlated with the number of casualties in the flooded area. 2. The graduality is estimated by evaluating the discharge damage function. A discontinuity indicates that damage increases dis-proportionally at a certain discharge level, subsequently indicating the possibility of a disaster. 3. The recovery rate indicates the rate of return to a state better or equal, in terms of functionality, to the predisaster state. It is estimated qualitatively by measuring the system's physical, economic and social characteristics.
Su et al. (2018)	1. the severity of the flood impact 2. the variability of the flood impact 3. the graduality of the impact	1. The severity of the flood impact is estimated through the expected annual damage. 2. The variability of the flood impact is estimated through the standard deviation of the annual flood damage due to the variability of floods. 3. The graduality is estimated using the continuity of the discharge damage function, similarly to De Bruijn (2004).
Hazbavi et al. (2018)	the recovery time	Recovery time is the average time a system needs to rebound to a satisfactory state after reaching an unsatisfactory state.

Table 2.6: *Papers found in the literature that estimate resilience by quantifying the response of a system to floods.*

2.3 MMR Flood Hazards

The MMR's flood vulnerability, which is already at an undesirable level, is projected to increase due to climate change-induced (i) sea-level rise, (ii) increased rainfall, and (iii) intensified monsoons (Murali et al., 2020).

In this chapter, the second part of SQ1 will be answered based on an extensive literature review.

What drivers of land-use change and flood hazards are essential to the MMR?

This sub-question is discussed by first discussing the severity of the current flood situation, in Section 2.3.1. After that, we discuss the natural and artificial geography, in Sections 2.3.2 and 2.3.3, that together form the root of the problem. Lastly, the currently executed and planned adaptations to the artificial geography are mentioned in Section 2.3.4.

2.3.1 Historical perspective

The MMR experiences significant floods yearly, some of which result in such devastating consequences that they leave a mark on society. Such an event occurred on July 26, 2005 (MCGM, 2016). On this day, unprecedented rainfall took place. Within 24 hours (from 8:30, July 26, 2005 until 8:30, July 27, 2005), 944 mm precipitation was recorded, which is almost half of the annual average rainfall in Mumbai (Hallegatte et al., 2010). This amount of precipitation could not be handled by the MMR's stormwater drainage (SWD) system, which had remained largely unchanged since colonial times. The event resulted in unprecedented physical and emotional damage to the citizens of the MMR; 419 people and 6307 animals lost their lives, over 60% of Mumbai city was inundated to various degrees, the power, transportation and communication systems broke down, and buildings and cars were damaged. Estimations of the total flood-related losses range from 690 million US$ (Picciariello, 2021) to 1.7 billion US$ (Hallegatte et al., 2010). Smaller and bigger flooding events happen as often as 5 to 6 times per year in the low-lying areas of the MMR. This has resulted in the normalisation of nuisance, as becomes clear from a statement given by an employee of the municipality to Butsch et al. (2016): "in Bombay 10 or 20 cm is nothing, it is only when you have 60 cm, 80 cm, [...] otherwise we can't call it a flood".

The root cause of MMR's susceptibility to floods is its geography, which can be divided into two sub-causes: (i) MMR's natural geography and (ii) MMR's artificial geography. Both of these are discussed in the following sections.

2.3.2 Natural geography

Firstly, MMR's geographical location, on the coast in south Asia, leaves it exposed to a tropical wet-dry climate (as already discussed in Section 2.1.1). This climate is associated with relatively large amounts of annual rainfall, ranging between [1800, 2500] mm. This annual rainfall is strongly concentrated over the Kharif season of June until September when the southwest monsoon occurs (Vinayak et al., 2021). During these months, 96% of the annual rainfall occurs (Rana et al., 2012). Moreover, rainfall is heavily concentrated within these months since 50% of the rainfall that occurs during July and August, the wettest months, typically falls within 2 or 3 events (Hallegatte et al., 2010). Most extreme precipitation events that occur only last a single day, while only 17% of very heavy and 21% of extremely heavy precipitation events[13] last more than a day (MCGM Municipal

[13] An event is categorised as heavy rain in case of [64.5, 124.4] mm in a day, as very heavy rain in case of [124.5, 244.4] mm in a day and as extremely heavy in case of [244.5, ∞] mm in a day(MCGM Municipal Corporation of Greater Mumbai, 2022).

Corporation of Greater Mumbai, 2022). These extreme precipitation events often result in floods while simultaneously supplying the city with sweet water that is subsequently stored in seven lakes to ensure water availability throughout the year (Mishra et al., 2016).

Various authors project that climate change will increase the probability of such extreme precipitation events, and therefore flooding, in the future. CSTEP (2022) projects that, under RCP4.5, an optimistic future scenario, and RCP8.5, a business-as-usual scenario/pessimistic scenario, the number of rainy days, the amount of heavy rainfall and the amount of very heavy rainfall events in the MMR will increase. Ranger et al. (2011) did a similar analysis and estimated, through the application of the PRECIS model, the intensity of rainfall with a return period[14] of 50, 100, 150 and 200 years for the year 2080, relative to the year 2005. They concluded that, in the case of an SRES A2 scenario[15], the intensity of a 2 to 5-year return period event more-or-less doubled. Furthermore, they concluded that the return period of events similar to July 26, 2005, is more in the order of 90 years for 2080. In contrast, the return period of the July 26, 2005 flood was estimated to be 1 in 200 years for 2005 (Ranger et al., 2011). Rana et al. (2014) also did a similar type of analysis and estimated that total annual rainfall will increase by [300, 500] mm over the [2010, 2099] period and that a seasonal shift will result in a delayed onset of the monsoon season, i.e. precipitation will decrease in June and increase in September.

However, the accuracy of such city-scale rainfall projections is doubtful because of two reasons: (i) lengthy rainfall records for a city are often lacking and (ii) climate models are often still inadequate in projecting changes in rainfall at a city scale (IPCC, 2007). Hallegatte et al. (2010) indicates this inaccuracy by showing the diverging projections of various climate models for precipitation in northwest India for the period [1990, 2090]. Although on average, an increase in precipitation is estimated for the region, only half of the 21 evaluated models estimate an increase in precipitation. A trend analysis done by Rana et al. (2012) on rainfall in Mumbai over the period [1951, 2004] also goes against the idea that rainfall has increased in the region. Based on linear regression, they estimated that there is a long-term negative trend of annual precipitation, monsoon precipitation, and maximum precipitation in a day.

At the same time, recent precipitation patterns for the whole of India suggest that we are witnessing an increase in maximum rainfall per day and an increase in the amount of very heavy rainfall events (Gupta, 2020; MCGM Municipal Corporation of Greater Mumbai, 2022). In accordance with this, IPCC (2022a, 2021) estimated, for South Asia in general, with high, medium, and medium confidence that annual mean precipitation, summer monsoon precipitation and extreme precipitation events will respectively increase, with increasing flood risk as a consequence (medium confidence).

Secondly, the MMR's coastal location, in combination with its low elevation levels, also results in increased flood vulnerability, which is expected to increase further due to climate change-induced sea-level rise. Patil and Deo (2020) established SLR scenarios associated with two IPCC scenarios and estimated SLR for the Arabian Sea at the MMR to increase by 0.21 m (0.24 m) in 2050 and 0.50 m (0.74 m) in 2100 for RCP4.5 (RCP8.5). IPCC (2022a) stated with *very high confidence* that risk related to sea-level rise, among which coastal flooding, is expected to increase for low-lying coastal areas. Abadie et al. (2020) estimated that Mumbai will become one of the most damaged cities of the world due to sea-level rise, with an approximated damage of 112.4 and 162.2 billion US$ annually by 2050 for the climate scenarios of RCP8.5 and a high-end scenario, respectively.

Lastly, the situation could be further worsened due to climate change-induced, more frequent

[14]The return period is a measure of the frequency of occurrence. it is commonly interpreted as "the inverse of the probability (p_r) that a certain flood level will be exceeded in any one year" (Foudi et al., 2015). Hence, $RP = 1/p_r$, where p_r is the annual exceedance probability.

[15]This scenario is at the upper band of the various IPCC climate scenario.

and intensified storm surges (Ranger et al., 2011; MCGM Municipal Corporation of Greater Mumbai, 2022). In accordance with this, IPCC (2014a) estimated that Mumbai will be one of the Asian cities most influenced by coastal flooding in terms of the exposed population. Shaji et al. (2014) estimated the impact of a storm of 40 m/s and concluded that this results potentially in 1.5 m surge amplitude and 4.5 m maximum water level[16]. Potential consequences of the combination of such water elevation and SLR would be detrimental to the city.

2.3.3 Artificial geography

The city of Mumbai was once, allegedly,[17], an archipelago consisting of seven islands. Land reclamation transformed this into one all-encompassing island over the past three centuries. However, most of these reclaimed grounds have been heightened only just above mean sea level and rarely above high-tide lines, resulting in increased flood vulnerability of these grounds, especially during high tide through their interaction with the SWD system (Hallegatte et al., 2010). The issue becomes clear by elaborating on the functioning of the SWD system.

Of the SWD system, only six of the 186 outfalls[18] lie above the high tide line, 135 lie above mean sea level but below the high tide line, and 45 are below mean sea level (Chatterjee, 2019). Since the SWD system works based on gravity, this results in problematic situations when intense precipitation and high tide coincide. In these circumstances, the drainage system cannot transport rainwater to the sea, while the reclaimed grounds become the lowest point where all the water moves towards (Gupta, 2007; Hallegatte et al., 2010; MCGM, 2016). This occurred during the floods of July 26, 2005, when rainfall peaked during the high tide, resulting in the water being unable to drain out to the sea (Gupta, 2007). This already dysfunctional situation is threatened to worsen due to projected sea-level rise, which would place an even larger portion of the SWD outfalls below the surface of the sea.

Furthermore, the MMR's SWD system suffers from some structural deficiencies, mainly because a large critical part (the part that drains stormwater from Mumbai city) has hardly been updated in the last 150 years (MCGM, 2016). In the city, the SWD system consists of a 440 km-long network of underground drains and laterals. In the suburbs, it consists of roadside surface drains ($\approx$ 2000 km), major Nallas[19] ($\approx$ 215 km), minor Nallas ($\approx$ 156 km) and, as earlier mentioned, 186 outfalls (MCGM, 2016; Chatterjee, 2019). This network can handle rainfall intensity of 25 mm/h at low tide and even less during high-tide (Chatterjee and Chattopadhyay, 2020; MCGM Municipal Corporation of Greater Mumbai, 2022). To put this in perspective: during the period [1999, 2004], for the two data stations of Santa Cruz and Colaba, the lowest maximum rainfall intensity measured within a year was 64 mm/h (Santa Cruz in 2002 and 2003), while for more than half of the years the stations measured maximum rainfall intensities in the range [80, 120] mm/h (Rana et al., 2014). Furthermore, the network is designed for a runoff coefficient[20] of 0.5 (Chatterjee and Chattopadhyay, 2020). In comparison, the runoff coefficient for large parts of Mumbai has undoubtedly surpassed the value of 0.5.[21] This can mainly be attributed to urban development that has resulted in a shift from natural ecosystems to high-density built-up, characterised by little infiltration, adsorption and storage (MCGM Municipal Corporation of Greater Mumbai, 2022).

[16] Maximum water level is an addition of *storm surge elevation* and *wind waves* (Shaji et al., 2014).

[17] According to Riding (2018) the islands were separated by land barely underwater. 'The British', however, framed the area as an archipelago consisting of seven islands, hereby exaggerating their land reclamation to showcase colonial power.

[18] An outfall is where the SWD system empties into the sea, a river, or a lake.

[19] These are gullies, which are also often called Nullahs.

[20] The runoff coefficient is a dimensionless number in the range [0, 1] that represents the ratio of runoff (water that runs off the surface) to rainfall.

[21] Runoff coefficients for urban environments are generally in the range of [0.6, 1] (USDA, 1986).

Also, a large portion[22] of the SWD system are roadside open drains, which are in general more susceptible to clogging and contamination (MCGM Municipal Corporation of Greater Mumbai, 2022).

Last but not least, the natural drainage capacity of the city has also significantly reduced due to development on flood plains. Consequently, the Mithi River in the North of the MMR lost nearly 54% of its original flow capacity (Gupta, 2007).

Gupta (2007) analysed MMR's SWD system and arrived at a list of problems associated with the drainage system of Mumbai city and the suburban areas. The various problems specified are structured in Table 2.7, some of which have already been discussed.

City area	**Suburban area**
low elevation of outfalls	Siltation of drains/Nallas
Dilapidated drains	Obstructions of utilities
Obstructions of utilities	Encroachment along Nallas
Siltation of drains/Nallas	Slums along outfalls
Urbanisation and loss of holding ponds	Garbage dumping in SWDs/Nallas, mainly in slums
Increase in runoff coefficient	No access for desilting

Table 2.7: *Main problems associated with the SWD system that contribute to flooding in the MMR, as according to Gupta (2007).*

2.3.4 Future and current adaptations to the stormwater drainage system

Since July 26, 2005, various measures were proposed, implemented and planned to increase MMR's flood resilience, which focused either on (i) the artificial SWD system, (ii) the natural SWD system, (iii) the runoff coefficient, (iv) the mapping of the region, or (v) the monitoring of flood levels. Time-wise, the first phase of the Brihanmumbai Stormwater Drainage (BRIMSTOWAD) Project, of which the project plan was already submitted in 1993, started in 2005. No year later, in 2006, the BRIMSTOWAD project was revised, and a second phase (BRIMSTOWAD-II) was added. BRIMSTOWAD-I got designed for rainfall intensities up to 50 mm/h and a runoff coefficient of 1, BRIMSTOWAD-II got designed to increase the maximally manageable rainfall intensity to 100 mm/h (Gupta, 2007). Construction was planned to take five years; however, both have yet to be finished. Furthermore, costs have turned out at least three times higher than expected (Chatterjee, 2019), and, to make things worse, rainfall intensities of 100 mm/h are already surpassed (Rana et al., 2014). However, progress has been made MCGM (2016). In addition to BRIMSTOWAD, MCGM (2016) suggested several flood risk management actions. While MMR's most recent climate action plan MCGM Municipal Corporation of Greater Mumbai (2022) also mentions several flood risk management actions.

The following adaptations have been implemented or are currently being implemented:

- Restore the natural SWD system of the city by removing silt from rivers, widening the rivers by removing structures on flood planes and creating buffer zones along rivers and creeks (MCGM, 2016).

[22] An exact percentage seems contested since (MCGM Municipal Corporation of Greater Mumbai, 2022) stated that 64% of the total length of the SWD system consists of roadside surface drains, while the statistics on the length of the various drainage components, as reported by (MCGM, 2016), indicate that 71% of the total length of the SWD system is roadside surface drainage.

- Upgrade the artificial SWD system by cleaning, widening, deepening, extending, desilting and repairing the drains, Nallas, flood gates and outfalls, and providing stormwater pumping stations (MCGM, 2016).
- Reduce the runoff coefficient by maintaining permeability in all public open spaces (MCGM, 2016).
- Increase the detail of the region mapping by preparing contour maps with smaller intervals (MCGM, 2016).

For the coming years [2022, 2030], the following goals have been described:

- Restore the natural SWD system of the city by rehabilitating encroachment and cleaning up of disposed waste (MCGM Municipal Corporation of Greater Mumbai, 2022).
- "Reduce the surface runoff coefficient and increase the permeable surface by conserving the existing green and blue spaces, retrofitting[23] land surfaces with recycled material and introducing hybrid (grey and green) and nature-based solutions, especially at mid-stream to avoid surface runoff into low-lying areas" (MCGM Municipal Corporation of Greater Mumbai, 2022).

Several medium- and long-term goals have also been mentioned for [2031, 2040]:

- Make the installation of Rooftop Rainwater Harvesting (RWH) mandatory in the existing and new government and private buildings (MCGM Municipal Corporation of Greater Mumbai, 2022).
- Monitor the flood levels of rivers, tributaries and estuaries with greater detail (MCGM Municipal Corporation of Greater Mumbai, 2022).

[23] "Reinforcement or upgrading of existing structures to become more resistant and resilient to the damaging effects of hazards" (United Nations Office for Disaster Risk Reduction (UNDRR), 2020).

Chapter 3

Conceptualisation

In this thesis, we execute a land-use modelling case study that (i) couples a land-use model with flood hazard maps and (ii) assesses the resilience of land-use scenarios associated with various implementations of urban planning. The execution of such a case study requires the construction of various components. The general concepts and applied procedures applied to construct these various components are discussed in this chapter. Firstly, Section 3.1 discusses how the land-use model was conceptualised. Secondly, Section 3.2 discusses the relation between urban planning and resilience and how resilience was assessed. Lastly, Section 3.3 discusses how the flood hazard maps and the flood risk-land-use interaction were conceptualised.

3.1 Land-Use Modelling

This section discusses how a land-use model for the MMR was constructed based on the knowledge derived from the literature review. First, in Section 3.1.1, the applied land-use modelling framework is discussed. Subsequently, Section 3.1.2 mentions the applied methods to calibrate the land-use model. Furthermore, Section 4.1.5 addresses the manner of performance assessment of calibration. After that, in Section 3.1.4, the establishment of a model for the future is considered. In addition, Section 3.1.5 discusses the validation procedure through expert interviews. Lastly, Section 3.1.6 examines the applied Monte Carlo procedure that was applied to incorporate a stochastic factor in the derived land-use maps.

3.1.1 Metronamica land-use modelling framework

In this thesis, the constrained-relaxed cellular automata (CA) based land-use modelling framework *Metronamica*, from the Research Institute for Knowledge Systems (RIKS), is applied (van Delden and Hagen-Zanker, 2009; RIKS, 2012). In CA-based land-use change models, land-use change is primarily simulated with recursive equations; land-use at time t is primarily determined by the state of cells and their neighbourhoods at time $t-1$ (Koomen and Stillwell, 2007; Lantman et al., 2011). A CA model is typically made up of five components: cell space, cell states, neighbourhood, time steps, and cell transition rules (Kim, 2012; Nemiche et al., 2019). These transition rules can be based on statistical analyses or expert-knowledge (Lantman et al., 2011). Furthermore, *constrained* indicates that the amount of cells that change in a CA model is constrained by an external variable; often, in the case of land-use modelling, this is the demand for the various incorporated land-use classes (Wickramasuriya et al., 2009). Lastly, *relaxed* refers to the fact that the cells are not uniform but have varying specifications, resulting in a heterogeneous space.

Land-use simulation

Changes in land use are driven by four factors in Metronamica, *Suitability*, *Spatial Planning*, *Accessibility*, and *neighbourhood rules*.

Suitability is represented by one map per land-use class and indicates the appropriateness of a cell, in physical terms, to host a particular land-use class. The suitability maps are based on (i) layers that describe the physical environment, such as elevation, slope and soil, and (ii) rules describing the appropriateness of physical environmental factors to land-use classes.

Spatial Planning is represented by one map per land-use class and indicates the appropriateness of a cell, in urban planning terms, to host a particular land-use class. The spatial planning maps are based on (i) several layers that describe urban planning policy, such as nature reserves and world heritage, and (ii) the reaction of land-use classes to these plans.

Accessibility is represented by one map per land-use class and indicates the appropriateness of a cell, in infrastructure network terms, to host a particular land-use class. The accessibility maps are based on (i) several layers of infrastructure networks, such as road networks and train stations, and (ii) the rules describing the desire of land-use classes to be located close to a particular network.

Neighbourhood rules are represented by inertia points, conversion points, self-influence tails and cross-influence tails that respectively indicate (i) the intransigence of a land-use class to stay at a particular location, (ii) the desire to transition from one land-use class to another and (iii) the desire of land-use classes to be located in the proximity of oneself or (iv) other land-use classes. These are an indicator of human clustering behaviour.

The simulation of land-use change in Metronamica, based on these four factors, is most easily described using Figure 3.1. Herein is visualised that the model is in a time loop, for which the suitability maps, urban planning maps, accessibility maps and interaction rules (neighbourhood rules) are determined every time step. These, together with the stochastic factor α, result in transition-potential maps that indicate the potential for a land-use class at a specific cell. Land-use classes are subsequently allocated to the cells with the highest transition potential until their demand is met. For more information concerning the functioning of Metronamica, we refer to RIKS (2012).

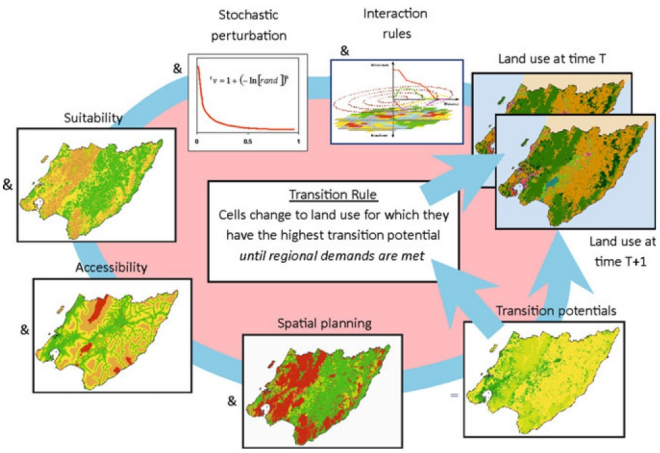

Figure 3.1: *A figure that visualises the time loop through which land-use change is simulated in the Metronamica model (Delden and Vanhout, 2018).*

3.1.2 Calibration: applied methods

After the model was set up (details concerning this are discussed in Section 4.1.1), calibration for the period [1996, 2016] was executed. Calibration was executed by combining semi-automated, statistical, and manual calibration methods while constantly comparing simulated land-use change with the historical 2016 land-use map. The historical land-use maps for 1996 and 2016 can be found in Appendix B.2. A conceptual overview of the applied methods per land-use change-influencing factor is given in this section. Where required, Sections 4.1.2, 4.1.3, and 4.1.4 give a more technical in-depth review.

Neighbourhood rules

Neighbourhood rules are at the core of CA-based land-use models. To arrive at calibrated neighbourhood rules, a semi-automatic calibration method, as developed by Newland (2018), was applied to arrive at initial values. After that, manual calibration was applied that visually compares simulated land-use change with historical land-use change in light of several calibration parameters.

The semi-automatic calibration method consists of the following steps. First, the various neighbourhood interactions are calculated from the available land-use maps. After that, a coarse calibration is initiated on a statically significant and reduced complexity subset of the interaction rules. This coarse calibration optimises coherence between the various neighbourhood interactions

according to the metrics: Kappa, Kappa-Simulation and Area-Weighted Clumpiness Error (AWCE). This coarse calibration results in a first coarse estimation of neighbourhood interactions, which act as a starting point for the fine calibration. The fine calibration further refines the coarse calibration by searching for local optima around the, by coarse calibration established, coarse estimation of the neighbourhood interactions. This is done in line with the same set of metrics as used in the coarse calibration. All the executed steps are in accordance with Newland (2018).

Suitability

First, a statistical analysis was executed on the historical 2016 map to determine calibrated suitability rules. This statistical analysis resulted in basic knowledge of the slope, soil and elevation type suitable for the various land-use classes. This knowledge was subsequently used as a starting point for calibrating the suitability factor. After that, similarly to the neighbourhood rules, manual calibration was applied to optimise calibration in light of the calibration performance indicators.

Accessibility

To arrive at calibrated accessibility rules, first, a statistical analysis was executed on the historical 2016 map. This statistical analysis resulted in basic knowledge of the impact of the various types of transport networks on the spatial distribution of the various land-use classes. This knowledge was subsequently used as a starting point for calibrating the accessibility factor. After that, similarly to the neighbourhood and suitability rules, manual calibration was applied to optimise calibration in light of the calibration performance indicators.

Spatial planning

The calibration of spatial planning policies was based on the policies discussed in Section 2.1.4. They eventually included plans are coastal regulation zones (Maharashtra CZMA, 2019), no development zones (Maharashtra CZMA, 2019), Cessed Buildings (UDRI, 2017), Heritage Precincts (UDRI, 2017), World Heritage (UDRI, 2017), MIDC IT areas (MIDC, 2020), Industrial location policy 1992 (MMR, 1995), Recreational zones (MMR, 1995), and Bhiwandhi industrial location policy 2008 (MMRDA, 2008). Special economic zones and central business districts were not included due to the unavailability of spatial data.

3.1.3 Calibration: performance assessment

The calibration of the various land-use model components was done as described in Section 3.1.2. The quality of the calibration is assessed statistically and visually. In this section, first, the statistical assessment of performance is discussed. After that, the visual assessment of performance is discussed.

Statistical assessment

The calibration performance was statistically assessed by comparing the simulated land-use map for 2016 with the historical land-use map for 2016. This statistical assessment was done based on calibration performance indicators. First, a selection of calibration performance indicators was applied that quantifies both locational agreement ($Kappa$, K_{Sim}, FK, and FK_{Sim}) and landscape pattern structure ($CLUMPY$). Then, the model's performance was assessed by putting the

performance indicators into perspective. This was done by comparing the performance of the calibrated model with two neutral models: the random constraint match (RCM) model and the null model, which the calibrated model should outperform.

The RCM model was constructed by applying the same demand for land-use classes as the calibrated model while erasing all the calibrated land-use rules. Hence, this results in random allocation while having the same quantitative distribution of land-use classes as the calibrated model (Hagen-Zanker and Lajoie, 2008).

The null model was constructed by applying the same demand for land-use classes as in the calibrated model while only applying an elementary set of neighbourhood rules (van Vliet et al., 2013b).

The results of the statistical assessment of the performance of the calibrated model are satisfactory and are discussed in depth in Section 4.1.5.

Visual assessment

Apart from a statistical assessment, a visual assessment of the performance of the calibrated model was executed. This was done by visually comparing the output of the calibrated model for 2016 with the historical 2016 land-use map through a game of 'spot the difference'. The main regions of incoherence for the land-use classes of interest are discussed in this section. The land-use classes of interest are the urban and industrial land-use classes since these are most relevant concerning the executed case study.

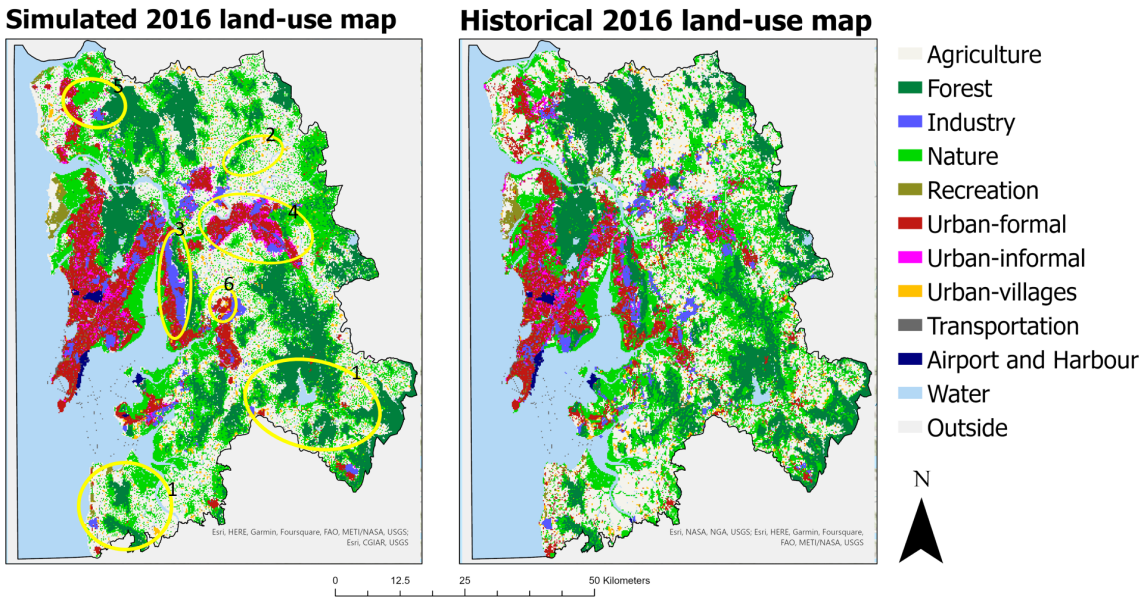

Figure 3.2: *A figure that compares the simulated land-use map of 2016 with the historical land-use map of 2016. The main problem areas are circled.*

Areas 1 In these areas, the growth of urban formal on the outskirts is not well simulated. This can be explained by the fact that (i) both an urban core and rural periphery are simulated in the same model using the same rules, and (ii) growth at the periphery exhibits different

characteristics than growth in the core. Consequently, not both types of growth can be modelled accurately in the same model and a choice is required. For this study, the urban core was considered more important; hence urban sprawl at the periphery was modelled with less accuracy.

Area 2 Modelling industrial growth at the periphery is, similarly to modelling urban formal at the periphery, problematic. The accuracy of modelling industrial growth in the urban core was considered more important; hence industrial growth at the periphery was modelled with less accuracy.

Area 3 Navi Mumbai's modelling was troublesome for two reasons. Firstly, in Navi Mumbai, industrial areas are converting to urban areas (Shaw, 2004). This was problematic to model since the industrial area of Navi Mumbai is located in a large MIDC area, located in an advantageous location with respect to the urban core, with suitable soil, height, slope, and infrastructure. Enabling the transition of areas such as these to Urban-Formal while preventing the conversion of other industrial areas in the urban core to Urban-Formal, is problematic. Also, the definition of what constitutes Industry is changing. Industry in the MMR is transforming from heavy, polluting industries to more high-tech and non-polluting industries (MMR, 1995; Shaw, 2004). This emergence of non-polluting industries often goes hand-in-hand with industrial areas transforming into office buildings. Dubious, in this case, is if these areas should still be considered Industry and what constitutes the pecise dichotomy between Urban-Formal and Industry.

Area 4 In general, urban clusters are more concatenated in the simulated land-use map than in the historical one.

Area 5 Urban-Informal is highly unpredictable in its growth. Therefore, few clear rules could be defined, and a significant area such as 5 is consequently missed.

Area 6 The historical map also contains some errors. For example, historical analysis of satellite data indicates that area 6 was built-up in 2016.

3.1.4 Future model

The model for the future has been established by (i) implementing future demand for the various land-use classes, (ii) adopting various urban planning and accessibility changes and subsequently extrapolating for the future. The proposed road network, planned harbour and airport development and planned industrial areas were all derived from MMR (2016). The inclusion of urban planning for the land-use classes 'industry' and 'airport and harbour' was deemed valid since these classes generally comply with urban planning.

The calculation of land-use demand for the future was based on future growth projections found in the literature. However, relevant detailed literature did not exceed the year 2036. Therefore, the trend for the period [2016, 2036] was extrapolated for the period [2036, 2050]. Table 3.1 gives an overview of the future land-use demands. A more detailed overview of the calculation of future demand is given in Section 4.1.6.

LUC	2016 land-use	Implemented growth	Applied references
Urban-formal	457.44 km^2	705.32 km^2 [2036] 851.18 km^2 [2050]	MMR (2016)
Urban-informal	83.04 km^2	106.50 km^2 [2036] 122.92 km^2 [2050]	Nijman (2008, 2012); MMR (2016)
Urban-villages	97.88 km^2	97.88 km^2 [2036] 97.88 km^2 [2050]	X
Industry	141.84 km^2	214.97 km^2 [2036] 266.16 km^2 [2050]	MMR (2016)
Forest	807.88 km^2	1038.16 km^2 [2036] 1199.36 km^2 [2050]	MMR (2016)
Nature	1099.12 km^2	794.50 km^2 [2036] 581.42 km^2 [2050]	MMR (2016)
Recreation	43.96 km^2	55.18 km^2 [2036] 63.03 km^2 [2050]	MMR (2016)

Table 3.1: *A table on the estimated future land-use demand for the various land-use classes that are driven by external demand in the Metronamica land-use model. Note that no data on Urban-Villages was found and hence no growth was assumed.*

3.1.5 Validation

No historical land-use map for a third timestep was available. Hence, the quality of the calibrated model could not be quantitatively assessed. An expert consultation was held with planning specialists working on the MMR to, to some extent, compensate for this significant shortcoming. During this consultation we presented a demo of the in-progress model and discussed its performance. This section mentions the key takeaways of these interviews concerning the performance of the model for the calibration period and the future.

Calibration period [1996, 2016]

- Designated protected forests have grown for the [1996, 2016] period. This concerns no real growth of the forests but growth of the area governed by the forest department. Hence, this growth only occurs on paper. This is done to seemingly balance urban growth for those concerned about the environment.
- Significant growth in the Northwest in Vasai occurs due to urban growth outside the MMR boundary. In this case-study, the MMR is modelled as if it is an island, while it is not. This also partly explains problem area 5 delineated in Figure 3.2.
- There is a nuclear power plant near the city of Mumbai, which is designated as Industry. In the model, this converts to urban formal, while in reality, such a transition is unlikely. The model does not account for this distinctive form of Industry.
- Informal settlements mainly pop up at locations that are problematic for other built-up land-use classes, such as steep slopes and along river banks.

Future [2016, 2050]

- Problem areas 1 seem less of a problem for the future. Urban growth on the outskirts takes place, however highly clustered.
- Significant urban growth appears in the model in the Northwest (Vasai), as expected in relation to the urban growth that occurs just outside the model boundary. Hence, although we model the MMR as an island, this expected urban growth is captured.
- Urban-Villages showed themselves capable of counteracting major infrastructural developments and, in all probability, will do so in the future. I.e. the high inertia of Urban-Villages is expected to persist in the future.
- Future development projects and legal decisions are difficult to predict and, therefore, fundamentally problematic to model.
- A lot of political agendas are at play in the considered region. The various political interests significantly influence urban growth and produce patterns that cannot be modelled with the available parameters of the land-use model.
- Connectivity corridors with other regions are about to get finished. As soon as this happens, growth will occur along them.

3.1.6 Monte Carlo simulation

A stochastic factor α is present in the land-use model, which depends on a seed. During calibration, the seed was kept constant to ensure replicability and to arrive at a single land-use map that could be implemented in the land-use model for the future. Now, for the future, we execute a Monte Carlo simulation of 50 runs per scenario that varies the random seed to consider the uncertainty of individual model runs. The Monte Carlo simulation results in probability maps for the various land-use classes. Herein the probability of a land-use class for a cell is equal to the fraction of runs a land-use class got allocated to that cell.

To acquire a single land-use map for visualisation purposes, the probability maps are combined according to a threshold of 20%. I.e. an urban land-use class is only located in case it has a probability of allocation larger than 20%. Figure 3.3 displays the resulting land-use map.

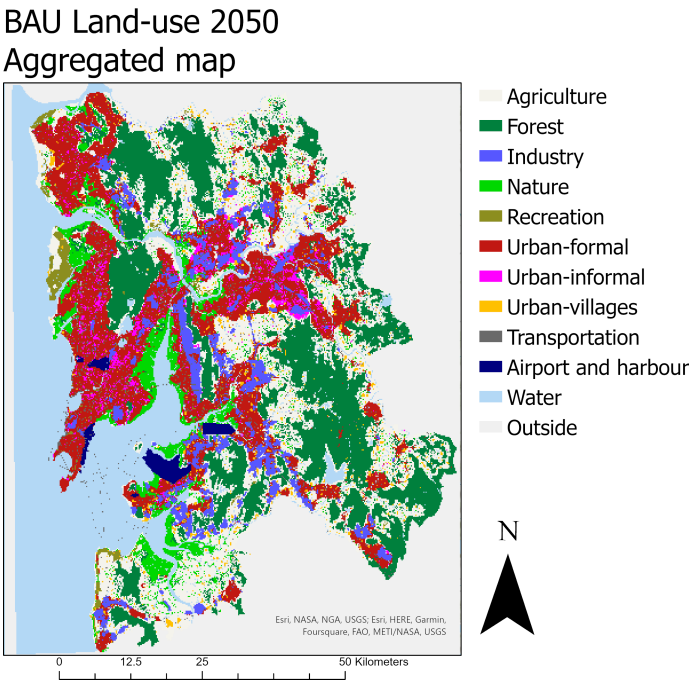

Figure 3.3: *A figure that visualises the projected land use for 2050 in case of business-as-usual (BAU) growth. A threshold of 20% is applied concerning the allocation of urban and industry land-use classes, as described in Section 4.1.7.*

Concerning the estimation of aggregated resilience indicators per cell, a procedure is executed that applies the weighted average of the various land-use classes that have a probability of being allocated at that location.

A more in-depth technical discussion concerning the applied Monte Carlo simulation can be found in Section .

3.2 Resilient Urban Planning

Section 2.2 discusses the literature on resilient urban planning. Based on the knowledge derived in that section, we discuss in this section (i) what constitutes resilient urban planning, (ii) how it is connected with the flood risk-land-use interaction and (iii) how resilience is quantitatively assessed in this thesis.

These various sections together answer the earlier defined SQ2 in conceptual terms:

How can resilient urban planning be conceptualised and assessed for the MMR?

3.2.1 Urban planning

According to the literature discussed in Section 2.2, flood adaptation (i) corresponds with the socio-ecological perspective on resilience, which is the suitable resilience paradigm to apply for urban environments facing climate change, and (ii) can contribute to the urban flood resilience of urban environments by reducing flood risk. Adapting the physical landscape through urban planning is one of the ways flood adaptation can be applied and is especially relevant to societies sensitive to climate change (Jafino et al., 2019; Smajgl et al., 2015). Urban planning can transform the urban environment in the face of urban floods, without attempting to change the flood regime but by guiding the structure of the city in a way that flood-vulnerable land-use classes are mainly located away from flood-prone areas. This can subsequently reduce overall flood risk and increase resilience. Note that in this linkage between urban planning and resilience, resilience is considered to be negatively correlated with flood risk. I.e. low flood risk is associated with high resilience and the other way round.

After arguing that urban planning can contribute to the resilience of an urban environment through the reduction of flood risk, one can argue that urban planning that results in a larger reduction of flood risk can be considered a more resilient form of urban planning. Consequently, it is key to determine how urban planning can, as effectively as possible, influence land-use to reduce flood risk.

In this thesis, the strictness of urban planning and the perception of future climate are varied to acquire knowledge on what kind of urban planning can be considered ‘resilient urban planning’. Both these alter the flood-risk-land-use interaction and are hence discussed in Section 3.3.4.

3.2.2 Resilience assessment

In Section 3.2.2, a literature review was conducted on flood resilience indicators that directly assess flood resilience through estimating flood risk. This approach assumes that a flood-resilient city experiences little flood impact and subsequently that low flood risk is associated with high resilience and the other way around (Hammond et al., 2015). This approach has been applied to various types of natural hazards (Bruneau et al., 2003; De Bruijn, 2004; Su et al., 2018; Hazbavi et al., 2018). In this thesis, we apply this direct approach to assessing flood resilience.

As already stated by De Bruijn (2004), “Indicators will always be partial and imperfect reflections of reality". Still, a variety of indicators needs to be selected. This is done based on the resilience indicators discussed in Section 3.2.2. The *recovery rate* and *recovery time* applied by respectively De Bruijn (2004); Hazbavi et al. (2018), seem unreasonable to apply in this thesis since time scales in this thesis are in the order of years, not in the order of hours and days. Assessing resilience through *graduality*, as done by (De Bruijn, 2004; Su et al., 2018), is only relevant when the flood impact that communities experience with increasing flood depth, flood duration or flow velocity is non-constant. E.g. a square meter of land will experience more flood damage in the

future when experiencing the same inundation depth. For the MMR, no knowledge is available on how the relation between flood parameters and damage will change. Therefore graduality is a constant, resulting in it being unusable for the assessment of resilience. This leaves us with the *severity* of the flood impact[1], and the variability of the flood impact. To limit the scope of this thesis, only severity is considered. Concerning severity, similarly to De Bruijn (2004); Su et al. (2018), we limit ourselves to the direct tangible impacts and direct intangible impacts.

Direct tangible impacts

The direct tangible impacts are the damages caused by the "ïmmediate physical contact of flood water with humans, property and the environment" that can be quantified in monetary terms (Hammond et al., 2015). The exact distinction between direct and indirect tangible loss is contested in literature. This thesis applies the distinction as defined by Messner (2007); Van der Veen et al. (2003). Hence, property damage is considered a direct tangible impact, while business interruption costs and economic multiplier effects are considered indirect tangible impacts. Since we focus solely on direct tangible impact, only damage to infrastructure, agriculture, properties and their interiors are considered.

Estimating direct tangible impact can be done using the *expected annual monetary damage* (EAMD) indicator. The EAMD is the average monetary flood damage experienced in a year, which can be calculated for the whole map, per land-use class, or for a given cell. How this is specifically done can be found in Section 4.2.2.

Troublesome concerning the EAMD is its de-levelling nature. If one based policy solely on the EAMD, one would prioritise land-use classes with more monetary value over land-use classes with less monetary value. The relative impact of a monetary loss is not taken into account here. Therefore, a relative monetary impact metric needs to be added that indicates the relative impact of monetary loss on the population, enabling a more 'fair' comparison between the various land-use classes (Huizinga et al., 2017). *Percentage annual income lost* (PAIL) is therefore also included as a resilience indicator. The PAIL is the average percentage of annual income lost per household in a year. In light of the earlier described purpose of PAIL of comparing the relative impact of monetary loss for the various land-use classes, PAIL is only evaluated per land-use class. How this is specifically done can be found in Section 4.2.4.

Direct intangible impacts

The direct intangible impacts are the damages caused by the "ïmmediate physical contact of flood water with humans, property and the environment" that can not be readily expressed in monetary terms (Hammond et al., 2015). It includes direct health impacts and the direct impact on the natural environment. Quantifying health impacts is deemed troublesome and rarely goes beyond estimating the number of people affected (Hammond et al., 2015). Due to the high-aggregation level associated with our time scale and modelling methodology, we deem it unsuitable to apply more detailed metrics than the number of people affected. Also, the direct tangible damage to the natural environment was not considered due to the difficulty associated with such estimations.

Estimating the number of people affected can be done using the *expected annual population affected* (EAPA) indicator. EAPA can be calculated for the whole map, per land-use class, or for a given cell. How this is specifically done can be found in Section 4.2.3.

[1]By De Bruijn (2004), this is defined as the amplitude of the reaction.

3.3 Flood-Risk-Land-Use Interaction

This section discusses how the applied flood-hazard maps were derived and how they were subsequently linked to the land-use model to result in a flood-risk-land-use interaction. First, Section 3.3.1 discusses the applied flood hazard maps and how they were derived. After that, Section 3.3.2 discusses the combination of the various flood hazard maps through the multi-model mean. Subsequently, Section 3.3.3 discusses how flood-risk assessment was conducted. Furthermore, the various urban planning configurations are discussed in Section 3.3.4. Lastly, Section 3.3.5 gives an overview of the constructed scenarios. Jointly, these various sections answer SQ3:

How can the flood-risk-land-use interaction be conceptualised for the MMR?

3.3.1 Riverine flood hazard maps

To limit the scope of analysis, solely riverine floods are considered in this thesis. Riverine flood hazard can be represented by inundation maps indicating inundation extent and depth. Inundation maps for several return periods (RPs)[2], based on two climate scenarios and five climate models, were extracted from the Aqueduct Floods tool (Ward et al., 2020). How Ward et al. (2020) derived these flood-hazard maps is visualised in Figure 3.4 and discussed in this section.

Figure 3.4: *Workflow applied by Ward et al. (2020) in deriving riverine flood hazard maps.*

Future flood hazard maps

Concerning flood hazard maps for the future, two climate scenarios were considered: Representative Concentration Pathways (RCPs) 4.5 and 8.5. Herein, RCP4.5 indicates an “intermediate" scenario wherein the radiative forcing[3] stabilises at 4.5 W/m^2 without ever exceeding that value (IPCC, 2014b). RCP4.5 assumes that climate policies are implemented to achieve the stabilisation of radiative forcing (Thomson et al., 2011) and is considered by Ward et al. (2020) to be an optimistic future scenario. RCP8.5 indicates a worst-case climate scenario in which radiative forcing equals 8.5 W/m^2 in 2100 (Schwalm et al., 2020). In RCP8.5, no climate policy is implemented to reduce the amount of radiative forcing (IPCC, 2014b). RCP8.5 is considered by Ward et al. (2020) to be the business-as-usual scenario/pessimistic scenario. These scenarios will be referred to as RCP4.5 and RCP8.5 in the remainder of this thesis.

Radiative forcing data was extracted from the Inter-sectoral Impact Model Intercomparison Project (ISI-MIP) for the period [2030, 2069] and was subsequently implemented in a cluster of five global climate models (GCMs) to arrive at rainfall data for [2030, 2069] (Hempel et al., 2013). The cluster of applied GCMs consists of MIROC-ESM-CHEM, NorESM1-M, IPSL-CM5A-LR, HadGEM2_ES, and GFDL-ESM2M.

[2]The return period is a measure of the frequency of occurrence. it is commonly interpreted as “the inverse of the probability (p_r) that a certain flood level will be exceeded in any one year" (Foudi et al., 2015). Hence, $RP = 1/p_r$, where p_r is the annual exceedance probability.

[3]Radiative forcing is a measure describing the energy gained by the surface-troposphere system due to excess of energy inflow over outflow (Shine et al., 1990).

The outputted rainfall data by the GCMs for the period [2030, 2069] is then inserted in a hydrological model called PCRaster Global Water Balance, version 2 (PCR-GLOBWB-2) to convert rainfall data into discharge and subsequently inundation data for the period [2030, 2069] (Ward et al., 2020).

Lastly, the outputted inundation data by the hydrological model is fitted using a Gumbel Extreme Value (GEV) distribution on the annual extremes. Consequently, a set of flood hazard maps is derived for 2050 for RPs of 2, 5, 10, 25, 50, 100, 250, 500, and 1000 years. The resolution of these maps of 5′ × 5′ flood is then converted through a volume spreading flood model to a resolution of 30" × 30" (Ward et al., 2020).

Consequently, this procedure resulted in a cluster of five flood hazard map sets (each derived by one of the GCMs) per climate scenario.

Present flood hazard maps

Flood hazard maps for the present were derived similarly to the flood hazard maps for the future. However, they differ concerning radiative forcing data and rainfall data. Rainfall data was extracted from European Union Water and Global Change (EUWATCH) for the period [1960, 1999] to arrive at flood hazard maps for 2010 (Weedon et al., 2011). Hence, the first step of Figure 3.4 was skipped. Also note that rainfall data for the period [1960, 1999] was assumed to be valid for 2010 (Ward et al., 2020) and that the 2-year RP flood hazard map is not available for the flood hazard maps of the present.

3.3.2 Multi-model-mean of flood hazard maps

Flood hazard maps for five GCMs were extracted from the Aqueduct flood tool (Ward et al., 2020). These together form a multi-model ensemble. The multi-model ensemble is generally defined as a set of model simulations from structurally different models that are simulated for an ensemble of initial conditions (Doblas-Reyes et al., 2005). Through the inclusion of multiple models, both structural uncertainties and parametric uncertainties can be taken into account. Consequently, more reliable and consistent model forecasts are generally derived (Doblas-Reyes et al., 2005; Tebaldi and Knutti, 2007).

State-of-the-art methods for combining models include Bayesian methods and weighted averages (Tebaldi and Knutti, 2007). However, this study applies the quick-and-dirty *equally-weighted-multi-model-mean* approach for simplicity. This approach, which was also applied in earlier reports of the IPCC (Tebaldi and Knutti, 2007), usually agrees better with observations than any single model (Lambert and Boer, 2001).

Hence, the equally-weighted-multi-model-mean approach is applied to the flood hazard maps extracted from the Aqueduct Floods Tool (Ward et al., 2020). This is done by calculating the mean flood depth of the various GCMs for all locations of the area of interest. This results in nine (2, 5, 10, 25, 50, 100, 250, 500, and 1000-year RP) flood hazard maps for each of the two climate scenarios.

These multi-model mean flood hazard maps are used throughout this thesis when flood risk is estimated.

3.3.3 Flood-risk-land-use interaction: flood risk assessment

In this thesis, a knowledge gap is filled by modelling the interaction between flood risk and land use for a city in the Global South. The interaction between flood risk and land use consists of various aspects, two of which are considered in this thesis. The first of both is discussed in this section.

The first included aspect, corresponding to *arrow:1* in Figure 1.1, considers that a particular land-use configuration leads to a certain flood risk. This relationship is subsequently modelled as follows.

Firstly, a flood hazard map for a specific RP is laid on top of a land-use map. After that, if (i) a cell is estimated to experience inundation and (ii) a flood-vulnerable land-use class is present at that cell that contains a damageable part, flood risk is estimated for the RP associated with the evaluated flood. This procedure can be summarised using the relationship given by Kron (2005):

$$Flood\ Risk = Hazard \cdot Values \cdot Vulnerability \tag{3.1}$$

where, *Hazard* refers to the threatening natural event including its probability of occurrence, *Values* refers to the total value at risk[4], and *Vulnerability* refers to the fraction of value damaged in case certain flood characteristics occur [5].

However, since we do not consider only one RP flood but a whole set of them, these flood risk estimates need to be combined based on their probability of occurrence to result in expected annual flood risk. This is done by taking the integral over the probability of occurrence associated with the various flood hazard maps. This leads to the following equation Kron (2005); Foudi et al. (2015):

$$Expected\ Annual\ Flood\ Risk = \int_0^1 Flood\ impact(p_r)\ dp_r \tag{3.2}$$

where $Expected\ Annual\ Damage$ is a measure of flood risk and indicates the flood damage that can be annually expected, $Flood\ impact(p_r)$ is the flood impact associated with a particular RP flood, and p_r is the probability associated with a particular RP flood, or more specifically, it is the probability that a certain flood level associated with a particular RP flood will be exceeded in a year Foudi et al. (2015).

This calculation results in an estimation of the expected annual flood damage for a specific cell. The various cells can be combined through addition to arrive at (i) the total expected annual flood damage for the region or (ii) land-use-class-specific knowledge concerning expected annual flood damage.

3.3.4 Flood-risk-land-use interaction, consequences for urban planning

In this thesis, a knowledge gap is filled by modelling the interaction between flood risk and land use for a city in the global South. The interaction between flood risk and land use consists of various aspects, two of which are considered in this thesis. The second aspect is discussed in this section.

The second included aspect, corresponding to *arrow:2* in Figure 1.1, considers that flood risk leads to land-use change if policies that alter the land-use configuration are based on flood hazard maps. In this modelling case study, various forms of urban planning based on flood hazard maps are compared to assess what type of urban planning results in the land-use configuration that experiences the least amount of flood risk and hence is most flood resilient. The varied factors concerning the construction of urban planning policy are (i) the perception of future climate and (ii) the strictness of urban planning. Both these varied factors are discussed in the following sections.

[4]This is often referred to as the maximum damage.

[5]This is often referred to as the normalised stage-damage function

Perception of future climate

Depending on the future flood risk one perceives, a different area is considered in urban planning. However, future flood risk is uncertain due to the uncertainty associated with climate change, and the consequently uncertain future precipitation patterns, as discussed in Section 2.3.2. Therefore, in this thesis, the resilience contribution of urban planning for two Representative Concentration Pathways (RCPs) is compared to acquire knowledge on the flood resilience achieved by urban planning based on various considered climate futures. I.e. the acquired resilience by urban planning based on RCP4.5 flood hazard maps, a moderate climate scenario, is compared with the acquired resilience by urban planning based on RCP8.5, a worst-case climate scenario. These scenarios were selected since these scenarios span a large portion of the possible future climate scenarios, giving us an indication of the maximum impact the perception of future climate potentially has.

Flood-risk zones (FRZs) must be defined to implement urban planning based on flood-hazard maps. Three flood zones are created: a low flood-risk zone (low FRZ), a medium flood-risk zone (medium FRZ) and a high flood-risk zone (high FRZ). The area delineated as low FRZ experiences a flood event of > 0.5 m inundation at least every 1000 years, the area delineated as medium FRZ experiences a flood event of > 0.5 m inundation at least every 100 years, and the area delineated as low FRZ experiences a flood event of > 0.5 m inundation at least every 10 years. The resulting FRZs are visualised in Figure 3.5.

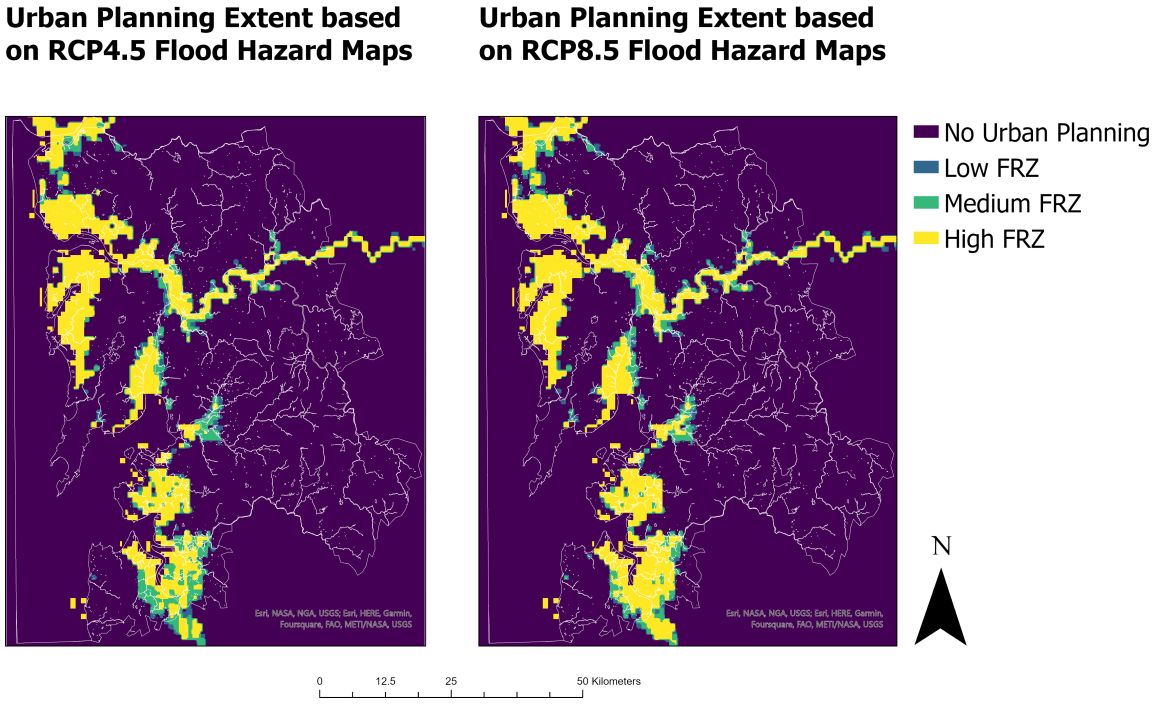

Figure 3.5: *Maps of urban planning based on the RCP4.5 and RCP8.5 scenarios.*

The 0.5 m inundation depth is based on the vulnerability of the land-use classes. The vulnerability of the land-use classes can be derived from the, in Section 4.2 discussed normalised-stage-damage functions that relate flood characteristics with the fraction of damaged value. The applied flood-depth-damage functions indicate that significant damage already occurs at inundation

depths as low as 0.5 m; hence urban planning based on this threshold was deemed considerate.

Furthermore, The three RPs on which the FRZs are based were decided upon somewhat arbitrarily and were arrived at by splitting the set of RP floods into three.

Strictness of urban planning regulations

Problematic concerning defining urban planning in light of future flood risk is the 'strictness' with which these urban planning policies need to be implemented and regulated to achieve desired resilience. The term 'strictness' herein encloses both (i) the strictness of the policies on paper, and (ii) the strictness with which the policies are enforced.

Three degrees of strictness (weak, mediocre, and strict) were applied, and their acquired resilience was compared to acquire knowledge on the flood resilience achieved by urban planning of various strictness. The three degrees of strictness were implemented in relation to the low, medium, and high FRZs. This was done as visualised in Table 3.2. The zoning state value (ZSV) is a parameter that reflects the urban planning strictness in the Metronamica land-use model. To put these values into perspective: in general, actively stimulated locations have $ZSV = 1.5$, allowed locations have $ZSV = 1$, weakly restricted locations have $ZSV = 0.5$ and strictly restricted locations have $ZSV = 0$. Note that urban planning was only applied to the land-use classes for which resilience indicators could be estimated and that could react to zoning in our land-use model. Also note that, in this approach, all land-use classes are treated equally if located in the same FRZ.

	Low FRZ	Medium FRZ	High FRZ
Weak urban planning	0.9	0.7	0.5
Mediocre urban planning	0.7	0.5	0.3
Strict urban planning	0.5	0.3	0.1

Table 3.2: *A table with the zoning state values for weak, mediocre and strict urban planning.*

3.3.5 Scenarios

The variation of expected future climate and strictness leads to various urban planning scenarios and, subsequently, various land-use scenarios for 2050 that are thereafter overlaid with the flood hazard maps for RCP4.5 and RCP8.5 for 2050 to determine their flood resilience. Urban planning is only initialised from 2023 to increase relevance for the present. This procedure is visualised in Figure 3.6.

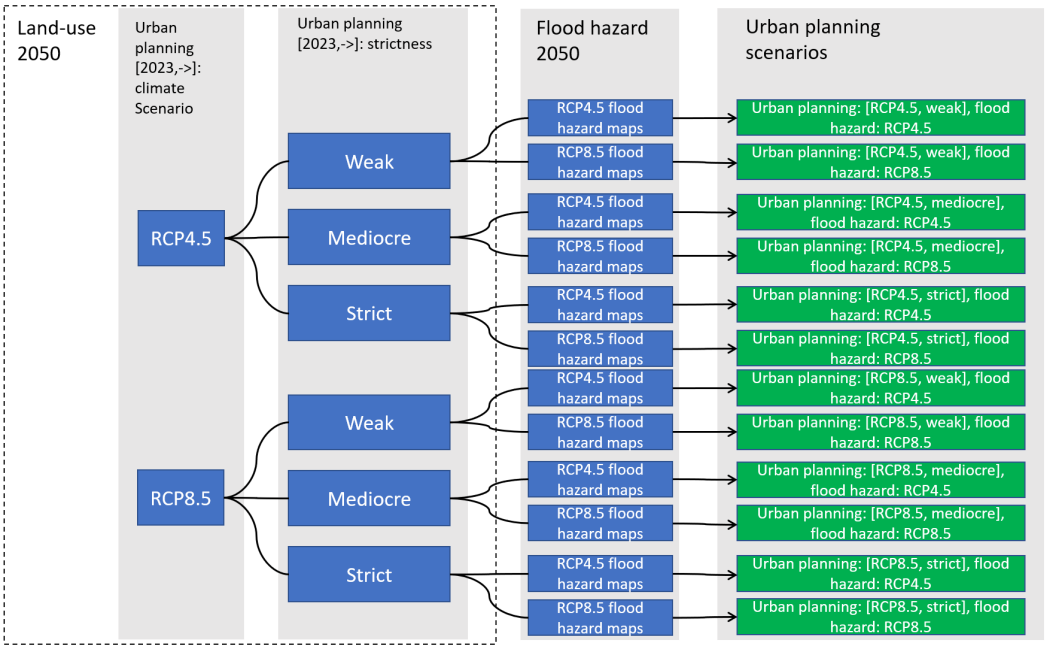

Figure 3.6: *A flow chart concerning the creation of urban planning scenarios. In total 12 scenarios are constructed that explore all possible combinations of the 'considered climate future' (RCP4.5 and RCP8.5), the 'strictness of urban planning' (weak, mediocre, and strict), and the flood hazard scenario (RCP4.5, RCP8.5).*

These scenarios are thereafter compared with: the past (2010) and the future (2050) in case of no urban planning. These no-urban-planning scenarios are described as business-as-usual (BAU) scenarios. Figure 3.7 shows how these were derived.

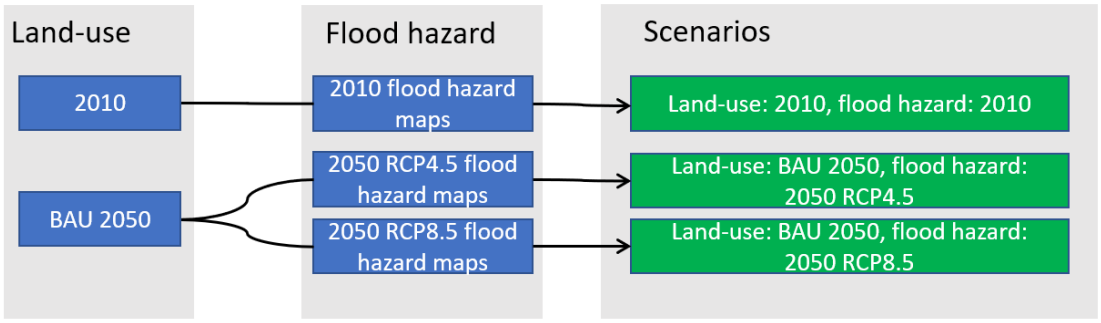

Figure 3.7: *A flow chart concerning the creation of no-urban planning scenarios. In total three scenarios are considered. One of which concerns the situation of 2010, two of which concern the situation of 2050 in case of two possible climate futures (RCP4.5 and RCP8.5).*

Chapter 4

Operationalisation

In Chapter 3, the conceptualisation of the case study was discussed. In this Chapter, in-depth, more technical discussions take place on the required topics. Firstly, Section 4.1 zooms in on the land-use model where necessary. After that, Section 4.2 discusses the flood risk assessment that supplies us with resilience indicators.

4.1 Land-Use Modelling

In Section 3.1, the conceptualisation of the land-use model is discussed. This section elaborates on the parts of the land-use modelling exercise that require a more in-depth technical discussion.

First, in Section 4.1.1, the basic model set-up is discussed. After that, in Sections 4.1.2, 4.1.3, and 4.1.4, an in-depth discussion on the statistical and semi-automated calibration methods takes place. Furthermore, in Section 4.1.5, the statistical assessment of calibration performance is considered. Thereafter, in Section 4.1.6, the calculation of the implemented future demand is discussed. Lastly, in Section 4.1.7, the executed Monte Carlo simulation is addressed.

4.1.1 Model set-up

Concerning cell space, the 506x398 square cells of 200x200 m form a rectangular euclidean space of 101.2x61.6 km. The cell size was decided upon by comparing various cell sizes. The 200x200 m cell size gave sufficient detail while limiting the model's computational weight. The urban core and periphery are intimately connected due to the urban growth that occurs towards the periphery; hence these cannot be separated, and the whole MMR, as defined in (MMR, 2016), is considered as the model boundary. The considered rectangular grid encloses the model boundary. Concerning cell states, the evaluated land-use classes are: *Agriculture*, *Forest*, *Industry*, *Nature*, *Recreation*, *Urban-formal*, *Urban-informal*, *Urban-villages*, *Transportation*, *Airport and Harbour*, *Water* and *Outside*, referring to the area inside the rectangular grid but outside the MMR. For these land-use classes, the following distinction was made. Agriculture was assigned to be a *vacant* land-use class, indicating that Agriculture was modelled as having no external demand. Consequently, it only changes due to changes in the active classes. Transportation, Airport and Harbour, Water and Outside, were considered *feature*; i.e. these do not change over time. The other land-use classes were considered *function* classes, i.e. these do change over time due to external demand.

Concerning the timestep, a timestep of one year is standard practice in Metronamica. Concerning the neighbourhood, a maximum neighbourhood of 8 cells is considered for the neighbourhood interactions.

The required vector and shape files were acquired by Malki (2022). An overview can be found in Table 4.1.

Data	**Source**
Regional boundary map	MMR (2016)
Land-use map 1996	UDRI (2017)
Recreational area 1996	OpenStreetMap (2017); MMR (1995)
Slum boundaries 1996 and 2016	UDRI (2017)
Coastal road	UDRI (2017)
Roads, rail and ferry line	OpenStreetMap (2017)
Land-use map 2016	UDRI (2017); OpenStreetMap (2017)
Industry and recreation 2016	OpenStreetMap (2017)
Digital elevation map	UDRI (2017)
Soil map	MMR (1995)

Table 4.1: *A table on the data applied to setup the land-use model and their origins.*

4.1.2 Calibration: neighbourhood rules

Neighbourhood rules are at the core of CA-based land-use models. To arrive at calibrated neighbourhood rules, a semi-automatic calibration method, as developed by Newland (2018), was applied to arrive at initial values. After that, manual calibration was applied that visually compares simulated land-use change with observed land-use change in light of several calibration parameters. The semi-automatic calibration procedure is discussed in this section. All credits are hereby attributed to (Newland, 2018). These can be found in Appendix B.2.

Step 1: Calculation of the neighbourhood interactions

In this first step, the neighbourhood interaction rules are calculated. The neighbourhood interactions can be subdivided into inertia points, conversion points, self-influence tails and cross-influence tails. These were derived from a contingency table and enrichment curves extracted from the available historical land-use maps. A discussion on the calculation of the various neighbourhood interactions can be found in Appendix C.1.

Step 2. Interaction elimination

In this second step, the statistical significance of the various neighbourhood interactions is evaluated to exclude the meaningless ones subsequently. This is done to reduce the problem's complexity and arrive at a statically significant subset of the neighbourhood interactions. Statistical significance is evaluated using the Mann-Whitney U-test. We refer to Newland (2018) for a detailed overview of this. Typically, the inertia points and self-influence tails are not reduced in their dimensionality since it is presumed that land-use classes always exhibit some form of interaction with themselves. Hence, only the dimensionality of the conversion points and tails is reduced.

Step 3. Parameter categorisation

In this third step, the complexity of the problem is further reduced by categorising the, in step 2 derived, meaningful neighbourhood interactions in low, mid and high categories. The ranges that determine the categorisation were based on an empirical analysis of the neighbourhood interaction values and were aimed at dividing the data into relatively equal proportions. If a particular neighbourhood interaction (i) falls within the high domain, it gets assigned the number 3, (ii) falls within the mid domain, it gets assigned the number 2, and if it (iii) falls within the low domain, it gets assigned the number 1. The following ranges were chosen:

Interaction Type	Low	Mid	High
Inertia point	$[0, 0.7]$	$[0.7, 0.9]$	$[0.9, \rightarrow]$
Conversion point	$[0, 0.25]$	$[0.25, 0.5]$	$[0.5, \rightarrow]$
Self-influence tail	$[0, 0.2]$	$[0.2, 0.4]$	$[0.4, \rightarrow]$
Cross-influence tail	$[0, 0.2]$	$[0.2, 0.4]$	$[0.4, \rightarrow]$

Table 4.2: *A table on the categorisation intervals applied in step 3 of the by Newland (2018) derived, semi-automatic calibration method.*

Step 4. Parameter initialisation

Now that the complexity of the problem is reduced significantly through elimination and categorisation, coherence needs to be established between the various types of neighbourhood interactions.

To achieve this, meta-parameters (θ_{CP}, θ_{ST} and θ_{CT}) are introduced that link the various neighbourhood interactions by specifying their inter-type importance relative to the inertia points. These meta-parameters typically fall within the [0, 0.1] domain. This results in the following representation of the neighbourhood interactions:

$$\begin{cases} w_{i,i,0} = \tilde{w}_{i,i,0} \\ w_{i,j,0} = \theta_{CP} \cdot \tilde{w}_{i,j,0} \\ w_{i,i,d} = \theta_{ST} \cdot \tilde{w}_{i,i,1} \cdot u(d) \\ w_{i,j,d} = \theta_{CT} \cdot \tilde{w}_{i,j,1} \cdot u(d) \end{cases} \tag{4.1}$$

where θ_{CP}, θ_{ST} and θ_{CT} are the meta-parameters. Also $\tilde{w}_{i,i,0}$ are the inertia points, $\tilde{w}_{i,j,0}$ are the conversion points, and $\tilde{w}_{i,i,1}$ and $\tilde{w}_{i,j,1}$ are the self and cross-influence tails at $d = 1$, all of which take values from the discretised parameter space; in our case $\{1, 2, 3\}$. While $u(d)$ governs the distance decay that the tails exhibit, which is, in our case, equal to 1 at $d = 1$, 0.1 at $d = 2$ and then degrades linearly to 0 at $d = 5$. Resulting from these equations are the coherent neighbourhood interactions $w_{i,i,0}$, $w_{i,j,0}$, $w_{i,i,d}$ and $w_{i,j,d}$.

Step 5. Coarse parameter adjustment

In this fifth step, a first coarse approximation of coherent neighbourhood interaction rules ($w_{i,i,0}$, $w_{i,j,0}$, $w_{i,i,d}$, $w_{i,j,d}$) is derived with the help of the set of equations 4.1. This is done by implementing the categorised parameters of step 3, iterating over various values for the meta-parameters and measuring and comparing model performance for the various meta-parameter values. Model performance is assessed by comparing the simulation with the historical land-use map of 2016 for the metrics: Kappa, Kappa Simulation and Area-Weighted Clumpiness Error (AWCE), of which Kappa and Kappa Simulation quantify locational agreement and AWCE quantifies landscape pattern structure. The Pareto optimum solutions are extracted, and the solution that balances the chosen metrics is chosen. The meta-parameters of the chosen solution are subsequently inserted in Equation 4.1 to arrive at the first coarse approximation of coherent neighbourhood interaction rules.

Step 6. Fine parameter adjustment

In this sixth step, the neighbourhood interaction rules derived by step 5 are refined by zooming in on all the individual neighbourhood interaction rules. Hence, our focus shifts from the overarching meta-parameters to the individual neighbourhood interaction rules. One-by-one, local optima are found for the neighbourhood interaction rules using the Golden-section search algorithm,[1] while the other interaction rules are set at the values derived in step 5.

Whenever a neighbourhood interaction rule is optimised, it is used in subsequent optimisations. The structure of optimisation is as follows. First, the algorithm loops through the interaction types in order of importance; hence consecutively, inertia points, self-influence points, conversion points, and cross-influence tails. This order of importance was decided upon by evaluating the meta-parameters. Per interaction type, the algorithm also loops through all the land-use classes. This is again done in order of importance. First, the residential land-use classes (Urban-Formal, Urban-Informal and Urban-Villages) are evaluated, then work-related land-use classes (Industry), subsequently recreational land-use classes (Recreation) and then the others.

[1] For an elaborate discussion on this optimisation algorithm, we refer to Newland (2018).

Model performance is assessed with the same metrics used in the coarse parameter adjustment step. However, for optimisation purposes, the three metrics needed to be reduced to one performance indicator. This is achieved by taking the weighted sum of the metrics. Equal value was given to locational agreement as landscape pattern structure, hence $weight_{kappa} = \frac{1}{5}$, $weight_{ksim} = \frac{2}{5}$, $weight_{AWCE} = \frac{1}{5}$.

4.1.3 Calibration: suitability

To arrive at calibrated suitability rules, first, a statistical analysis was executed on the historical 2016 land-use map to gain basic knowledge on what kind of slope, soil, and elevation are suitable for the various land-use classes. After that, similarly to the neighbourhood rules, manual calibration was applied. The executed statistical analysis is discussed in this section.

- Firstly, the Zonal Histogram tool from *ArcGIS Pro* was applied on the 2016 land-use map in combination with soil, slope, and elevation maps to derive histograms that indicate at what height, soil and slope land-use classes were mainly located.
- Thereafter, these histograms were normalised to take into account that some heights, slopes and soils are more present than others. This is done by dividing the number of cells of a specific land-use class within a specific domain by the total number of cells within that same domain. By domain, we refer to a certain height or slope domain or soil type.

The described analysis was executed for the 2016 map instead of the cells that changed from 1996 to 2016. This was deemed sufficient since the relation between the suitability indicators: *slope*, *elevation* and *soil* and the spatial distribution of the various land-use classes was expected to be more-or-less time-independent. Furthermore, this approach resulted in the analysis of more cells, hence more data availability.

Figure 4.1 visualises an example histogram derived from the described analysis. The histogram illustrates that the urban-formal land-use class takes up $\approx 20\%$ of the area with a slope smaller than $5.71°$, while it hardly takes up any area with a slope bigger than $20°$.

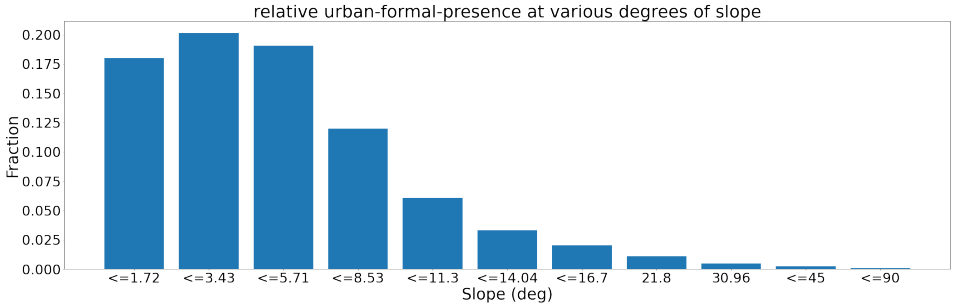

Figure 4.1: *A histogram that visualises the relative presence of the land-use class Urban-Formal at various degrees of slope.*

This analysis was executed for all land-use classes and the three suitability factors: slope, height and soil.

4.1.4 Calibration: accessibility

To arrive at calibrated accessibility rules, first, a statistical analysis was executed on the historical 2016 map to gain basic knowledge on the impact of the various types of transport networks on the spatial distribution of the various land-use classes. After that, similarly to the neighbourhood and suitability rules, manual calibration was applied. The executed statistical analysis is discussed in this section.

1. Firstly, the Euclidean Distance tool from *ArcGIS Pro* was applied on the transport networks to arrive at raster maps indicating the distance from the various transport networks.
2. Subsequently, the Zonal Histogram tool from *ArcGIS Pro* was applied on a [1996, 2016] land-use map[2] in combination with the various maps that originated from the Euclidean Distance tool.
3. After that, normalisation was executed by dividing the number of cells of a specific land-use class within a specific domain by the total number of cells within that same domain. By domain, we refer to a certain 'distance from a network' domain.

In contrast with the suitability analysis, this analysis was executed solely for the cells that changed from 1996 to 2016, as the relation between the transport networks and spatial distribution of the various land-use classes was expected to be time-dependent.

In Figure 4.2, the histogram illustrates that of all the newly allocated cells at $[0, 600]$ m from a major road, $\approx 30\%$ was Urban-Formal. In contrast, only a tiny fraction of the newly allocated cells at $[5400, \rightarrow]$ m was Urban-Formal.

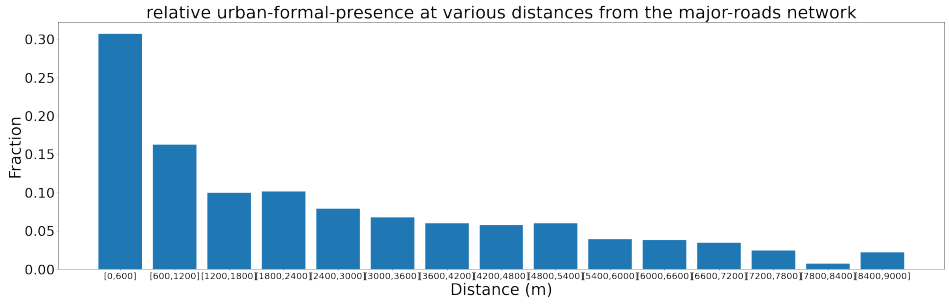

Figure 4.2: *A histogram visualising the relative presence of the land-use class Urban-formal at various degrees of slope.*

This analysis was executed for all land-use classes and the various transport networks: *minor roads*, *major roads*, *highways*, *railways*, *mono and metro railways*, *ferry lines*, *bus centroids*, *ferry terminals*, *metro stations* and *railway stations*.

4.1.5 Calibration performance

After the various land-use model components were calibrated, calibration performance was assessed as described in Section 3.1.3. This section discusses the statistical assessment of calibration performance in depth. This is done by first describing the applied calibration-performance indicators; subsequently, the implementation of the various indicators is discussed; and lastly,

[2]We refer to a map that only incorporates the cells that have changed from 1996 to 2016.

the performance of the land-use model concerning these calibration-performance indicators is reviewed.

Calibration-performance indicators

A selection of calibration-performance indicators was applied that quantifies locational agreement (on a cell-by-cell basis and in a fuzzy logic manner) and landscape pattern structure. The selected indicators include $Kappa$, K_{Sim}, FK, and FK_{Sim} and $CLUMPY$. Details on these calibration performance indicators are discussed in this section.

$Kappa$ is a coefficient indicating the agreement of two data sets, corrected for the agreement as can be expected by chance. In the context of map comparison, it is estimated by multiplying $K_{Histogram}$, which indicates the similarity in quantity, with $K_{Location}$, which indicates the similarity in spatial allocation. $Kappa$ values range from -1, indicating no agreement, to 1, indicating perfect agreement. $Kappa = 0$ indicates agreements as can be expected by chance (van Vliet et al., 2011).

Problematic concerning $Kappa$, is that in the case of little change over time, $Kappa$ will be high irrespective of the quality of the model. To account for this problem of "land-use persistence" (van Vliet et al., 2011), the Kappa Simulation (K_{Sim}) coefficient can be applied. K_{Sim} is computed in a similar way as $Kappa$, except that only the changed cells are evaluated. K_{Sim} values, similarly to $Kappa$ values, range from -1, indicating no agreement, to 1, indicating perfect agreement, with 0 indicating as-good-as-random performance. K_{Sim} values are generally significantly lower than $Kappa$ values due to the focus on changed cells (van Vliet et al., 2011).

Both $Kappa$ and K_{Sim} function (i) on a cell-by-cell basis and (ii) do not account for similarities between land-use classes. Hence, if the newly allocated cell is allocated one cell away from its prescribed location, it is counted as erroneous. This misses the point of modelling land-use patterns. The Fuzzy Kappa (FK) coefficient was applied to account for nearly correct allocation. FK is a fusion of the $Kappa$ coefficient and fuzzy logic, where fuzzy logic, as opposed to two-value logic, enables the inclusion of degrees of locational agreement. FK values, similarly to $Kappa$ values, range from -1, indicating no agreement, to 1, indicating perfect agreement, with 0 indicating as-good-as-random performance. FK values are generally higher than $Kappa$ values since also truth is seen in just erroneous cells (Dou et al., 2007).

FK however, also experiences the same problem as $Kappa$, concerning land-use persistence. Therefore, Fuzzy Kappa Simulation (FK_{Sim}) is included which combines Fuzzy logic, and $Kappa$, while only evaluating the changed cells. FK_{Sim} values, similarly to $Kappa$ values, range from -1, indicating no agreement, to 1, indicating perfect agreement, with 0 indicating as-good-as-random performance. FK_{Sim} values are generally higher than K_{Sim} values since also truth is seen for just erroneous cells, but lower than $Kappa$ and FK, since only changed land-use cells are evaluated (van Vliet et al., 2013a).

The various Kappa coefficients quantify locational agreement. To also quantify landscape pattern structure, the Clumpiness index ($CLUMPY$) is incorporated. $CLUMPY$ is a measure of adjacency indicating the fragmentation or clumping that a land-use class portrays over the evaluated area (Cushman and McGarigal, 2008). $CLUMPY$ equals -1 for a maximal dis-aggregation to 1 for maximal clumping, with 0 indicating a random distribution over space (Hewitt et al., 2014). The clumpiness of each land-use class for the simulated land-use map is desired to be the same as the clumpiness of each land-use class for the observed map. Therefore the difference per land-use class is evaluated and desired to be equal to 0.

Calibration-performance indicators assessment

The selected indicators were all assessed with the *Map Comparison Kit 3* application from the Research Institute for Knowledge Systems (RIKS) (Visser and de Nijs, 2006). The FK and FK_{Sim} indicators were applied with a neighbourhood radius of four cells with linear decay. Linear decay was deemed reasonable since this results in finite fuzziness, i.e. the correctness ends after four cells. Furthermore, a neighbourhood radius of four cells was deemed reasonable concerning the size of the studied area. The assessment of $Kappa$, and K_{Sim} cannot be specified, hence does not have to be discussed.

Statistical calibration performance

The various performance indicators need to be put into perspective to decide on the sufficiency of the model performance. This is done by comparing the performance of the calibrated models with two neutral models: the random constraint match (RCM) model and the Null model, which the calibrated model should outperform.

The RCM model is constructed by applying the same demand for land-use classes as the calibrated model but erasing all the calibrated land-use rules. Hence, this results in random allocation while having the same quantitative distribution of land-use classes as the calibrated model (Hagen-Zanker and Lajoie, 2008).

The null model is constructed by applying the same demand for land-use classes as in the calibrated model, while only applying a very simple set of neighbourhood rules; the inertia point is set to 100 for all land-use classes, the conversion point is set to 1 for all possible conversions and the neighbourhood rules at distance > 0 (van Vliet et al., 2013b).

The achieved performance by the calibrated model, the RCM model and the Null model, concerning locational agreement, is visualised in Table 4.3. Herein is visible how the calibrated model outperforms the RCM and the Null model, considering all the calibration performance indicators that are taken into account.

	$Kappa$	K_{Sim}	FK	FK_{Sim}
Calibrated model	0.763	0.180	0.854	0.294
RCM Model	0.727	0.002	0.787	0.006
Null Model	0.712	0.000	0.776	0.005

Table 4.3: *A table on the performance indicator values for the calibrated, RCM and null models. The calibration model outperforms both the RCM and the Null model.*

The achieved performance by the calibrated model, the RCM model and the Null model concerning landscape pattern structure, is visualised in Table 4.4. Herein is visible how the calibrated model outperforms the RCM and the Null model, considering almost all the calibration performance indicators that are taken into account. Only concerning Industry, the calibrated model is outperformed by both the Null and the RCM model, and concerning Urban-Formal, it is outperformed by the Null model. This results from focusing on locational agreement instead of landscape pattern while applying manual calibration methods.

	Calibrated model	RCM Model	Null Model
Agriculture	0.044	0.026	0.197
Forest	-0.018	0.321	0.301
Industry	-0.125	**-0.051**	**-0.054**
Nature	-0.001	-0.131	-0.128
Recreation	0.002	-0.047	-0.059
Urban-Formal	-0.081	0.082	**-0.075**
Urban-Informal	0.066	0.180	0.174
Urban-Villages	-0.022	0.033	0.032

Table 4.4: *A table on the clumpiness index performance indicator for the various land-use classes of the calibrated, RCM and null models.*

4.1.6 Land-use model for the future

The calculation of land-use demand for the future was already touched upon in Section 3.1.4. A more in-depth calculation can be found in this section, with help from Table 4.5. Exact details on the reasoning behind the estimates can be found in Appendix C.2.

LUC	2016 land-use	Growth calculation	Implemented growth
Urban-Informal	83.04 km^2	1. $urban\ informal_{2036} = 0.9 * \frac{urban\ informal_{2016}}{built\ up_{2016}} * built\ up_{2036}$ (Nijman, 2008, 2012) (a) $built\ up_{2016} = urban\ formal_{2016} + urban\ informal_{2016} + urban\ villages_{2016} =$ 638.36 km^2 (b) $built\ up_{2036} = growth\ rate * built\ up_{2016} =$ 909.70 km^2 i. $growth\ rate =$ 1.425[2016, 2036](MMR, 2016)	106.50 km^2 [2036] 122.92 km^2 [2050]
Urban-Villages	97.88 km^2	1. $urban\ villages_{2050} = urban\ villages_{2036} = urban\ villages_{2016}$	97.88 km^2 [2036] 97.88 km^2 [2050]
Urban-Formal	457.44 km^2	1. $urban\ formal_{2036} = built\ up_{2036} - urban\ informal_{2036} - urban\ villages_{2036}$ (a) $built\ up_{2036} = growth\ rate * built\ up_{2016} =$ 909.70 km^2 i. $growth\ rate =$ 1.425[2016, 2036](MMR, 2016)	705.32 km^2 [2036] 851.18 km^2 [2050]

LUC	2016 land-use	Growth calculation	Implemented growth
Industry	141.84 km^2	1. $industry_{2036} = 214.97$ km^2 (MMR, 2016)	214.97 km^2 [2036] 266.16 km^2 [2050]
Forest	807.88 km^2	1. $forest_{2036} = growth\ rate * forest_{2016}$ (a) $growth\ rate = 1.285$ [2016, 2036] (MMR, 2016)	1038.16 km^2 [2036] 1199.36 km^2 [2050]
Nature	1099.12 km^2	1. $nature_{2050} = frac\ nature_{2050} * green\ space_{2050}$ [3] (a) $frac\ nature_{2050} = frac\ nature_{2036} = frac\ nature_{2016} = 0.458 = nature_{2016}/green\ space_{2016}$ [4] (b) $green\ space_{2036} = growth\ rate * green\ space_{2016} = growth\ rate * (agriculture_{2016} + nature_{2016}) =$ 1734.71 km^2 i. $growth\ rate = 0.723[2016, 2036]$ (MMR, 2016)	794.50 km^2 [2036] 581.42 km^2 [2050]
Recreation	43.96 km^2	1. $recreation_{2036} = growth\ rate * recreation_{2016}$ (a) $growth\ rate = 1.26$ [2016,2036] (MMR, 2016)	55.18 km^2 [2036] 63.03 km^2 [2050]

Table 4.5: *A table on the estimated future land-use demand for the various land-use classes that figure as function land-use classes in the Metronamica land-use model. All non-referenced numbers have been extracted from the land-use maps.*

4.1.7 Monte Carlo simulation

A stochastic factor α is present in the land-use model, which depends on a seed. During calibration, the seed was kept constant to ensure replicability and to arrive at a single land-use map that could be implemented in the land-use model for the future. Now, for the future, we apply a Monte Carlo simulation that varies the random seed to take the uncertainty of individual model runs into account. The Monte Carlo simulation results in probability maps for the various land-use classes.

[3] $green\ space_{2050}$ is derived from $green\ space_{2036}$ through linear extrapolation.
[4] Nature is assumed to be the same fraction of green space in 2036 and 2050 as it was in 2016.

Figure 4.3 shows an example probability map. Herein is visible how the presence of a land-use class at a certain cell is not either 0 or 100%, but falls in the range [0, 100]%. The percentage follows from the fraction of runs a land-use class got allocated to a cell.

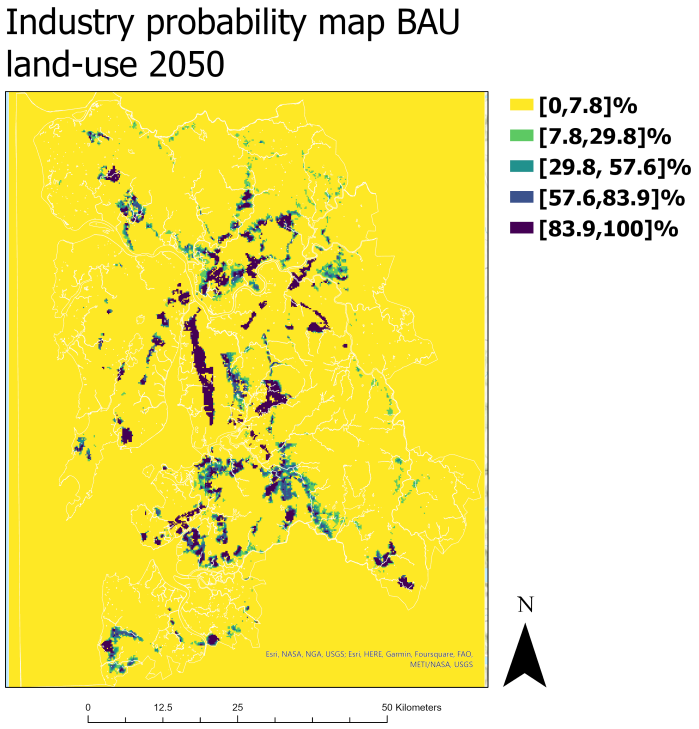

Figure 4.3: *A figure that visualises an example probability map for the Industrial land-use class that follows from a Monte Carlo simulation.*

For each scenario[5],50 runs are executed. Problematic concerning the Monte Carlo simulation is that we are now not dealing anymore with a single map but a cluster of maps based on probabilities instead of booleans. The handling of these maps concerning visualisation and calculation of resilience indicators is discussed in the following sections.

Visualisation

The probability maps can be combined for visualisation purposes to form a single land-use map. This can be done in the following manner.

- If urban formal, urban-informal, urban-villages, or industry has a probability of allocation $> 20\%$, then this land-use class is allocated to the cell.
- If multiple urban or industrial land-use classes have a probability of allocation $> 20\%$ for a cell, then the land-use class with the highest potential is allocated.
- If non of the urban or industrial land-use classes has a probability of allocation $> 20\%$, then a cell is filled by the non-urban or industrial land-use class with the highest potential.

This approach is applied since our focus is on the urban-formal, informal, villages and industrial

[5]The scenarios are described in Section 3.3.4

land-use classes. The threshold of 20% was based on expert knowledge.[6] Figure 3.3 is derived using the described approach.

Resilience indicators

The construction of a single map from the various probability maps was not considered a suitable method when estimating aggregated resilience indicators, for two reasons. Firstly, a single map with a threshold of 20% leads to flood risk estimates that are independent from the allocation probability. Also, a threshold of 20% results in a land-use map with more urban and industrial areas for 2050 than the estimated 2050 demand. To account for these problems, a different approach is applied when estimating aggregated resilience indicators. In this approach, the allocation probability is taken into account, and the flood impacts per land-use class are summed to arrive at a total impact per cell for a certain RP flood. Subsequently, the expected annual flood damage for a cell is calculated by taking into account the probability of occurrence of the several RP floods. This is done in the following manner:

$$\begin{aligned} &Expected\ annual\ flood\ damage\ cell = \int_0^1 Flood\ impact\ cell(p_r)\ dp_r \\ &= \int_0^1 \sum_{luc} cell\ allocation\ probability(luc) * flood\ impact(luc, p_r)\ dp_r \end{aligned} \tag{4.2}$$

where $Expected\ annual\ flood\ damage\ cell$ is a measure of flood risk and indicates the flood damage that can be annually expected, $Flood\ impact\ cell(p_r)$ is the flood impact associated with a particular RP flood for a specific cell, and p_r is the probability that a certain flood level associated with a particular RP flood will be exceeded in a year Foudi et al. (2015). Furthermore, $flood\ impact\ cell(p_r)$ is the flood impact for a certain cell associated with a a flood of a certain RP flood, $cell\ allocation\ probability(luc)$ is the probability that a land-use class is allocated to a cell and $flood\ impact(luc, p_r)$ is the flood impact associated with a certain RP flood for a certain land-use class.

Unlike the earlier discussed visualisation approach, this approach estimates higher projected flood impact for cells with a higher allocation probability. Also, the applied demand for 2050 is taken into account.

However, even though Equation 4.2 might be useful to calculate aggregate resilience indicators (such as total EAMD and total EAPA), application for spatial analyses of the resilience indicators for single land-use classes is less suitable. An example best explains this.

In the case of informal settlements, the uncertainty of allocation is large for all newly allocated areas. Now image applying Equation 4.2 to acquire knowledge on the spatial distribution of the most vulnerable informal settlements in 2050. This would subsequently result in higher resilience indicator estimates for the already existing informal settlements and the downplaying of the expected flood risk at newly allocated areas. This is problematic since this results in a potential overlooking of newly allocated areas. Therefore, concerning spatial analyses of resilience indicators for individual land-use classes, maps are constructed as discussed in the visualisation section. However, for spatial analyses of the aggregate resilience indicators, equation 4.2 is applied since these spatial analyses are executed to acquire a more general image of the area.

[6] This threshold was suggested through e-mail by Mrs. Hedwig van Delden on Sept 30, 2022.

4.2 Flood Risk Assessment

In Section 3.2.2 is discussed how the assessment of resilience for the MMR was conceptualised as an assessment of flood risk. After that, in Section 3.3.3, a conceptual discussion takes place concerning assessing flood risk through coupling a land-use model and flood hazard maps. This section discusses the flood risk assessment in more technical and detailed terms.

First, in Section 4.2.1, the general methodology is discussed. Thereafter, in Section 4.2.2 the procedure for estimating the expected annual monetary damage is addressed. Furthermore, in Section 4.2.3 the procedure for estimating the expected annual population affected is conversed. Lastly, in Section 4.2.4 the procedure for estimating the percentage of annual income lost is discussed.

Together these sections answer the assessment part of SQ2 in depth:

How can resilient urban planning be conceptualised and assessed for the MMR?

4.2.1 General methodology

In accordance with Foudi and Osés-Eraso (2014); Foudi et al. (2015); Penning-Rowsell et al. (2005), flood risk is assessed using a four-step approach: (i) hazard assessment, (ii) exposure assessment, (iii) vulnerability assessment and (iv) risk assessment, leading to quantifications for the in Section 2.2 discussed indicators: EAMD, EAPA, and PAIL. This approach is visualised in Figure 4.4 and discussed in depth below.

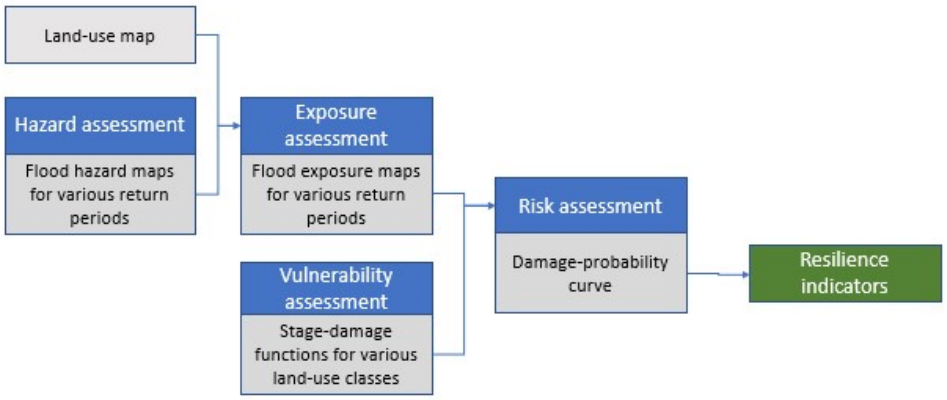

Figure 4.4: *An overview of the four-step approach as applied in this thesis. In blue, the various assessments, in grey, their associated outputs and inputs and, in green, the desired indicators are visualised.*

Hazard assessment

Hazard assessment assesses the flood hazard that corresponds with floods of various RPs, and results in flood hazard maps for each RP flood. For the MMR, solely flood-depth data was available. Henceforth, flood-depth was used as a proxy for flood hazard. How the applied flood hazard maps were derived is discussed in Section 3.3.1.

Exposure assessment

In exposure assessment, the flood hazard maps for various RPs are one by one combined with a land-use map. By overlaying, one gains knowledge (i) on the land-use classes located in flood-prone areas for a particular RP flood and (ii) on the flood hazard a land-use class will be exposed to if located in a flood-prone area. The derivation of the various land-use maps applied in this thesis is discussed conceptually in Section 3.1 and more in-depth in Section 4.1.

Vulnerability assessment

The flood impacts associated with exposure to a particular flood hazard are assessed in the vulnerability assessment. This can be done using stage-damage functions. Stage-damage functions estimate the flood impacts associated with specific flood parameters, such as flood depth, flood duration and flow velocity. In general, flood depth is considered the most critical parameter concerning direct flood damage (de Moel and Aerts, 2011); hence the usage of flood depth as a proxy for flood hazard seems reasonable. To arrive at land-use specific impact estimates, a unique stage-damage function was generated for each relevant land-use class for each resilience indicator.

Risk assessment

In risk assessment, the outputs of the hazard assessment, the exposure assessment and the vulnerability assessment all come together to arrive at a flood risk estimate. This is done by, first, overlaying a land-use map with a flood hazard map for a particular RP. After that, through the application of the stage-damage functions, flood impacts associated with such a flood hazard are assessed. Subsequently, the flood impacts of the floods of various RPs are coupled with their annual probability of occurrence through the construction of *damage-probability curves*. Figure 4.5 shows an example damage-probability curve.

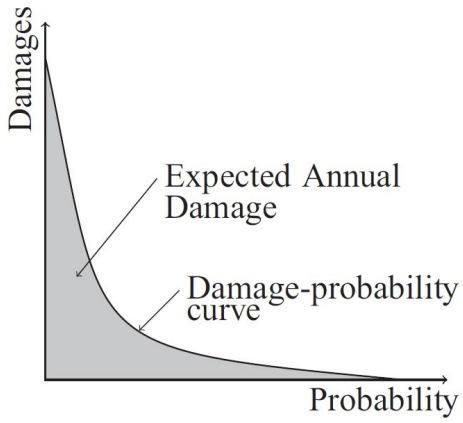

Figure 4.5: *An example damage-probability curve that enables the assessment of expected annual damage (Foudi et al., 2015).*

From the damage-probability curve, one can derive the *expected annual damage*, where the expected annual damage is the average flood damage experienced in a year. The expected annual

damage can be estimated by calculating the surface below the damage-probability curve, using the following equation from Foudi et al. (2015)[7]:

$$EAD = \int_0^1 D\left(p_r\right) dp_r \tag{4.3}$$

where $D\left(p_r\right)$ is the damage-probability curve, p_r is the annual exceedance probability for a particular flood event, and EAD is the expected annual damage. Note that EAD is an umbrella concept under which EAMD, EAPA and PAIL all fall.

The estimation of EAD can be done for the whole evaluated region for all land-use classes combined, for the whole evaluated region for a single land-use class, or spatially explicitly and hence for each cell separately.

Damage-probability curve

A damage-probability curve is required that spans a wide selection of RP floods to arrive at reasonable expected annual damage estimates. The set of flood hazard maps available from the Aqueduct Floods tool does not include extremely high ($p_r = 1$) and low ($p_r \to 0$) probability floods. Therefore, estimates of flood damage associated with such floods were made.

Estimates for the damage associated with $p_r = 1$ (1 year RP) and $p_r = 0.002$ (500 year RP) were estimated based on damage estimates for the other RP floods. Foudi et al. (2015) “arbitrarily" estimates the damage to be equal to 0 at $p_r = 1$ and estimates $D(0.002)$ to be equal to $1.5 \cdot D(0.02)$. Concerning $p_r = 0.002$, applying the same approach seems reasonable since this approximately follows the rest of the damage-probability curve. For the uncertainty bounds, a similar multiplication approach with a factor of 1.5 was applied. Concerning $p_r = 1$, a different approach was applied since, in some cases, the damage estimate of 0 at p_r appears to be not in line with the rest of the curve and results in a relatively low estimate for the MMR. Consequently, for the best estimate, the slope between $p_r = 0.2$ and $p_r = 0.5$ is extrapolated while ensuring that $damage \geq 0$. The uncertainty bounds at $p_r = 1$ are made equal to the uncertainty bounds at $p = 0.5$, also ensuring that $damage \geq 0$.

An example of a damage-probability curve derived using the above-described procedure is visualised in Figure 4.6.

[7] This equation was already mentioned in Section 3.3.3.

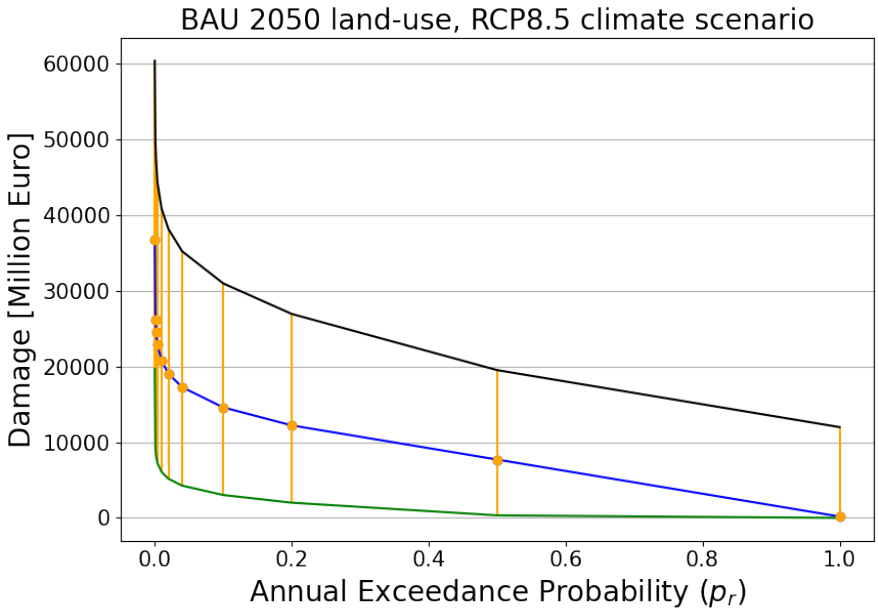

Figure 4.6: *A damage-probability curve of EAMD, constructed for the business-as-usual scenario land-use scenario of 2050 and the RCP8.5 climate scenario.*

4.2.2 Expected annual monetary damage

The Expected Annual Monetary Damage (EAMD) is the average[8] monetary flood damage experienced in a year. It can be derived for a cell, a land-use class, or a region using the methodology discussed in Section 4.2.1. Hence required, besides flood hazard maps and a land-use map, are stage-damage functions for the various land-use classes that associate flood depth with monetary damage. These so-called monetary flood-depth damage functions or monetary damage functions (MDF) were not readily available for India or the MMR. Therefore they were constructed using the methodology of Huizinga et al. (2017). MDFs were available and hence constructed for the land-use classes: *Urban-formal*, *Urban-informal*, *Urban-villages*, *Industry*, *Transportation*, and *Agriculture*. The damage experienced by Agriculture is estimated to be marginal when compared with the other land-use classes. Therefore Agriculture is not further taken into account.[9]

The applied methodology concerning the construction of MDFs and the constructed MDFs are discussed in the following sections.

MDFs derivation methodology

An overview of the workflow that was applied by Huizinga et al. (2017) to arrive at MDFs is visualised in Figure 4.7.

[8] This is an average over time.
[9] The MDF for Agriculture is still discussed in the Appendix D.

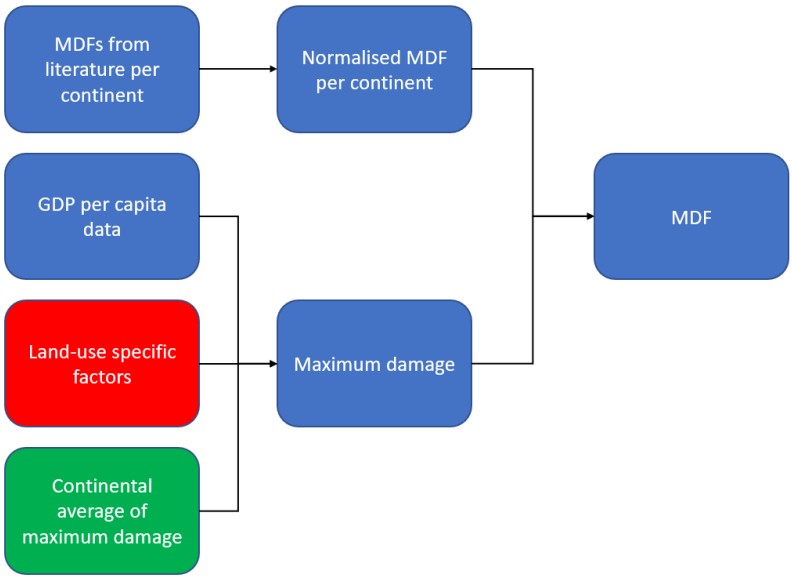

Figure 4.7: *An overview of the methodology of Huizinga et al. (2017) to arrive at MDFs. Blue indicates that an element was used to estimate MDFs for all land-use classes. Red indicates that an element was solely used to estimate MDFs for the land-use classes Urban-Formal, Urban-Informal, Urban-Villages, and Industry. Green indicates that an element was solely used to estimate the MDF for the transportation land-use class.*

First, the *normalised MDF* and the *maximum damage* are estimated. The normalised flood-depth damage function describes the relation between flood depth and the fraction of the economic loss that is done to the damaged object, which ranges from zero (no damage) to one (maximum damage). These are estimated by Huizinga et al. (2017) by averaging over flood depth damage functions available in the literature that apply to the same continent.[10]

Second, the maximum damage (Euro/m^2) is estimated based on the GDP per capita of a certain location.[11] For the GDP per capita input, we applied the estimation done by Suzuki (2020), who estimated that the MMR's GDP per capita was 4803 Euro (5328 $) in 2015. Furthermore, for the land-use classes Urban-Formal, Urban-Informal, Urban-Villages, and Industry, also various land-use specific factors were considered, such as (i) the depreciation of the structure, (ii) the undamagable fraction of a structure, (iii) the material worth of a structure, (iv) the value of the content inside the structure relative to the value of the structure and (v) the fraction of land covered by structures. The specific values of these various factors differ per land-use class and have been implemented as prescribed by Huizinga et al. (2017). For the transportation LUC, the GDP per capita data is combined with the continental average of the maximum damage to arrive at maximum damage for a specific location.

Finally, the MDF can be derived through the multiplication of the normalised MDF and maximum damage.

To get insight in the certainty associated with the estimated MDFs, we took into account the uncertainties in (i) the estimated normalised damage function and (ii) the GDP per capita-construction cost relation. Both these uncertainties were derived from Huizinga et al. (2017). In addition, we also included relative uncertainties of 5% for the land-use-specific factors, to account

[10] In our case-study, we use the available flood depth damage functions for the Asian continent.

[11] This was deemed valid since a correlation between GDP per capita and construction cost was found, enabling the estimation of construction cost in case GDP per capita is known.

to some degree for their uncertainty. The resulting 90% confidence intervals are included in the MDFs visualised in the following Sections.

Note that the normalised damage functions, as supplied by Huizinga et al. (2017), are no smooth fits but concatenations of points. Therefore, smooth functions were established that allow swift damage estimation for continuous flood depth. For the urban-formal, urban-informal, urban-villages and industry land-use classes, a power-law fit of the form $y = a \cdot x^b$ was applied. For the transportation land-use class, a poly-logarithmic fit of the form $y = a * log(x)^2 + b * log(x) + c$ was applied since this resulted in higher R^2 values. Fitting was also applied to the 90% confidence intervals to allow the estimation of the uncertainty in flood damage for continuous flood depth.

Appendix D provides a complete overview of the applied calculations.

Urban-formal

Based on the earlier described methodology, the urban-formal MDF was estimated. The normalised MDF for damage class 'residential' was applied as a proxy for urban-formal. In terms of land-use-specific factors, urban-formal was deemed to have: (i) high material worth of the structure, (ii) an undamageable fraction, and (iii) a small fraction of land covered by structures. The smooth MDF (orange), the 90% upper-bound fit (black) and the 90% lower-bound fit (yellow) are visualised in Figure 4.8, together with the data points and their uncertainties. All fits have R^2 values higher than 0.97.

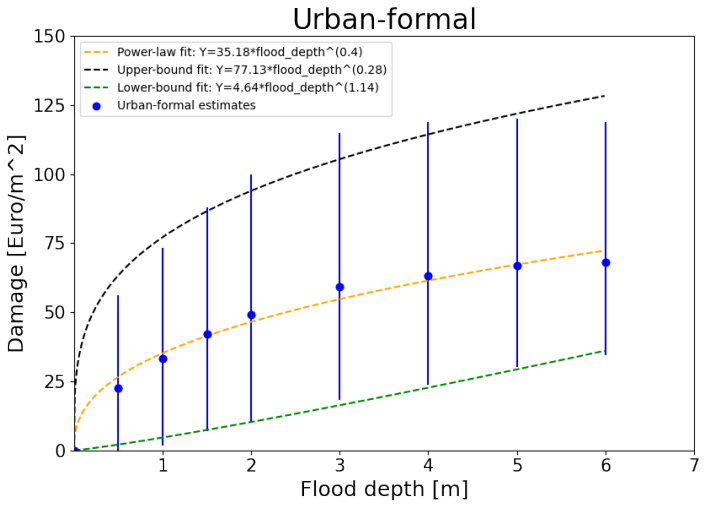

Figure 4.8: *In this figure, the smooth MDF (orange), the 90% upper-bound fit (black) and the 90% lower-bound fit (yellow) for Urban-Formal are visualised together with the data points. The power-fits have the following R^2 values:* $R^2_{MDF} = 0.984, R^2_{upperbound} = 0.976, R^2_{lowerbound} = 0.985$.

Urban-informal

Based on the earlier described methodology, the urban-informal MDF was estimated. The normalised MDF for damage class 'residential' was applied as a proxy for urban-informal. In terms of land-use-specific factors, Urban-Informal was deemed to have: (i) structures with little material worth, (ii) no undamageable fraction, and (iii) a significant fraction of land covered by structures. The smooth MDF (orange), the 90% upper-bound fit (black) and the 90% lower-bound

fit (yellow) are visualised in Figure 4.9, together with the data points and their uncertainties. All fits have R^2 values higher than 0.97.

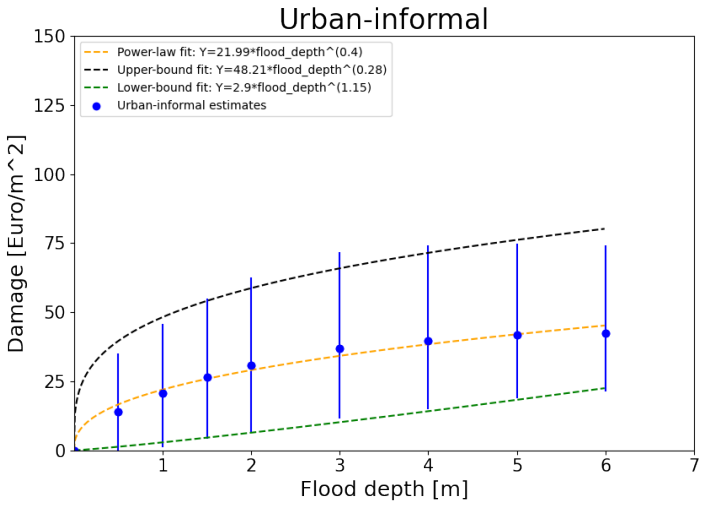

Figure 4.9: *In this figure, the smooth MDF (orange), the 90% upper-bound fit (black) and the 90% lower-bound fit (yellow) for Urban-Informal are visualised together with the data points. The power-fits have the following R^2 values:* $R^2_{MDF} = 0.984, R^2_{upperbound} = 0.976, R^2_{lowerbound} = 0.985$

Urban-villages

Based on the earlier described methodology, the urban-villages MDF was estimated. The normalised MDF for damage class 'residential' was applied as a proxy for Urban-Villages. In terms of land-use-specific factors, Urban-Villages was deemed to have: (i) structures with little material worth, (ii) no undamageable fraction, and (iii) a small fraction of land covered by structures. The smooth MDF (orange), the 90% upper-bound fit (black) and the 90% lower-bound fit (yellow) are visualised in Figure 4.10, together with the data points and their uncertainties. All fits have R^2 values higher than 0.97.

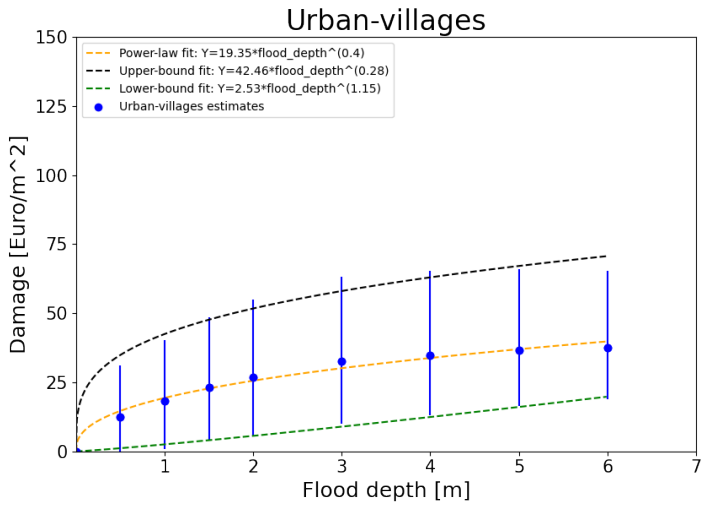

Figure 4.10: *In this figure, the smooth MDF (orange), the 90% upper-bound fit (black) and the 90% lower-bound fit (yellow) for Urban-Villages are visualised together with the data points. The power-fits have the following* R^2 *values:* $R^2_{MDF} = 0.984, R^2_{upperbound} = 0.976, R^2_{lowerbound} = 0.985$

Industry

Based on the earlier described methodology, the industry MDF was estimated. In terms of land-use-specific factors, Industry was deemed to have: (i) structures with high material worth, (ii) an undamageable fraction, (iii) a mediocre fraction of land covered by structures, and (iv) high interior value. The smooth MDF (orange), the 90% upper-bound fit (black) and the 90% lower-bound fit (yellow) are visualised in Figure 4.11, together with the data points and their uncertainties. All fits have R^2 values higher than 0.96.

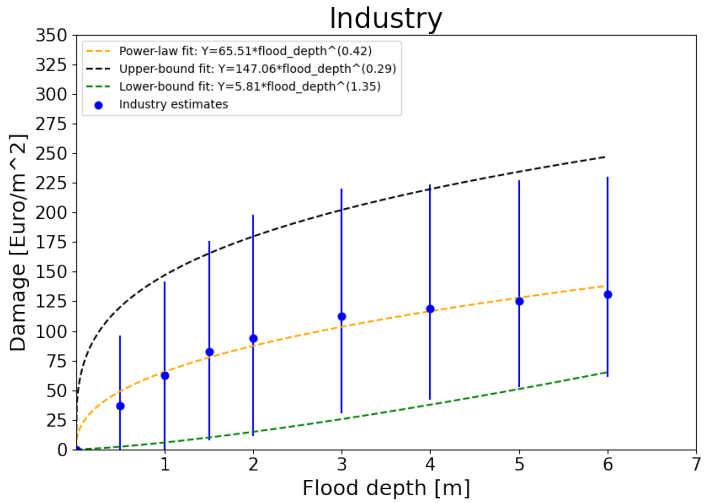

Figure 4.11: *In this figure, the smooth MDF (orange), the 90% upper-bound fit (black) and the 90% lower-bound fit (yellow) for Industry are visualised together with the data points. The power-fits have the following* R^2 *values:*$R^2_{MDF} = 0.976, R^2_{upperbound} = 0.963, R^2_{lowerbound} = 0.976$

Transportation

Based on the earlier described methodology, the transportation MDF was estimated. The smooth MDF (orange), the 90% upper-bound fit (black) and the 90% lower-bound fit (yellow) are visualised in Figure 4.12, together with the data points and their uncertainties. All fits have R^2 values higher than 0.95.

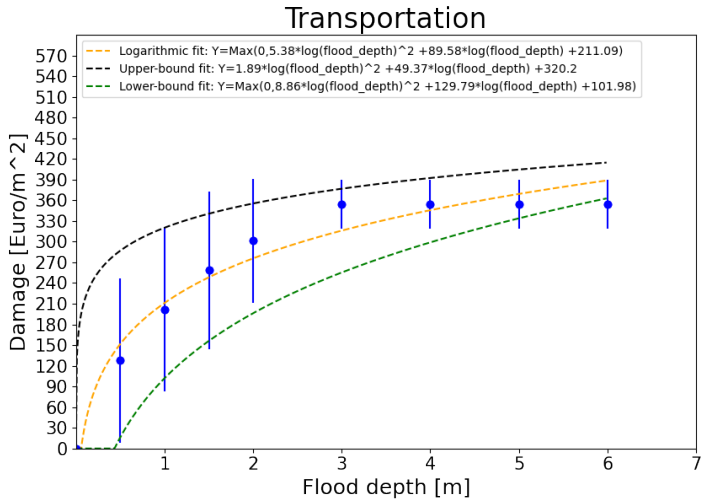

Figure 4.12: *In this figure, the smooth MDF (orange), the 90% upper-bound fit (black) and the 90% lower-bound fit (yellow) for Urban-Informal are visualised together with the data points. The power-fits have the following* R^2 *values:* $R^2_{MDF} = 0.965, R^2_{upperbound} = 0.963, R^2_{lowerbound} = 0.950$

4.2.3 Expected annual population affected

The Expected Annual Population Affected (EAPA) is the average population affected by floods in a year. It can be derived for a cell, a land-use class, or a region using the methodology discussed in Section 4.2.1. Hence required, besides a land-use map and flood hazard maps, are stage-damage functions that associate flood depth with the population affected. The applied stage-damage functions for EAPA of a cell, contrary to the MDFs, do not steadily increase with increasing flood depth but function as a binary step function of the form:

$$Population\ affected(flood\ depth) = \begin{cases} 0 & \text{for } flood\ depth = 0 \\ Population & \text{For } flood\ depth > 0 \end{cases} \tag{4.4}$$

In other words, if a cell is flooded, all people living in that cell are considered to be affected. As a result, we assume that people are affected at any inundation level, which is not necessarily the case. However, since we do not know the inundation levels land-use classes can experience without suffering negative consequences, we deem the assumption of 'any inundation leads to negative consequences' to be the most neutral one. According to Equation 4.4, $Population\ affected$ is equal to $Population$ in case of $flood\ depth > 0$. $Population$ is, however, troublesome to acquire data for and problematic to generalise for land-use classes. Most suitable seem the estimations made by Hu et al. (2021) based on Sentinel data, that estimate the population density of Mumbai city's low-density, high-density and average-density urban areas. Problematic concerning applying these estimates for the city centre to the entire study area is that they most likely result in an overestimation of $Population$ for cells on the outskirts. However, since the most flood-prone areas are located towards the coast and coincide with the denser regions of the MMR, we deem the estimates made by Hu et al. (2021) most suitable to apply. Also assumed was that solely the land-use classes of Urban-Formal, Urban-Informal and Urban-Villages contain population. An overview of the applied population densities is visualised in Table 4.6.

	Derivation	Population density ($10^3/km_2$)
urban-formal	The average population density of Mumbai (Hu et al., 2021).	37
Urban-informal	The population density for complex, high-density slum structures in Mumbai (Hu et al., 2021).	47
urban-villages	The population density for open, low-density area in Mumbai (Hu et al., 2021).	34

Table 4.6: *Population density for the land-use classes urban-formal, urban-informal and urban-villages as derived from Hu et al. (2021).*

4.2.4 Percentage of annual income lost

The percentage of Annual Income Lost (PAIL) is the average percentage of annual income lost by a household due to floods in a year. It is derived from the EAMD and a cluster of statistics portrayed in Table 4.7. Including this resilience indicator results in insight into the real-world impact of EAMD. Establishing PAIL is done by relating the $EAMD\ per\ household$ to the *yearly mean income per household* for the various land-use classes. To subsequently be able to

compare the maximum percentage of income lost by a household due to floods for the various land-use classes.

	Derivation yearly mean income per household	Yearly mean income per household (Euro/Year (2015))	Average population per household
Urban-Formal	1. *median monthly income per household* = 20000 Rs/month(2008)[12] (MCGM, 2016) 2. 37768 Rs/month(2015)= 20000 Rs/month(2008) (Scripbox, 2022) 3. 524.98 Euro/month (2015)= 37768 Rs/month(2015) (ExchangeRates.org, 2022) 4. 6300 Euro/year (2015)≈ 524.98 Euro/month(2015)	6300	4.39 (MMR, 2016)
Urban-Informal	1. *mean monthly income per household* = 2978 Rs/month(2002) (MMR, 2002) 2. 7413 Rs/month(2015)= 2978 Rs/month(2002) (Scripbox, 2022) 3. 103.04 Euro/month(2015)= 7413 Rs/month(2050) (ExchangeRates.org, 2022) 4. 1236 Euro/year (2015)≈ 103.04 Euro/month(2050)	1236	4.39 (MMR, 2016)
Urban-Villages	Constitutes a subcategory of informal settlements. Therefore it is treated equally to urban-informal.	1236	4.39 (MMR, 2016)

Table 4.7: *A table concerning the derivation of various statistics required for the estimation of PAIL.*

PAIL is calculated in two steps. First, the EAMD per household is calculated through:

$$EAMD\ per\ household = \frac{total\ EAMD\ per\ cell}{households\ per\ cell} = \frac{total\ EAMD\ per\ cell}{\frac{population\ per\ cell}{average\ population\ per\ households}} \tag{4.5}$$

where, *total EAMD per cell* follows from the EAMD analysis, and *population per cell* and *average population per households* follow from Table 4.7.

Subsequently, PAIL for a cell is estimated through:

$$PAIL = \frac{EAMD\ per\ household}{yearly\ mean\ income\ per\ household} \tag{4.6}$$

[12]This was calculated for Greater Mumbai.

where, *yearly mean income per household* follows from Table 4.7.

Significant assumptions of the applied methodology can be found in both Equation 4.5 and 4.6. Firstly, Equation 4.5 assumes that all damage done to buildings and interiors of a particular land-use cell is equally split over the households of that cell. This implies that everyone experiences the same damage and denies the presence of other parties in a land-use cell, such as companies, government agencies, and others. Secondly, Equation 4.6 aggregates the situation significantly by taking the mean yearly income per household. It also assumes that a household loses the amount of money equivalent to the experienced damage, which denies the existence of insurance. Also, this assumes that people living in a house also own it, which is not accurate in general, but especially not for the formal sector of Mumbai housing. This becomes clear when considering that the median household income is 20000 Rs/month (2008), while a single-bedroom public housing unit starts from 1.4 Million Rs. Hence, most people cannot afford to own a house in the formal sector (MCGM, 2016).

No uncertainty bounds were available for the statistics of Table 4.7. However, these uncertainties are considered significant due to averaging over space, aggregation of land-use classes and extrapolation over time and space. Solely including the uncertainties for EAMD for the calculation of PAIL was deemed to give a false 'sense of certainty'; hence uncertainties were not included but can be considered more than significant.

Chapter 5

Results

In this chapter, the results of the land-use modelling case study are discussed. Results were derived concerning three topics. Firstly, the various flood hazard scenarios are discussed in Section 5.1. After that, in Section 5.2, the flood resilience associated with the business-as-usual growth scenario is discussed. Furthermore, Section 5.3 discusses the flood resilience associated with various urban planning scenarios.

5.1 Flood Hazard

In this section, the analysis of the flood hazard maps is discussed. First, the inter-model differences are discussed in Section 5.1.1. After that, in Section 5.1.2, the multi-model mean flood maps are discussed. Lastly, the intermediary conclusions are stated in Section 5.1.3.

5.1.1 Inter-model differences

The flood hazard maps derived by Ward et al. (2020) were analysed to gain knowledge on the differences in projected flood hazard for the various GCMs. They were analysed on the topics of inundation depth and extent. The results for RCP8.5 for inundation depth and extent are respectively visualised in Figure 5.1a and 5.1b. The results for RCP4.5 can be found in Appendix E.1 and are comparable to the ones visualised in this section.

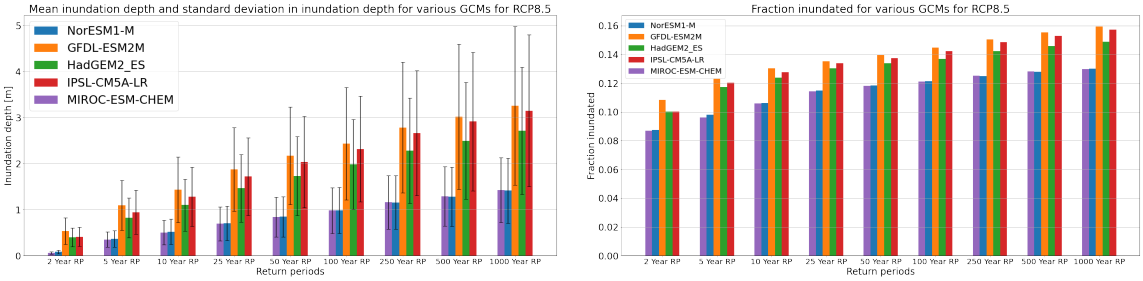

(a) *A histogram of the mean inundation depth and the standard deviation in inundation depth.*

(b) *A histogram of the fraction of surface inundated. This is calculated by dividing the total inundated area by the total evaluated area.*

Figure 5.1: *Histograms concerning the 5 evaluated GCMs for various RPs and climate scenario RCP8.5.*

Concerning inundation depth, significant differences are visible between the GCMs, as visualised in Figure 5.1a. The GFDL-ESM2M GCM and the IPSL-CM5A_LR GCM result, over the whole range of RPs, in twice as much mean inundation[1] as the NorESM1-M GCM and the MIROC-ESM-CHEM GCM. Also, the standard deviation in inundation depth varies significantly over the evaluated models, seemingly being positively correlated with inundation depth.

Concerning flood extent, the various GCMs agree significantly more. This follows from the fact that (i), according to Figure 5.1b, the fraction of inundated surface is similar for the various GCMs. And from the fact that (ii) the various GCMs predict similar spatial distributions of flood extent, as is visualised in Figure 5.2.

[1]Only inundated cells are incorporated in the mean.

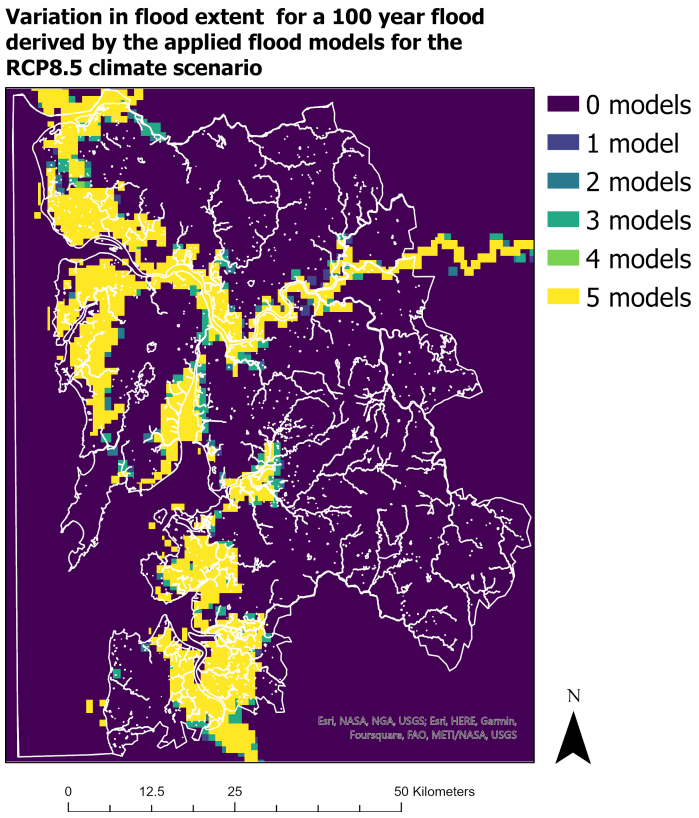

Figure 5.2: *A map for the projected inundation extent of a 100 year flood for RCP8.5 by the various GCMs.*

5.1.2 Multi-model mean flood hazard maps

As discussed in Section 3.3, sets of flood hazard maps, including RP floods in the range of [2, 1000] year, for the climate scenarios RCP4.5 and RCP8.5 for 2050 were arrived at by taking the equally weighted multi-model mean over the multi-model ensembles. These multi-model mean flood hazard maps are discussed in this section regarding their inundation depth and extent.

Inundation depth

Based on Figure 5.3, a discussion takes place in this section.

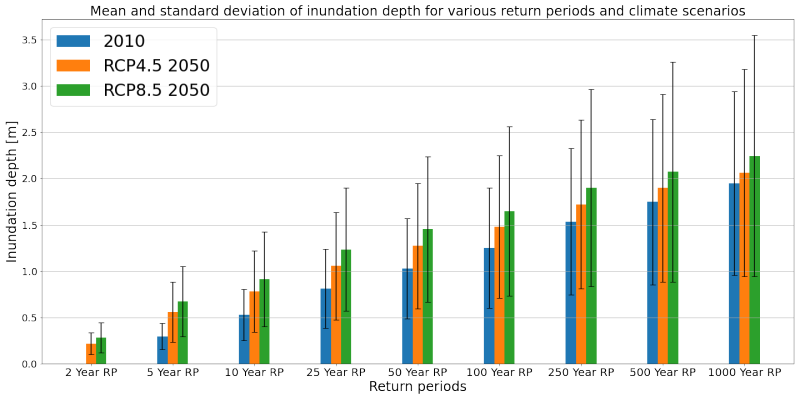

Figure 5.3: *A histogram concerning the projected inundation depth for various RP flood hazard maps, based on a multi-model mean of the available models from Aquaduct for climate scenarios RCP4.5 and RCP8.5, compared with the projected inundation depth for 2010. For 2010 the 2 year RP was not available.*

Concerning projected inundation depth, an increase in the mean inundation depth[2] can be observed for all RPs for RCP4.5 and RCP8.5 compared with 2010. This increase in mean inundation depth for 2050 is, in absolute terms, of a similar order of magnitude for the various RPs, resulting in, relatively, the largest increase for the shorter RPs (5 and 10 year). The relative increase from 2010 to the RCP scenarios for 2050 falls in the range of $[10, 160]$%. Furthermore, mean inundation depth increases significantly with increasing RP. In general, a 1000 RP flood results in 10 times the mean inundation depth of a 2 year RP flood.

Concerning the standard deviation, remarkable is that for both RCPs, -although it increases for longer return periods as expected- it remains relatively small for longer RPs. Consequently, this results in a relatively small standard deviation over the full range of RPs for both RCPs, which indicates that if a flood occurs, the majority of inundated land experiences a similarly high inundation depth.

Inundation extent

Based on Figure 5.4, a discussion occurs in this section.

[2]Only inundated cells are incorporated in the mean.

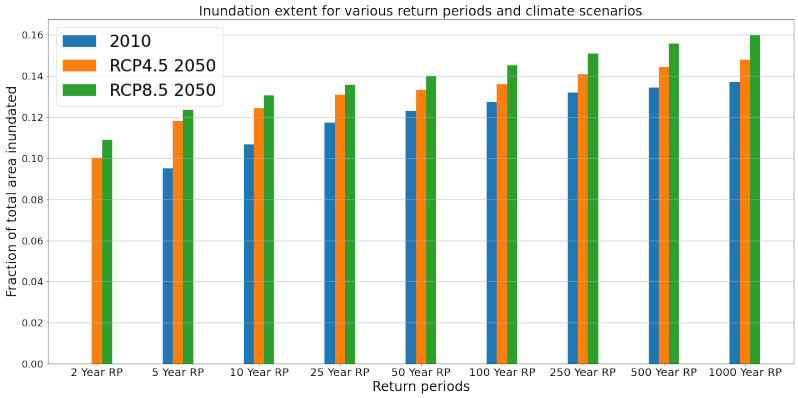

Figure 5.4: *A histogram concerning the projected inundation extent for various RP flood hazard maps, based on a multi-model model mean of the available models from Aquaduct for climate scenarios RCP4.5 and RCP8.5, compared with the projected inundation extent for 2010. For 2010 the 2 year RP was not available.*

Concerning projected inundation extent, an increase in the inundation extent can be observed for all return periods for RCP4.5 and RCP8.5 compared with 2010. This increase in inundation extent for 2050 is, in absolute terms, of a similar order of magnitude for the various RPs, resulting in, relatively, the largest increase for the shorter RPs (5 and 10 year). The relative increase from 2010 to the RCP scenarios for 2050 falls in the range of $[10, 35]\%$. When the relative increase in inundation extent is compared with the, in Figure 5.3 visualised, relative increase in inundation depth, one can conclude that the RCP scenarios predict a significantly greater relative increase in inundation depth than inundation extent.

Further notable is the relatively stable fraction of the total area inundated as a function of RP for the three scenarios. In general, a 1000 RP flood results in 1.5 times the inundated fraction of land of a 2-year RP flood, which indicates a relatively stable inundation extent, independent from the return period of the flood.

Spatial analysis

In this section, two of the most divergent flood hazard maps are evaluated (2010, 5 year RP and 2050 RCP8.5, 1000 year RP) to gain spatially explicit knowledge concerning the whole range of possible inundation extent and depth. Figure 5.5 illustrates the flood hazard maps considered in this section.

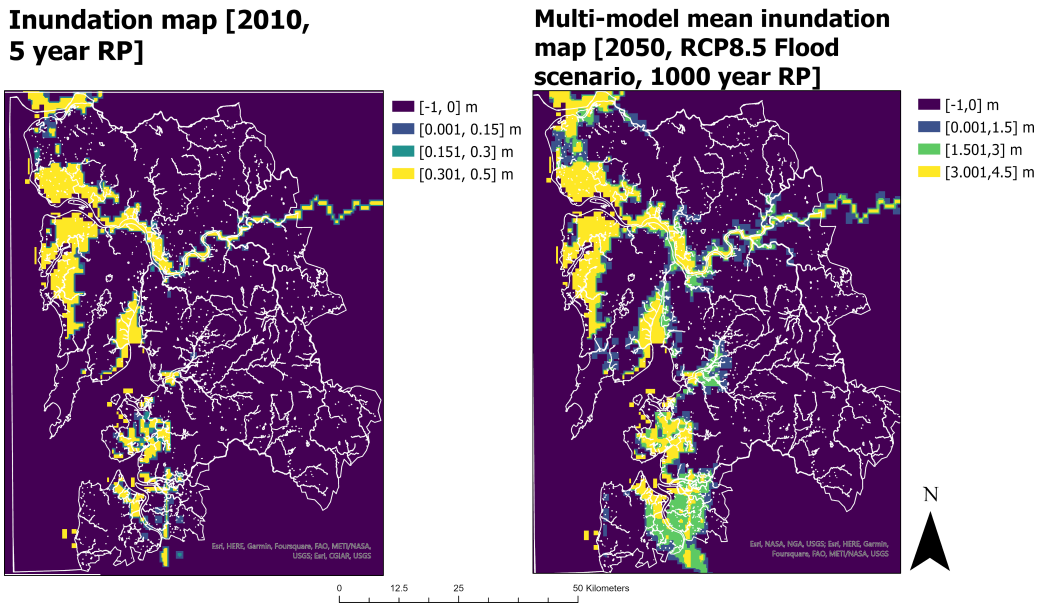

Figure 5.5: *Inundation maps for (i) a 2010, 5-year RP flood and (ii) 2050, 1000 year RP flood for RCP8.5, which is based on the multi-model mean. Note that the legends for both inundation maps are different, to indicate that their extent is similar.*

Firstly, Figure 5.5 confirms the relatively stable inundation extent for various return periods and climate scenarios, which was earlier hypothesised. Secondly, unlike the inundation extent, inundation depth significantly increases, as can be observed by comparing the legends. Thirdly, most inundated land is part of one inundation depth categorisation, resulting in almost binary maps with certain areas being heavily inundated and the rest experiencing no inundation. This is coherent with the discussed small standard deviation of the inundation depth.

Assuming that these evaluated maps span the whole range of inundation depth and extent, we can conclude that, over the various RP floods and climate scenarios, (i) the inundation extent is relatively stable, while (ii) the inundation depth varies in several orders of magnitude.

5.1.3 Conclusion

Several conclusions can be drawn from the analysis of the multi-model mean RCP4.5 and RCP8.5 flood hazard maps.

1. The various GCMs result in significantly different flood depths but similar flood extents.
2. Both mean inundation depth and extent will increase for future climate, according to the multi-model mean. However, inundation extent will experience, in relative terms, a less significant increase than mean inundation depth.
3. Concerning variability over time, the mean inundation depth varies strongly with increasing RP, while the inundation extent stays relatively constant with increasing RP.
4. Concerning variability over space, if a flood occurs, this results in most inundated areas experiencing similar inundation depths.

The analysis results indicate that the estimated inundation extent associated with riverine floods (i) is relatively independent of the GCM considered, (ii) is not highly uncertain in light of future climate, (iii) does not differ significantly per RP flood and (iv) is not projected to increase drastically for the future.

What is disputed for the future is the inundation depth, which varies significantly for the climate scenarios, and various RPs. However, what appears certain is that an increase in mean inundation depth can be expected for both the optimistic (RCP4.5) and the pessimistic (RCP8.5) climate scenario. Also, the variability over space appears to be limited.

5.2 Business-as-usual Scenarios

This section discusses the business-as-usual (BAU) land-use scenario and its flood resilience.

First, in Section 5.2.1, land use associated with BAU growth is discussed. After that, in Section 5.2.2, statistics concerning vulnerable areas are discussed. Furthermore, in Section 5.2.3, a statistical discussion occurs regarding the resilience indicators. Moreover, in Section 5.2.4, a spatially explicit discussion takes place regarding the resilience indicators. Lastly, the intermediary conclusions are stated in Section 5.2.5.

5.2.1 BAU land-use

In this section the most relevant land-use patterns, in case of BAU growth, are discussed. This is done by comparing land use in 2010 with land use in 2050, as visualised in Figure 5.6. The naming of regions is based on the designations as visualised in Appendix B.1.

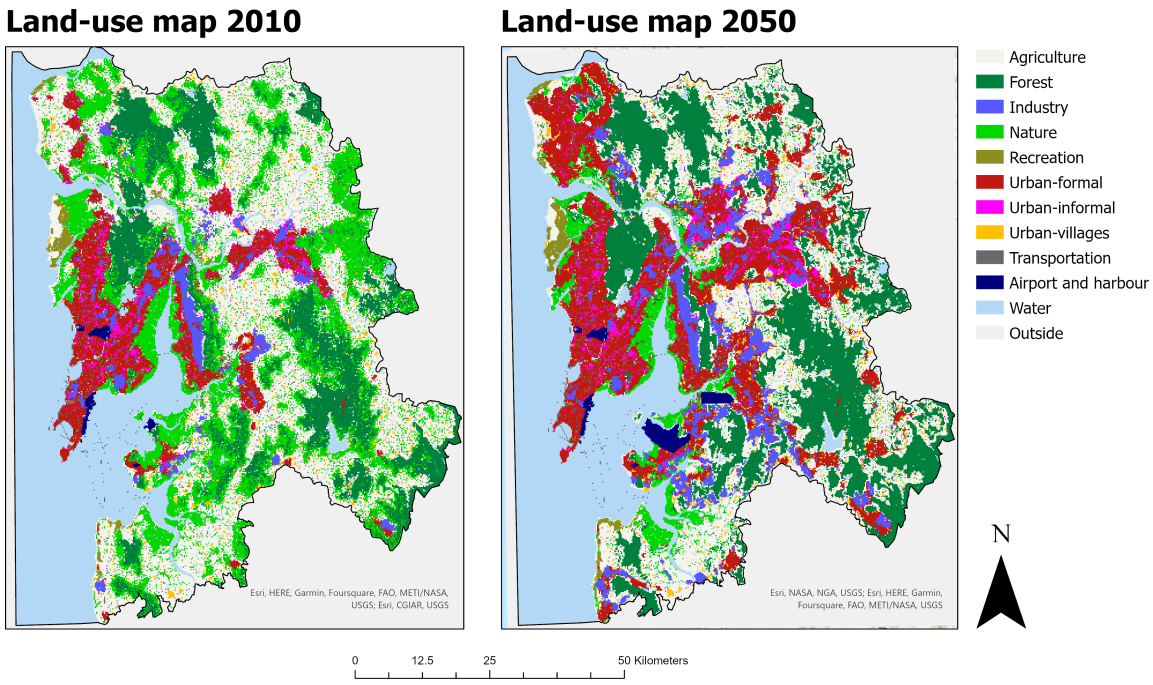

Figure 5.6: *A figure on the simulated land-use maps for 2010, and 2050. The land-use map for 2050 is generated based on a threshold value of 0.2. For further information on the derivation of the land-use map for 2050 we refer to Section 4.1.7.*

- Concerning Industry, growth can be observed more towards the periphery, while Industry in the urban core is reducing through take-over from Urban-Formal. Especially significant industrial growth is visible in the southern regions of Uran and Panvel and around the city of Bhiwandhi.
- Concerning Urban-Formal, all urban-formal clusters experience growth, and several new clusters emerge. More specifically, large urban-formal clusters emergence in Vasai, Ulhasnager, Kalyan and Panvel, while smaller urban-formal clusters emerge in Bhiwandi, Uran Khalapur, Karjat and Alibagh. Generally, Urban-Formal takes over from Agriculture, Nature, and in the core, from Industry.

- Concerning Urban-Informal, growth is mainly located near industrial areas and urban clusters. Concerning locations it was already located in 2010, persistence can be observed.
- Concerning Urban-Villages, little to no change occurs due to Urban-Villages' high inertia and stable demand.
- Concerning Transportation, no growth is observed since Transportation was modelled as a feature class and hence does not change over time. However, monetary damage curves were available; hence, Transportation is considered for the total EAMD estimate.
- Although Airport and Harbour was modelled as a feature class, growth can be observed. This is because these areas were manually changed for the period [2016, 2050] to account for the emergence of the Navi-Mumbai International Airport and the growth of the harbour, as described in MMR (2016). However, even though this growth is visible on the map, no monetary damage curves were available for this land-use class from Huizinga et al. (2017); hence Airport and Harbour was not considered for the total EAMD estimate.

5.2.2 Vulnerable areas

The earlier discussed BAU growth is accompanied by an increase in inundation extent, as discussed in Section 5.1. Together these factors increase the possibly affected area. A discussion concerning this takes place in this section based on Figure 5.7. Note that only the built-up classes of Industry, Urban-Formal, Urban-Informal, Urban-Villages, Transportation, and Airport and Harbour were considered to be affected by floods.

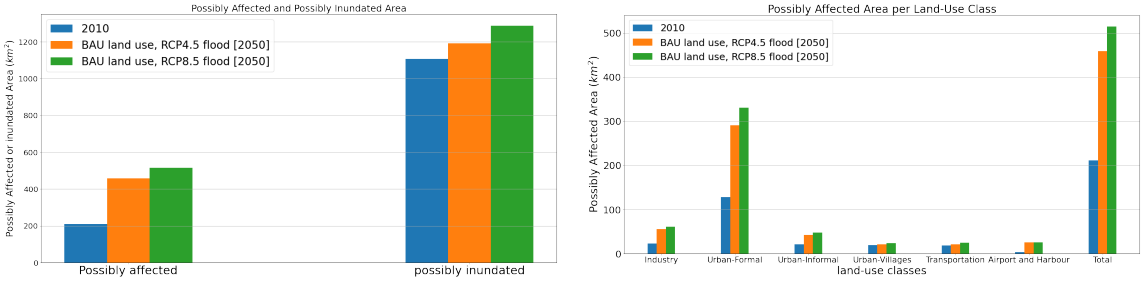

(a) *A histogram concerning the projected inundated and affected areas.*

(b) *A histogram concerning the projected affected areas for several land-use classes.*

Figure 5.7: *Histograms for the scenarios (i) BAU land-use, RCP4.5 flood, and (ii) BAU land-use, RCP8.5 flood, compared with estimations for 2010.*

From Figure 5.7a can be derived that an increase in the possibly inundated area can be expected for the future for both the RCP4.5 and the RCP8.5 climate scenario, subsequently resulting in a larger portion of built-up land getting affected by floods. Furthermore, the RCP8.5 climate scenario will result in more possibly inundated areas and more possibly affected areas than the RCP4.5 climate scenario. Additionally, in both the RCP4.5 and the RCP8.5 scenario, the amount of affected area will increase more than the amount of inundated area. This can only be explained by an increase in built-up in flood-vulnerable locations. Lastly, the difference in the possibly affected area is greater between the 2010 estimation and the RCP scenarios than between the two RCP scenarios, indicating that, independently from the exact climate future, undesired consequences will arise.

From Figure 5.7b can be derived that even though the possibly affected area increases for all the land-use classes, the total increase can mainly be attributed to the urban-formal land-use class.

Furthermore, relatively Airport and Harbour increases the most, while Industry, Urban-Formal, and Urban-Informal experience a doubling in possibly affected area.

5.2.3 Resilience BAU scenarios: statistics

In Sections 5.1 and 5.2.2 we have (i) confirmed that the inundation extent and depth will increase for all RP floods for 2050 in both the RCP4.5 and the RCP8.5 scenario and (ii) deduced that the possibly affected area will increase for both RCP4.5 and RCP8.5 due to the increase in inundation extent and the further growth of built-up land at flood-prone locations. This section discusses how these changes affect the system's resilience based on the earlier defined resilience indicators.

Expected annual monetary damage (EAMD) and Expected annual population affected (EAPA)

The EAMD and EAPA were derived by the in Section 4.2 discussed approach. A discussion on the EAMD and EAPA for the BAU scenarios compared with 2010 estimates takes place in this section based on Figure 5.8.

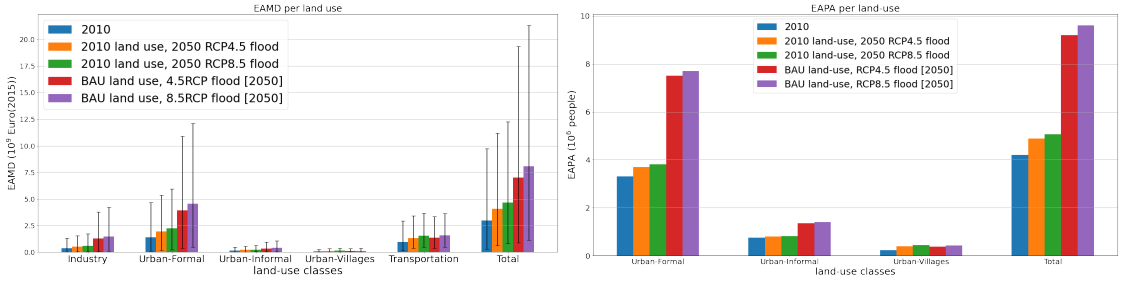

(a) *A histogram concerning the projected EAMD.* **(b)** *A histogram concerning the projected EAPA.*

Figure 5.8: *Histograms concerning the scenarios (i) BAU land use, RCP4.5 flood scenario, (ii) BAU land use, RCP8.5 flood scenario, compared with estimations for 2010.*

Firstly, Figures 5.8a and 5.8b visualise how, in the case of BAU urban growth and climate scenarios RCP4.5 and RCP8.5, both EAMD and EAPA are projected to increase. Concerning tangible monetary terms, Urban-Formal, Industry and Transportation contribute the most to the total EAMD. Concerning the intangible, Urban-Formal and Urban-Informal contribute most to the total EAPA.

Also remarkable is that the estimated EAMD and EAPA for RCP4.5 and RCP8.5 for the various land-use classes are relatively similar. This can be explained by (i) the similarity of the climate scenarios in terms of inundation extent and (ii) although inundation depth does differ for the two climate scenarios, this does not result in very big differences in estimated damage, due to the shape of the stage-damage functions, which flatten for higher flood depth in case of EAMD, and do not increase for higher flood depth in case of EAPA.

Furthermore, two additional scenarios were added in Figure 5.8. The first considers the land use of 2010 with the RCP4.5 flood scenario for 2050 and the second considers the land use of 2010 with the RCP8.5 flood scenario for 2050. These were added to allow differentiation between the impact of climate change and land-use change on the increase in EAMD and EAPA. In these additional scenarios, all added EAMD and EAPA relative to 2010 originates from climate change. Subsequently, the added EAMD and EAPA due to land-use change can be delineated when these

scenarios are compared with the 'BAU land-use and RCP4.5 flood' scenario and 'BAU land-use and RCP8.5 flood' scenario.

From the comparison of the various scenarios can be concluded that in case of BAU land-use and the RCP4.5 climate scenario, ≈ 27% (≈ 14%) of the increase in EAMD (EAPA) can be attributed to climate change and ≈ 73% (86%) of the increase in EAMD (EAPA) can be attributed to land-use change. While for RCP8.5, ≈ 33% (≈ 16%) of the increase in EAMD (EAPA) can be attributed to climate change and ≈ 66% (84%) of the increase in EAMD (EAPA) can be attributed to land-use change. Note that the significance of the EAMD is troublesome due to the large 90% confidence intervals associated with the EAMD calculation.

Percentage of annual income lost (PAIL)

The PAIL was derived by the in Section 4.2 discussed approach. A discussion on the PAIL for the BAU scenarios, compared with 2010 estimates, takes place in this section based on Figure 5.9. The fictive scenarios '2010 land-use, RCP4.5 flood' and '2010 land-use, RCP8.5 flood' were again included to differentiate between the impact of climate change and land-use change on the distribution of PAIL.

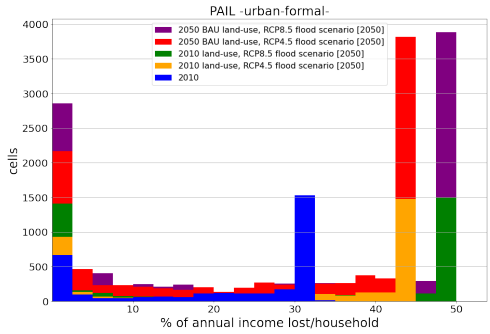

(a) *A histogram concerning the urban-formal land-use class.*

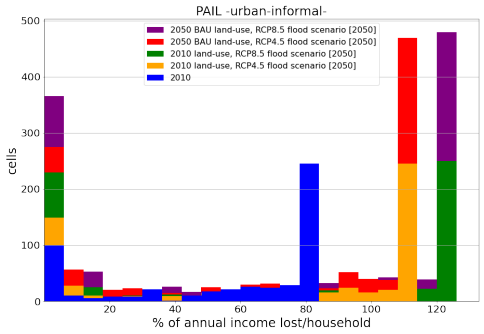

(b) *A histogram concerning the urban-informal land-use class.*

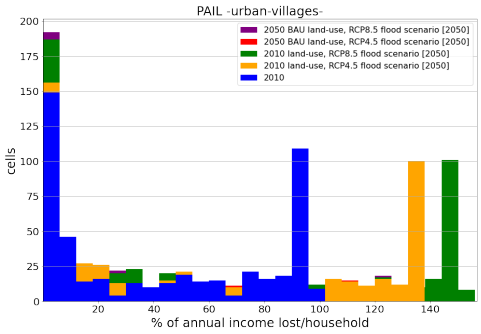

(c) *A histogram concerning the urban-villages land-use class.*

Figure 5.9: *Histograms of the percentage of annual income lost for the affected cells of the various land-use classes and various scenarios. For the individual visualisation of the various histograms, we refer to Appendix E.5.*

From Figure 5.9 can be observed that maximum PAIL is estimated to be more than double for

informal households (urban-informal and urban-villages) relative to formal households currently (2010) and in the future (RCP4.5 and RCP8.5). Also, considering the change of PAIL for the future, for all three land-use classes an increase in the spread of PAIL can be observed. Furthermore, RCP4.5 and RCP8.5 project that future climate will result, in absolute terms, in a greater increase of maximum PAIL for informal households than for formal households. In addition, one can observe how a large portion of the affected cells experiences maximum PAIL. This can be explained by the, in Section 5.1 discussed, fact that most cells are affected by similarly high inundation depths.

Furthermore, the included scenarios '2010 land-use, RCP4.5 flood' and '2010 land-use, RCP8.5 flood' lead to the conclusion that maximum PAIL depends on the climate scenario. In contrast, the distribution of PAIL is dependent on the land-use scenario. Hence, BAU land-use change is projected to result in the doubling of urban-formal and urban-informal cells in which the average household experiences maximum PAIL.

Lastly, the specific estimates for PAIL indicate that there are certain flood-prone areas where the average informal household will experience catastrophic monetary flood damage that exceeds its annual income. However, the uncertainty bounds for this calculation were projected to be large.[3] Therefore, we refrain from perceiving these exact statistics as truthful.

5.2.4 Resilience BAU scenario: spatial analysis

Based on Section 5.2.3, we can conclude that, in statistical terms, the MMR is projected to experience an increase in EAMD and EAPA, and, in general, households will experience more PAIL. This can be ascribed (i) to an increase in inundation extent and depth for both RCP4.5 and RCP8.5 and (ii) to the growth of built-up at flood-prone locations. A spatial analysis of the most vulnerable areas is discussed in this section. The naming of regions is based on the designations as visualised in Appendix B.1. For brevity, 2010 is only compared with RCP8.5. The Figures on RCP4.5 can be found in Appendix E.4.

Expected annual monetary damage (EAMD) and Expected annual population affected (EAPA)

The EAMD and EAPA were derived by the in Section 4.2 approach. A spatially explicit discussion on the EAMD and EAPA for the (2050 BAU land-use, 2050 RCP8.5 flood) scenario compared with 2010 takes place in this section based on respectively Figure 5.10 and 5.11.

[3] We refer to Section 4.2.4 for a discussion on this topic.

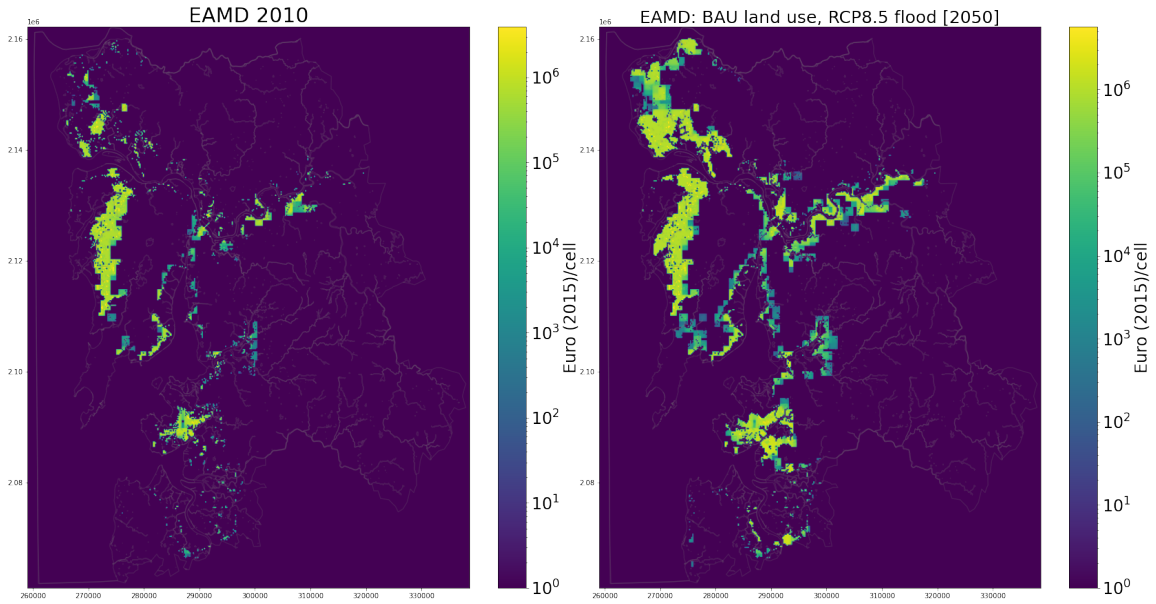

Figure 5.10: *Raster maps visualising the total EAMD spatially explicitly for the scenarios (i)2010 and (ii) BAU land use, RCP8.5 flood [2050].*

In Figure 5.10 is visible that new areas emerge in Greater Mumbai (Mumbai, Mumbai Suburban, Mira Bhayandar, Thane and Navi Mumbai), in the north (Vasai), in the north-east (Bhiwandhi), in the east along Ulhas River (Kalyan), in the south-east (Panvel) and in the south (Uran and Pen), which contribute to the increase in total EAMD. Compared with the land-use maps in Figure 5.6, one can observe that a large portion of these lands was built up over the [2010, 2050] period. This confirms the, in Section 5.2.2 discussed increase of built-up in flood-vulnerable locations. In general, the largest EAMD originates from (i) the Mumbai Suburban, Mira Bhayandar cluster, (ii) the Vasai area, (iii) the Kalyan area, and (iv) the Uran area.

Further notable is, by observing the color bar on the side, that the maximum EAMD experienced by a cell increases only from 6.6 Million Euros (2015) to 6.8 Million Euros (2015). This can be explained by the MDFs of Section 4.2.2, which flatten for higher flood depth.

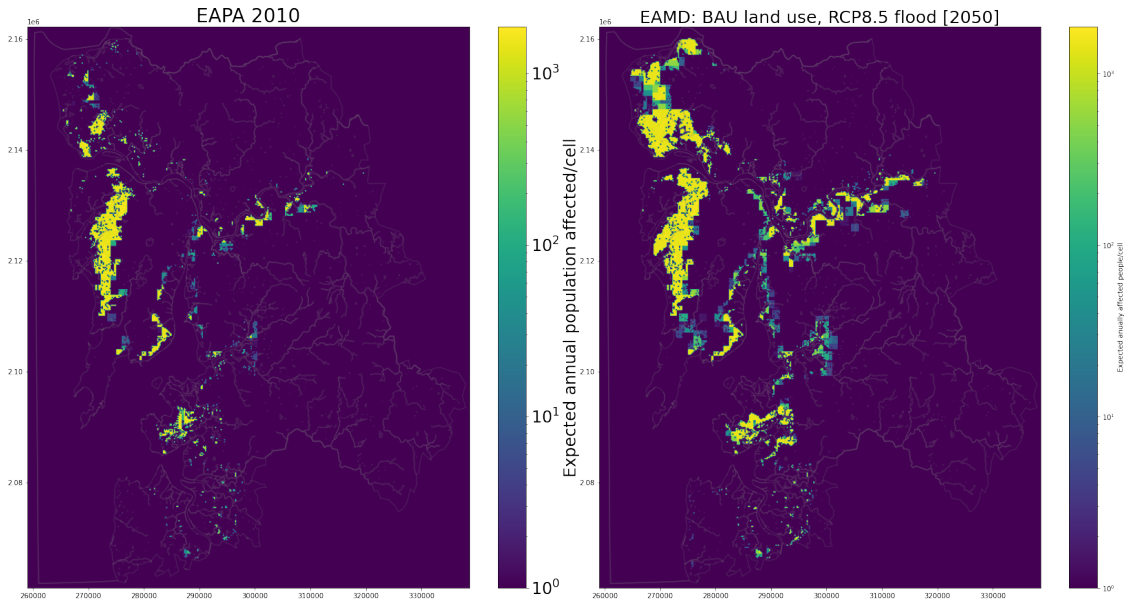

Figure 5.11: *Raster maps visualising the total EAPA spatially explicitly for the scenarios (i) 2010 and (ii) BAU land use, RCP8.5 flood [2050].*

Figure 5.11 shows that the delineated areas contributing to the total EAPA correspond to the same areas delineated by the EAMD analysis, minus the industry and transportation areas. There is no difference in maximal EAPA between 2010 and the '2050 BAU land-use, 2050 RCP8.5 flood' scenario. This can be explained by the fact that the population densities were considered constant over time, and the amount of affected people is calculated using a binary step function. We refer to Section 4.2.3 for an in-depth discussion.

Percentage of annual income lost (PAIL)

Section 5.2.3 concluded that the maximally impacted informal households already (2010) experience twice as much PAIL as the maximally impacted formal households. Also, maximum PAIL and the number of households experiencing it will increase even further due to projected land-use and climate change. Furthermore, projected land-use and climate change will hit informal households hardest. A spatial analysis concerning the most affected households is conducted in this section based on Figure 5.12.

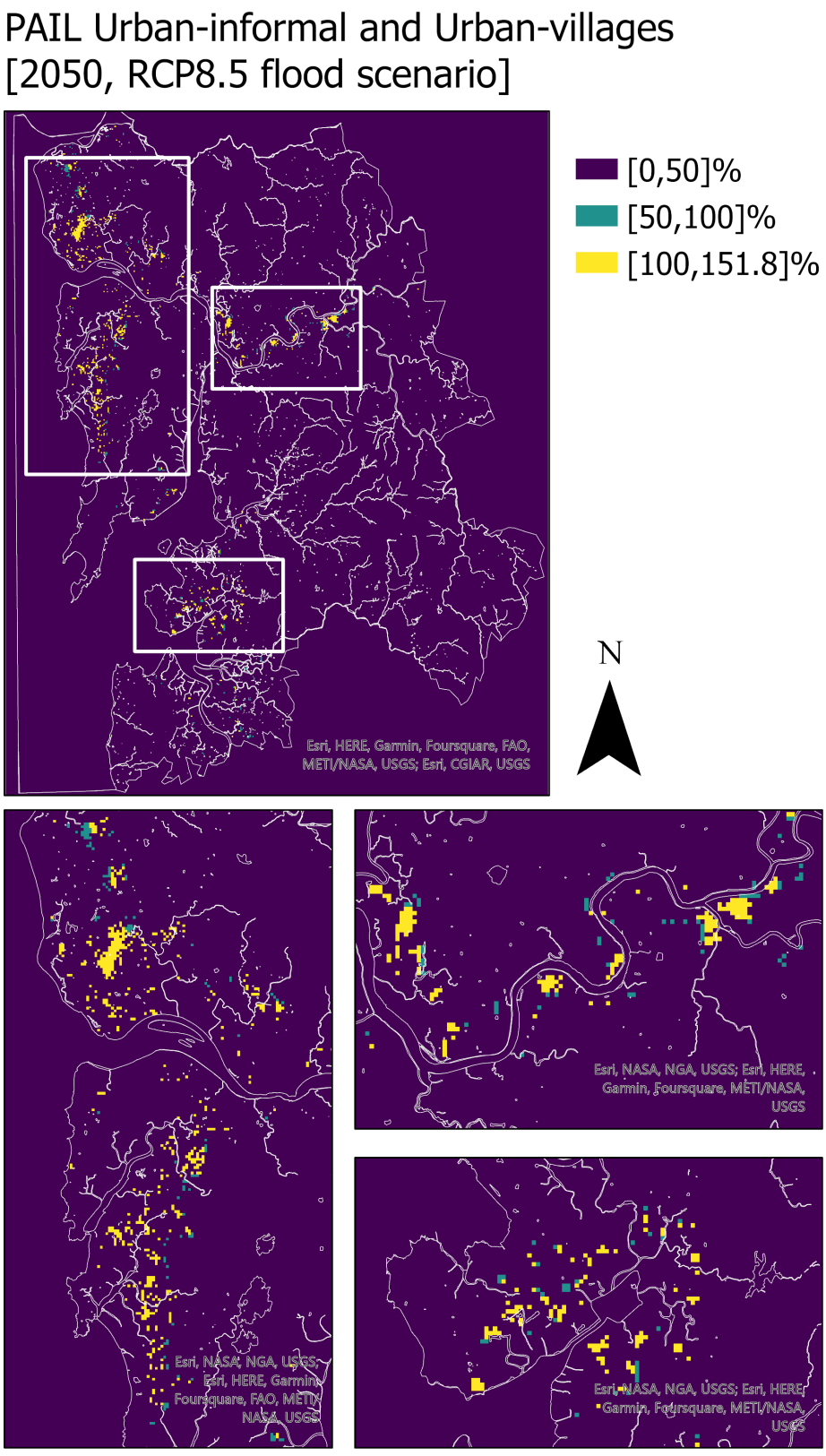

Figure 5.12: *Several high-detail maps of the areas where PAIL is* $> 50\%$*. Only land-use cells with at least a* 20% *chance of being informal in 2050 are considered, in the case of BAU land use and the RCP8.5 flood scenario.*

In Figure 5.12 the land-use cells with (i) at least a 20% chance of being informal in 2050 and (ii) with the average informal household experiencing PAIL $> 50\%$, are visualised. Three regions of major concern can be delineated.

Firstly, the north-western region (Mumbai Suburban, Mira Bhayandar and Vasai) is projected to be a major area of concern. In this region, the informal areas in Mumbai suburban and Mira Bhayandar were already present in 2010, while the informal areas in Vasai potentially appear over the [2010, 2050] period.[4] Furthermore, in the eastern region along Ulhas River (Kalyan), several informal areas are projected to experience major impacts from floods, most of which are projected to experience growth over the [2010, 2050] period. Lastly, several urban villages in the southern area of Uran are projected to experience major impacts due to floods.

5.2.5 Conclusion

Several conclusions can be drawn from the analysis of the BAU land-use scenarios.

- In case of BAU growth and RCP4.5 or RCP8.5 climate change, EAMD and EAPA, are expected to increase for all land-use classes.
- In case of BAU growth and RCP4.5 or RCP8.5 climate change, the maximum PAIL by a household and the number of households experiencing this maximum PAIL are expected to increase for all residential land-use classes.
- In relative terms, the most heavily affected households reside in informal settlements (Urban-Informal and Urban-Villages). These suffer more than twice as much relative monetary impact as the maximally impacted formal households.
- Growth of built-up area in flood-vulnerable locations contributes more to the increase in total EAMD and total EAPA, than climate change.
- In the case of BAU growth, RCP4.5 and RCP8.5 climate scenarios result in comparable total EAMD and total EAPA.
- BAU growth is projected to result in a doubling of the area where the average household experiences maximum PAIL.
- The increase in maximum PAIL can be ascribed to climate change.

The analysis results indicate how the projected BAU growth and climate scenarios result in reduced flood resilience for the MMR in light of the resilience indicators applied.

Furthermore, informal settlements will experience the most monetary damage in relative terms.

Also is derived that flood risk is comparable for the two evaluated climate scenarios.

Lastly, the majority of increased flood impact can be ascribed not to climate change but to the emergence of built-up in flood-prone locations.

For spatially explicit information on the areas that are projected to, relatively, suffer the most monetary damage, we refer to Figure 5.12.

[4] This can be observed by looking at the land-use maps in Figure 5.6.

5.3 Urban Planning Scenarios

In Sections 5.2.3 and 5.2.4 is discussed how the executed modelling exercise indicates that, in case of the projected BAU urban growth and the climate scenarios RCP4.5 and RCP8.5, (i) the MMR will experience more monetary damage, (ii) in the MMR more people will be affected by floods, (iii) in general, MMR households will lose a bigger portion of their annual income due to floods, and (iv) informal households will suffer the most significant relative impact. Therefore, the flood resilience of the MMR should be increased to counteract these undesirable developments. Hopeful, however, is that the growth in projected annual damage mainly originates from urban growth in flood-vulnerable locations, not climate change. This empowers the MMR and allows it to tackle a large part of the problem locally.

As discussed in Section 3.2, the adaptation of the urban environment through urban planning that alters the flood-risk-land-use interaction poses a valid option to decrease flood risk and subsequently increase urban flood resilience. Urban planning, in this case, aims to guide the city's structure so that flood-vulnerable land use is mainly located away from flood-prone areas. Furthermore, Sections 3.3.4 and 3.3.5 discuss how, in this thesis, two factors are varied that influence the flood-risk-land-use interaction; the perception of future climate and the strictness of urban planning. In this section, an analysis is executed on the two varied factors to gain knowledge on the potential pathways of land-use change towards resilience. Hence, this section aims to answer SQ4:

What are potential pathways of land-use change towards resilience considering flood risk-land-use interaction for MMR that can be derived from the results of the land-use simulations?

Firstly, in Section 5.3.1, the acquired flood resilience through urban planning based on RCP4.5 and RCP8.5 are compared. After that, in Section 5.3.2, the acquired flood resilience through urban planning with weak, mediocre and strict zoning are compared. These discussions are both based on Figures 5.13 and 5.14; hence these are displayed here. The '2010 land use, 2050 RCP4.5 flood' and '2010 land use, 2050 RCP8.5 flood' scenarios are again included. These can be considered hypothetical 2050 scenarios in which no growth occurred over the [2010, 2050] period. These scenarios again allow us to differentiate between the impact of climate change and land-use change on the increase in EAMD and EAPA, as was previously done in Section 5.2.3. Lastly, in Section 5.3.3, the intermediary conclusions are stated.

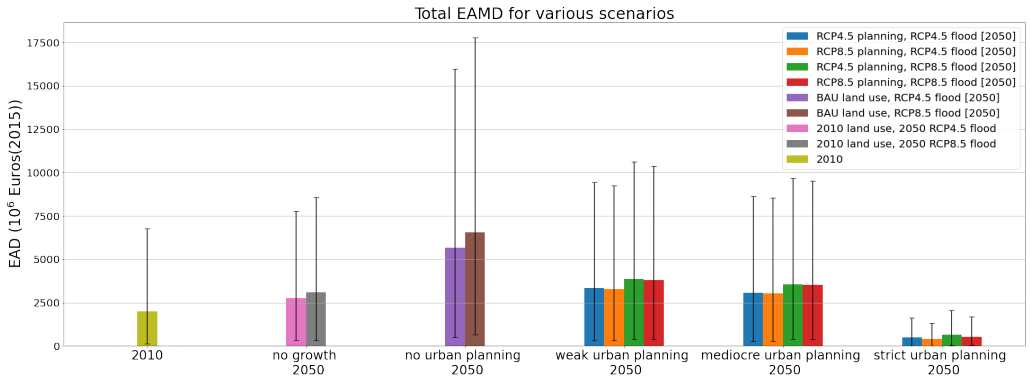

Figure 5.13: *A figure on the total EAMD for various scenarios. Concerning the included scenarios, the naming goes as follows. RCP4.5 planning indicates that urban planning was based on RCP4.5. RCP4.5 flood indicates that the flood hazard maps that were laid on top of the land-use map were coherent with RCP4.5. If '2050' is in square brackets at the end of the scenario name, it indicates that both land use and flood hazard were derived for 2050. Note, the total EAMD estimates only includes the land-use classes that could be influenced by urban planning: industry, urban-formal, urban-informal, urban-villages.*

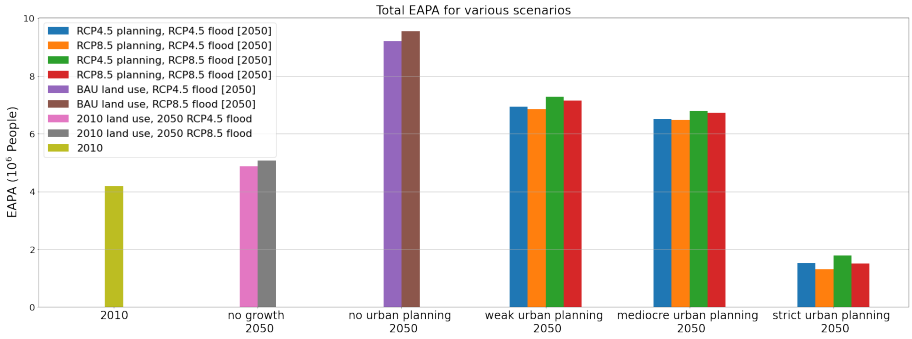

Figure 5.14: *A figure on the total EAPA for various scenarios. Concerning the included scenarios, the naming goes as follows. RCP4.5 planning indicates that urban planning was based on RCP4.5. RCP4.5 flood indicates that the flood hazard maps that were laid on top of the land-use map were coherent with RCP4.5. If '2050' is in square brackets at the end of the scenario name, it indicates that both land use and flood hazard were derived for 2050.*

5.3.1 Climate scenario

In Figures 5.13 and 5.14 can be seen how, by establishing urban planning based on the RCP8.5 scenario, instead of the RCP4.5 scenario, some decrease in total EAMD and EAPA can be achieved for any strictness, however only marginal. This same pattern can be observed for the EAMD and EAPA for individual land-use classes, which are respectively visualised in Figure 5.15 and Appendix E.6. The similarity of the resilience indicator values of urban planning based on RCP4.5 and RCP8.5, is explained by the similarity of the flood risk zones delineated based on the two climate scenarios, as visualised in Section 3.3.4.[5]

[5] A visual comparison between the various RP flood maps of the two climate scenarios was executed to analyse if more variation would be arrived at by basing the FRZs on other RP floods. In this analysis, the flood depth threshold for the various FRZs was kept at 0.5 m. However, for other RP floods, differences between the urban plans remained marginal.

Hence, one can conclude that if one applies the urban planning strategy as discussed in Section 3.3.4, basing the urban planning on the RCP8.5 climate scenario does only marginally result in an increase in acquired resilience over basing urban planning on the RCP4.5 climate scenario. However, note that this does not exclude the possibility that a *certain* urban planning strategy based on a different flood depth threshold and different delineation of the FRZs, does result in a significant increase in acquired resilience for urban planning based on the worst-case scenario over urban planning based on the optimistic scenario.

5.3.2 Urban planning strictness

Figures 5.13 and 5.14 show that the strictness of urban planning significantly impacts the resilience of the system. Weak and moderate urban planning result in a significant decrease in total EAMD and EAPA for 2050 compared to the BAU scenario (no urban planning), while strict urban planning results in less total EAMD and EAPA for 2050 than for 2010.

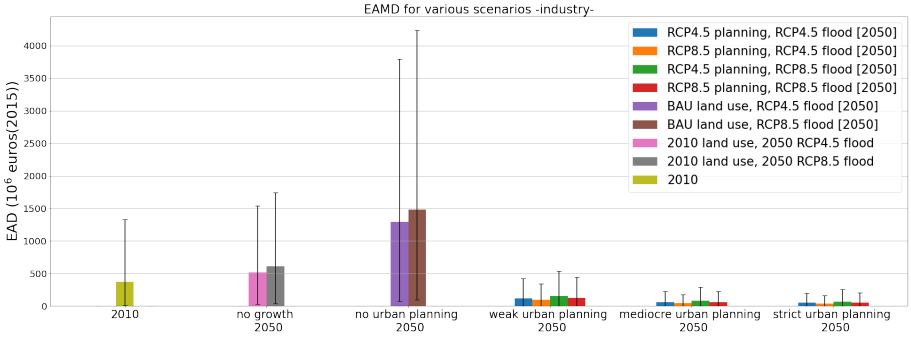

(a) *A figure concerning the industry land-use class.*

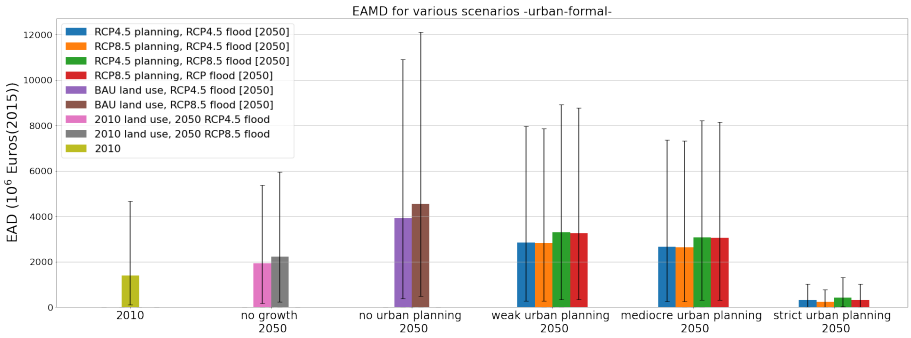

(b) *A figure concerning the urban-formal land-use class.*

Figure 5.15: *Figures on the EAMD per land-use class for various scenarios. Concerning the included scenarios, the naming goes as follows. RCP4.5 planning indicates that urban planning was based on RCP4.5. RCP4.5 flood indicates that the flood hazard maps that were laid on top of the land-use map were coherent with RCP4.5. If '2050' is in square brackets at the end of the scenario name, it indicates that both land use and flood hazard were derived for 2050.*

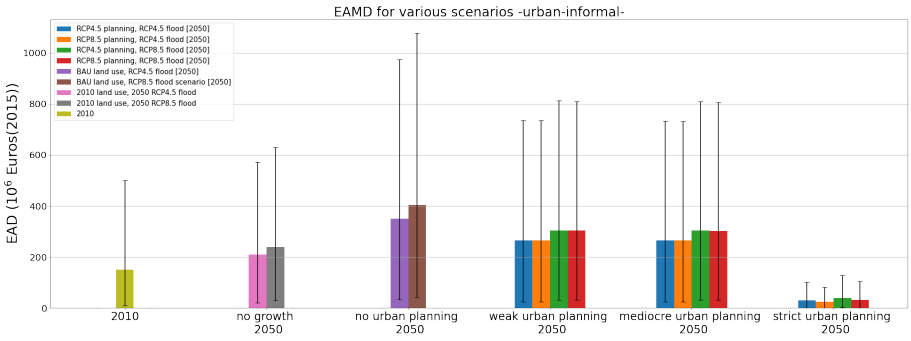

(c) *A figure concerning the urban-informal land-use class.*

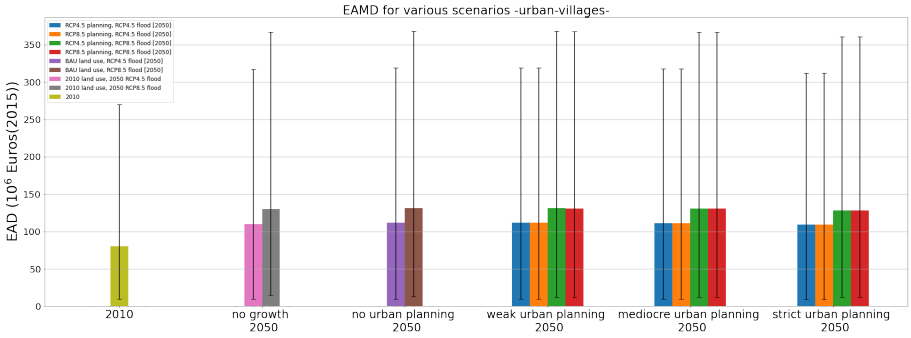

(d) *A figure concerning the urban-villages land-use class.*

Figure 5.15: *Figures on the EAMD per land-use class for various scenarios. Concerning the included scenarios, the naming goes as follows. RCP4.5 planning indicates that urban planning was based on RCP4.5. RCP4.5 flood indicates that the flood hazard maps that were laid on top of the land-use map were coherent with RCP4.5. If '2050' is in square brackets at the end of the scenario name, it indicates that both land use and flood hazard were derived for 2050.*

In Figure 5.15, the EAMD is visualised per land-use class.[6] Herein is shown how the decrease in EAMD as a function of urban planning strictness differs per land-use class. EAMD for Industry already reduces tot below-2010-levels at weak urban planning, EAMD for Urban-Formal and Urban-Informal only reduces to below 2010 levels at strict urban planning, and EAMD for Urban-Villages does not appear to vary with urban planning strictness.

This varying response to urban planning strictness originates from the fact that the land-use classes have varying characteristics and are therefore modelled differently, using varying configurations of the various land-use change influencing factors; neighbourhood rules, accessibility, suitability and urban planning policies. In real-world terms, this varying response indicates that some land-use classes are more disobedient than others or have nowhere else to go.

Helpful concerning the construction of land-use specific urban planning policies would be to acquire knowledge on the required urban planning strictness that directly results in the movement of particular land-use classes. I.e. the government needs to be very strict concerning land-use class A, but less strict urban planning is required for land-use class B. However, even though all land-use classes are treated equally,[7] it remains problematic to determine the direct response of land-use classes to urban planning. An example best explains this.

[6] EAPA can be found in Appendix E.6 and shows the same behaviour.

[7] In the applied urban planning approach, all land-use classes are treated with equal urban planning strictness if present in the same FRZ.

Consider a scenario where Urban-Formal and Urban-Informal are clustered in a region, Urban-Informal is attracted by Urban-Formal, and both land-use classes are considered in the urban planning approach with equal strictness. Suppose Urban-Formal responds to urban planning by reallocating to a different region, and Urban-Informal also moves away. In that case, one cannot delineate if the reallocation of Urban-Informal is directly caused by urban planning or indirectly by the reallocation of Urban-Formal. Problematic here is the fundamental interconnectedness of the various land-use classes through the neighbourhood rules. A multi-variate sensitivity analysis is required to determine how the various land-use classes are directly influenced by varying urban planning strictness.

Consequently, determining the direct response of land-use classes to urban planning is problematic. However, some land-use specific knowledge can still be deduced from Figure 5.15, by remembering that the varying response to urban planning strictness originates from the fact that the land-use classes are modelled differently. Therefore, one can derive some land-use-specific knowledge from a visual analysis of the land-use model and general knowledge of the configuration of the various land-use classes. Industry, for example, was calibrated to have significantly lower inertia than Urban-Formal, Urban-Informal and Urban-Villages, contributing to Industry responding at weak urban planning, in contrast to Urban-Formal, Urban-Informal and Urban-Villages. Furthermore, Urban-Informal and Urban-Villages were calibrated to have the same high inertia; however, Urban-Informal was calibrated to have an attraction to the land-use classes of Industry and Urban-Formal through the neighbourhood rules. This attraction of Urban-Informal to Urban-Formal and Industry appears to result in Urban-Informal moving away if Urban-Formal and Industry move away. On the other hand, Urban-Villages is generally not located next to Urban-Formal and Industry and was calibrated to experience less attraction to these same land-use classes. This appears to results, together with its high inertia, in the little reaction of Urban-Villages to urban planning. Note that the potential indirect response to urban planning[8] indicates that land-use classes might not have to be directly influenced to be removed from an area.

Furthermore, visual analysis of the land-use model concerning the impact of urban planning strictness on Urban-Formal indicates a two-step response. With weak and moderate urban planning, the *growth* of Urban-Formal is restricted in flood-prone areas. Apparently, a certain threshold is crossed that is located in between no urban planning and weak urban planning, which convinces cells to stop locating in flood-prone areas. Note that the observed difference between the EAMD for the 'no growth scenarios' and the weak and mediocre urban planning scenarios originates from the urban growth that took place during the period [2010, 2023].[9] In contrast, with strict urban planning, Urban-Formal present in flood-prone areas is directly 'evacuated'. Here again, a certain threshold is crossed that is located in between mediocre urban planning and strict urban planning, which results in the movement away from flood-prone areas by urban-formal cells.

Lastly, when comparing Figure 5.15b and 5.15c to Figure 5.13, and acknowledging the relevance of Urban-Formal concerning the total EAMD,[10] it appears that the evacuation response of Urban-Formal to strict urban planning is the cause of the significant decrease in total EAMD from mediocre urban planning to strict urban planning.

5.3.3 Conclusion

Several conclusions can be drawn from the analysis of the various urban planning scenarios.

[8] Again, to acquire certainty, a multi-variate sensitivity analysis is required.

[9] Recall that urban planning was implemented in 2023, as discussed in Section 3.3.5.

[10] We refer to Figure 5.7b for a visualisation of this.

- Basing urban planning on the pessimistic RCP8.5 climate scenario only results in a marginally more resilient urban environment over basing urban planning on the optimistic RCP4.5 climate scenario if urban planning is executed as discussed in this thesis.
- Application of the weak, mediocre and strict urban planning approaches all result in a more resilient urban environment for 2050 relative to the 2050 BAU land-use scenario.
- Application of the weak and mediocre urban planning approaches result in a stabilisation of total EAMD for 2050, relative to 2010.
- Application of the weak and mediocre urban planning approaches results in a decrease in total EAPA relative to the 2050 BAU land-use scenario.
- Application of the strict urban planning approach is far more effective than weak and mediocre urban planning in reducing total EAMD and EAPA and even results in lower values for the two resilience indicators for 2050 relative to 2010.
- Land-use classes vary differently with urban planning strictness, due to their varying characteristics.
- If urban planning is implemented as done in this thesis, EAMD for Industry already converges to zero if weak urban planning is applied. On the other hand, EAMD for Urban-Formal and Urban-Informal reduces for any urban planning strictness; however only converges to zero for strict urban planning, and Urban-Villages does not respond to either weak, mediocre, or strict urban planning.
- Land-use classes can also indirectly be affected by urban planning.

These conclusions confirm that the resilience acquired by urban planning is only marginally dependent on the exact climate future considered, in case an urban planning approach is applied similarly to the one applied in this thesis.

Secondly, these conclusions indicate that any application of urban planning for the MMR contributes to the resilience of the system, while more strict urban planning contributes most to the resilience of the system.

Also, these conclusions indicate that land-use classes react differently to urban planning and hence need land-use-specific treatment.

Lastly, these conclusions indicate that land-use classes can also indirectly be influenced through their interaction with other land-use classes.

Chapter 6

Conclusion

The conclusion of this thesis is discussed in this final chapter. First, in Section 6.1 the answers to the various sub-questions and main research question are discussed. After that, Section 6.2 discusses the scientific impact of this thesis. Subsequently, Section 6.3 discusses the societal impact of this thesis. Lastly, Section 6.4 addresses limitations and future research.

6.1 Answers to the research questions

The answers concerning the various sub-questions and the main research question are discussed in this section.

[SQ1] What drivers of land-use change and flood hazards are essential to the MMR?

In recent decades, the MMR's urban growth has mainly occurred in the suburbs and satellite towns. This growth pattern is driven by a combination of factors, namely (i) further-reaching transport networks (Vinayak et al., 2021), (ii) dispersal of industries and jobs, (iii) an overfull core (MMR, 2016) and (iv) less strictly enforced urban planning regulations at the periphery (Chatterjee and Chattopadhyay, 2020). This urban growth was accompanied by decreasing green space, forest, agriculture, water bodies, wetlands and coastal lands (MMR, 2016).

In the future, a further increase in urban areas is expected due to significant population growth. The local authority projects (i) that the total built-up area will increase by a factor of approximately 1.4 during the period [2016, 2036] and (ii) that the area covered by industry and quarries will more than double in the same period. This further expansion of built-up area will mainly come at the expanse of agricultural areas, but green space and water bodies will experience a decrease. Contrarily, forests, wetlands and coastal lands are planned to increase. Furthermore, the local authority plans to significantly decrease the fraction of informal settlements of built-up areas (MMR, 2016).

Various factors determine the spatial distribution of land use. Concerning built-up land, (i) growth mainly occurs on open and arable land. Also, built-up areas have a general desire to be located close to (ii) other built-up areas (Shafizadeh-Moghadam and Helbich, 2015), (iii) economically active areas that offer jobs (such as special economic zones and business districts) (Vinayak et al., 2021), and (iv) transport networks and hubs (Chatterjee and Chattopadhyay, 2020). Furthermore, (v) high altitude and slopes are generally not considered desirable for built-up areas (Shafizadeh Moghadam and Helbich, 2013). Consequently, forest land use is often designated to such regions. Concerning industrial land, growth mainly takes place in designated areas such as special economic zones and MIDC areas (MMR, 2016).

Furthermore, several governmental regulations guide land use. Firstly, concerning industrial land, several policies constrain the emergence of several industry types in various locations (MMR, 1995; MMRDA, 2008). In contrast, the emergence of industry is also stimulated for several regions by facilitating a suitable business environment (MIDC, 2020). Secondly, several coastal regulation zones attempt to ensure that no, or not too many, constructions emerge in environmentally critical areas and too close to the shoreline (Ministry of Environment, Forest and Climate Change, 2019). Furthermore, Mumbai's heritage list and UNESCO's world-heritage list limit development close to cultural, natural, or mixed heritage (MCGM, 2016; Alsalloum, 2018).

MMR's flood vulnerability is already at an undesirable level and is projected to increase due to climate change-induced (i) sea-level rise, (ii) increased rainfall, and (iii) intensified monsoons (Murali et al., 2020). MMR's flood vulnerability is related to two sub-causes: (i) MMR's natural geography and (ii) MMR's artificial geography.

Concerning MMR's natural geography, two aspects result in significant flood vulnerability. Firstly, the MMR has a tropical wet-dry climate characterised by heavy monsoons from June until September (Vinayak et al., 2021). These heavy monsoons constitute almost all the rainfall that occurs in a year and result in riverine and urban flooding events that happen as often as 5 to 6 times per year in the low-lying areas of the MMR (Butsch et al., 2016). To make matters worse, annual precipitation, monsoon precipitation and extreme precipitation events are expected to

increase due to climate change (IPCC, 2022a, 2021). Secondly, The MMR's coastal location and low elevation levels result in coastal flooding (Abadie et al., 2020). Again, climate change will exacerbate the problem by resulting in sea-level rise, and more frequent and intensified storm surges (Patil and Deo, 2020; Ranger et al., 2011). In this thesis, the focus is on riverine flooding.

Concerning MMR's artificial geography, several aspects result in significant flood vulnerability. Firstly, the MMR's stormwater drainage system was designed for rainfall intensities that are exceeded yearly, and for runoff coefficients that apply to rural environments, not to urban environments (Chatterjee and Chattopadhyay, 2020). Furthermore, various low-lying areas fill up like a bathtub when high tide and heavy precipitation coincide since the stormwater drainage system mainly relies on gravity. In these circumstances, the drainage system cannot transport rainwater to the sea, while the reclaimed grounds become the lowest point where all the water moves towards (Hallegatte et al., 2010). Furthermore, clogging of drains and urbanisation leading to loss of natural drainage capacity, further worsen the situation (Gupta, 2007; MCGM, 2016).

Several structural adaptations to the stormwater drainage system are being implemented to improve the situation. Problematic, however, is that (i) these adaptations are turning out to be very costly, (ii) the project is still not finished ten years after the initial deadline (Chatterjee, 2019), and (iii) climate change is catching up with the design capacity for which it is constructed (Rana et al., 2014).

[SQ2] How can resilient urban planning be conceptualised and assessed for the MMR?

This thesis argues that, through urban planning, one can transform the urban environment in the face of urban floods, without attempting to change the flood regime but by guiding the structure of the city in a way that flood-vulnerable land-use classes are mainly located away from flood-prone areas. In this manner, adapting the physical landscape through urban planning can contribute to the urban flood resilience of urban environments. What constitutes *resilient* urban planning is researched in this thesis by varying two factors that influence the effectiveness of urban planning concerning achieving resilience. These varied factors are discussed in relation to SQ3.

Concerning the assessment of resilience, a direct approach was applied. This direct approach assumes that a flood-resilient city experiences little flood impact and that low flood risk is associated with high resilience and the other way around (Hammond et al., 2015). Therefore, by assessing flood risk, one can assess resilience. Subsequently, flood risk was assessed by applying several flood-risk indicators, which can also be considered resilience indicators in the context of this thesis.

Firstly, the *expected annual monetary damage* (EAMD) was applied to cover direct tangible impacts. This indicates the annual monetary damage that can be expected for an area, land-use class or the whole region. Secondly, the *expected annual population affected* (EAPA) was applied to cover direct intangible damage. This indicates the annual affected population that can be expected for an area, land-use class or the whole region. Thirdly, the *percentage of annual income lost* (PAIL) was applied to get insight into relative monetary impact. This indicates the percentage of total income lost annually by the households of the various land-use classes.

[SQ3] How can the flood-risk-land-use interaction be conceptualised for the MMR?

The flood-risk-land-use interaction was conceptualised using two aspects.

The first aspect considers that a particular land-use configuration leads to a certain flood risk. Flood risk is subsequently estimated using a variety of steps. First, the multi-model mean was applied to flood hazard maps for various global climate models, which resulted in a set of flood hazard maps that indicate flood depth and extent for several return periods. After

that, each flood hazard map was laid on top of a land-use map to derive the associated flood impact. Thereupon, the resilience indicators were estimated by combining the flood impacts concerning their probability of occurrence. In several cases, land-use allocation probabilities were also considered when estimating flood risk. We refer to Section 4.1.7 for an in-depth discussion concerning the inclusion of land-use allocation probabilities when estimating flood risk.

The second aspect considers that flood risk leads to land-use change if policies that alter the land-use configuration are based on flood hazard maps. In this modelling case study, various forms of urban planning based on flood hazard maps are compared to assess what type of urban planning results in the land-use configuration that experiences the least amount of flood risk and hence is most flood resilient. These varied factors are the *perception of future climate* and the *strictness of urban planning*.

The 'perception of future climate' refers to the climate scenario the local authority considers when designing the urban planning strategy. The considered climate scenarios were a moderate climate scenario (RCP4.5) and a worst-case climate scenario (RCP8.5). Subsequently, flood risk zones were delineated based on the flood hazard maps associated with these climate scenarios. Three flood risk zones were defined per climate scenario: low, medium and high.

The 'strictness of urban planning' refers to (i) the strictness of the policies on paper, and (ii) the strictness with which the policies are enforced. Three degrees of 'strictness' were defined: weak, mediocre, and strict.

[SQ4] What are potential pathways of land-use change towards resilience considering flood-risk-land-use interaction for MMR that can be derived from the results of the land-use simulations?

The varied factors 'perception of future climate' and 'strictness of urban planning', that alter land use based on flood risk, were combined to form a collection of six land-use scenarios. These land use scenarios were thereafter overlaid with the flood hazard maps for the two climate scenarios to assess their resilience. Several potential pathways of land-use change towards resilience can be derived from these various scenarios and their associated resilience.

Firstly, a land-use configuration's resilience is largely independent of the 'perception of future climate' if the scenarios are constructed as done in this thesis. This is explained by the similarity of the flood risk zones delineated based on the two climate scenarios, as visualised in Section 3.3.4, which again originates from the fact that flood-prone regions are relatively independent of the climate scenario one perceives.

Secondly, the resilience of a land-use configuration is highly dependent on the 'strictness of urban planning'. Strict urban planning resulted in the most resilient urban environment by initiating forced evacuation of a large portion of the flood-vulnerable land-use classes away from flood-prone areas. Furthermore, mediocre and weak urban planning resulted mainly in the reduction of growth of flood-vulnerable land-use classes in flood-prone areas.

Furthermore, the various land-use classes reacted differently to the implemented urban planning policies. Especially the most vulnerable land-use classes were troublesome to reallocate. Hence, a land-use-specific treatment is required.

Lastly, the application of urban planning can also have an indirect impact. Since, sometimes land-use classes move away since other land-use classes move away, not as a result of urban planning.

[RQ] How will the interaction of flood risk and land use impact the long-term flood resilience of cities in the Global South?

IPCC (2022b) states with high confidence that heavy rainfall events will increase worldwide and lead to increased flood risk.[1] Cities in the Global South are more at risk since flood risk in these cities is, in general, less well controlled (Kovacs et al., 2017). To make matters worse, rapid urbanisation is taking place worldwide, approximately 90% of which occurs in the Global South (Yazdani and Dola, 2013). Subsequently leading to an increase in population in flood-prone areas if no action is taken (Kim and Newman, 2020). In other words, flood hazards and population in flood-prone areas are increasing in cities in the Global South, resulting in more flood risk. According to our conceptualisation of resilience, this is associated with less flood-resilient urban environments.

Our modelling case study confirms the described doomsday scenario. It was derived that, in case no governmental intervention occurs, riverine floods will result in more affected people and more monetary damage in the MMR. Furthermore, the most vulnerable communities will relatively suffer the most.

This increasing flood risk can mainly be attributed to urban growth in flood-prone areas; not climate change-induced increased flood hazards. Unstructured growth frequently occurs in cities in the Global South (Amponsah et al., 2022); hence it seems reasonable that urban growth in flood-prone areas will significantly contribute to the increase in flood risk for various cities in the Global South.

On a more positive note, population growth in flood-prone areas, contrary to climate change, can be handled locally. According to our case study, local handling of the problem through urban planning can significantly contribute to the flood resilience of an urban environment if applied effectively.

The effectiveness of urban planning policies varied significantly per land-use class and largely depended on the strictness with which these policies were implemented and enforced. Logically, the urban environment was deemed more resilient if stricter urban planning policies were implemented and enforced, since stricter urban planning leads to more movement away from flood-prone areas, subsequently resulting in a reduction of flood risk. Problematic was that the most vulnerable land-use classes, consisting of informal settlements, were least obedient to urban planning policies. Therefore, land-use-specific treatment is required to increase the overall resilience of the system.

Contrarily, the effectiveness of urban planning policies was largely independent of the perceived climate future. This was due to two reasons. Firstly, in the case study, the flood-prone areas were largely equal for an optimistic and a worst-case climate scenario. Secondly, uncertainty associated with future climate was present in the inundation depths that these flood-prone areas will endure; however, this does not affect the effectiveness of urban planning policies.

Future climate projections, of course, cannot be generalised for the Global South. However, the case study does indicate that significant flood-prone regions are possibly uncontested and that the application of urban planning policies for these uncontested regions can be promising for constructing more resilient urban environments.

[1] This thesis has only included riverine floods that result from increased heavy rainfall events in the modelling case study. Hence we constrain ourselves from discussing other flood types in this conclusion.

6.2 Scientific impact

This study has addressed several literature gaps, which were derived in Section 1.1.2. How these gaps were addressed, and the associated issues are addressed in this section.

6.2.1 Coupling a land-use model and flood hazard maps for a city in the Global South

To our knowledge, no studies have linked a land-use model and flood hazard maps while incorporating flood-risk-land-use interaction for an area in the Global South. This thesis addressed this gap by creating a land-use model, collecting flood hazard maps, and establishing an interaction between the two for the MMR. This process involved several issues.

Concerning the generation of the land-use model for the MMR, several problems arose. To begin with, collecting and processing data files that were required for the land-use model was a laborious exercise. Firstly, gaining access to vector data on land use, soil, elevation, transportation networks, and zoning policies for the MMR was highly problematic. Data was often inaccessible, inconsistent, incomplete, inaccurate, or undocumented. This resulted in extensive searching, waiting, scraping and editing. The majority of this work was executed by Malki (2022). Furthermore, the subsequent calibration of the land-use model was problematic due to loosely defined land-use classes that resulted from inconsistencies in the data and unexpected and largely unpredictable behaviour of several land-use classes. In addition, only two land-use maps were retrieved, limiting the land-use model quality significantly since no statistical validation could be executed. Expert consultation needed to be executed to compensate for this major shortcoming partly.

Concerning the obtainment of flood hazard maps for the MMR, several other problems arose. At first, flood hazard maps were not accessible due to their cost (Malki, 2022). Consequently, the construction of flood hazard maps was decided upon. This was done by first extracting daily rainfall data from NASA (2022) for the period [2000, 2020] and from Mishra et al. (2020) for the period [2035, 2065] for various GCMs. After that, rainfall for these periods and the various GCMs was disaggregated to shorter timesteps (12 hours, 6 hours, 3 hours, 1.5 hours and 45 minutes) using the disaggregation formalism described by Rana et al. (2013). Subsequently, the annual extremes of the resulting rainfall sequences were fitted using a Gumbel Extreme Value (GEV) distribution, resulting in estimates for the rainfall associated with 2, 5, 10, 20, 50, and 100 RP floods. After that, several design storms were created using one of the most popular frequency-based methods: the Alternating Block Method (Krvavica and Rubinić, 2020; Chow et al., 1988). These were subsequently implemented in the hydrologic modelling program HEC-HMS with elevation data to generate runoff and, after that, in the hydraulic modelling program of HEC-RAS to generate flood hazard maps. This procedure was jointly executed with Gautami Kushwaha, and took more than a month of full-time work. However, the derived flood hazard maps contained various errors. Therefore a second search for flood hazard maps was executed online. This resulted in the finding of the Aqueduct flood tool (Ward et al., 2020), which supplied us with, in total, 18 flood hazard maps for various RP floods for the climate scenario RCP4.5 and RCP8.5.

6.2.2 An elaborate flood risk assessment

To our knowledge, rarely flood risk assessments are executed when a land-use model is coupled with flood hazard maps. A flood risk assessment requires flood hazard maps for various return periods that can jointly result in 'expected annual damage' estimates. Generally, only a few flood

hazard maps are considered in studies in which a land-use model is coupled with flood hazard maps. Therefore these studies are unable to assess flood risk and solely estimate flooded built-up area. Only te Linde et al. (2011); Adnan et al. (2020) coupled a land-use model with flood hazard maps and included a flood risk assessment. However, they solely assessed 'expected annual monetary damage'.

In this case study, a more detailed flood risk assessment was enabled by collecting a large cluster of flood hazard maps for various RP floods from the Aqueduct flood tool (Ward et al., 2020). Hence, flood risk indicators for both absolute (expected annual monetary damage) and relative (percentage of annual income lost) direct tangible damage, as well as direct intangible damage (expected annual population affected), were assessed.

The assessment of the flood risk indicators required land-use-specific stage-damage functions. Unfortunately, these were unavailable for the MMR; hence these needed to be constructed based on various assumptions and inaccurate data. This resulted in enormous uncertainty bounds.

6.3 Societal impact

This thesis has resulted in increased knowledge on various topics relevant to MMR's society concerning the construction of a secure and inclusive society.

Firstly, this thesis indicates that the future looks bleak if no government intervention occurs and business-as-usual growth continues. In short, riverine floods will result in more affected people and more monetary damage. Furthermore, the most vulnerable communities will relatively suffer the most. However, also derived is that most of these problems can be attributed to urban growth in flood-prone areas, not climate change. This indicates that the MMR is not powerless, and a significant part of the problem can be handled locally, which can be considered a hopeful message for the society of the MMR.

Also, this thesis has spatially explicitly pointed out the major problem areas at present and in the future. These can be used as a starting point for more high-detailed studies on which subsequently urban policies can be based.

In addition, this thesis estimates that urban planning can contribute to the flood resilience of MMR's urban environment by restricting growth in flood-prone areas and evacuating flood-vulnerable land use from the areas at risk. This knowledge indicates that policymakers should consider including urban planning to increase the flood resilience of the MMR.

Furthermore, land-use classes' reactions to the various implemented urban planning policies differed significantly. Problematic concerning this is that the most vulnerable informal land-use classes were least responsive and required very strict urban planning. This knowledge indicates that urban planning requires a land-use-specific approach that also specifically targets these vulnerable communities.

Lastly, this thesis indicates that the effectiveness of the various implemented urban planning policies for the MMR was largely independent of the perceived climate future. This indicates that creating effective urban planning policies for the MMR is not significantly limited by climate uncertainty.

6.4 Limitations and future work

In this section, first, the limitations of this thesis are discussed in Section 6.4.1. After that, in Section 6.4.2, future work is discussed.

6.4.1 Limitations

The limitations concerning the land-use model, the flood model, the assessment of resilience and flood risk, and the urban planning scenarios are discussed in this section.

Land-use model

Fundamentally models have several limitations. These are mainly related to the procedure: calibration for the present and subsequent extrapolation for the future. This procedure is problematic (i) because nothing logically follows from historical replication (Tebaldi and Knutti, 2007), and (ii) because one can calibrate any land-use patterns with enough free parameters, which is more commonly described as Von Neumanns elephant (Dyson et al., 2004).

This problem is usually addressed by introducing a validation period, with which the quality of the model is statistically assessed. However, due to the unavailability of a third land-use map, such a statistical validation procedure was not executed in this study. A qualitative calibration procedure through expert consultation was executed to compensate for this shortcoming partly.

This qualitative validation resulted in knowledge concerning several limitations of the model. Firstly, there are multiple political forces at play in the MMR that jointly influence land use and cannot be captured by the land-use model. Secondly, the model considers the MMR to be an island that does not interact with elements outside its border, while this is, of course, fundamentally erroneous. Furthermore, the modelling boundary consists of both an urban core and a rural periphery, which require the application of different parameter values; hence the periphery was modelled inaccurately. Moreover, the applied data is erroneous in several aspects. Lastly, the delineation of land-use classes appeared to be fluid and to change over time.

Flood hazard maps

The flood hazard maps were derived from the Aqueduct flood tool. Concerning these flood hazard maps, several significant limitations can be pointed out. To begin with, only one hydrological model was applied by (Ward et al., 2020). Consequently, even though the multi-model mean is applied in this thesis, the biases present in the hydrological model are not balanced by another hydrological model that contains contrary biases. A problem that arises from this can be observed in Figure 6.1. Herein, the city of Mumbai is not considered part of the larger watershed, resulting in no inundation modelled for that specific area. This is problematic since the city of Mumbai is one of the major flood-prone areas of the region (Gupta, 2007).

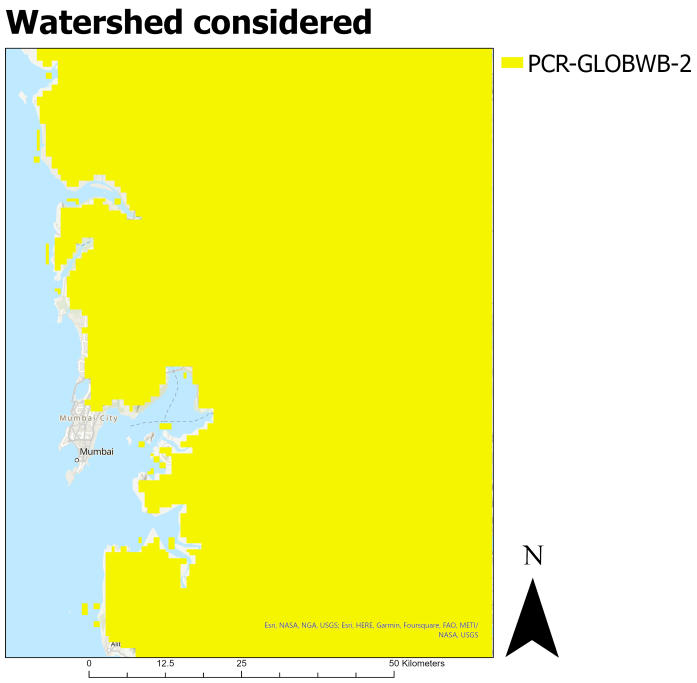

Figure 6.1: *A figure on the watershed considered by the flood hazard maps derived from the Aqueduct flood tool (Ward et al., 2020).*

Furthermore, runoff curve numbers and the stormwater drainage system were not considered in the hydrological model, and the generated grid has relatively large cells, compared to the land-use model, of 30" × 30" (≈ 1 km x ≈ 1 km) (Ward et al., 2020). Moreover, on the topic of extreme value computation, Ward et al. (2020) applied a Gumbel extreme value distribution fit, which, according to Koutsoyiannis (2003), frequently underestimates extreme values.

Lastly, the applied multi-model mean contains several other problems. This is, first of all, a relatively outdated method. More modern approaches are usually based on Bayesian statistics and weighted averages (Tebaldi and Knutti, 2007). Also, balancing biases through the combination of multiple models is based on the assumption that these models span a wide range of possible models. Concerning the 5 GCMs included, we are not sure of this; they were merrily selected based on their availability. This is called the "ensemble of opportunity" by Tebaldi and Knutti (2007).

Resilience assessment

In this thesis, flood resilience was assessed using a direct approach. However, some argue that resilience cannot be directly observed or measured and can only be measured indirectly through surrogates (Schipper and Langston, 2015). This thesis, however, assesses flood risk by estimating flood risk and assuming that low flood risk is associated with high resilience. This methodology is hence contested. For an in-depth discussion, we refer to Schipper and Langston (2015).

Flood risk assessment

Flood risk assessment was executed based on flood-depth damage functions. First, these functions generalise the situation by only evaluating flood depth while excluding other relevant factors

such as flood duration and flow velocity (de Moel and Aerts, 2011). Also, these functions were constructed based on various assumptions and inaccurate data, resulting in very large uncertainty bounds (Huizinga et al., 2017).

Urban planning scenarios

First, the considered degrees of urban planning strictness do not span the whole parameter space, which troubled the derivation of land-use-specific knowledge. This can be addressed by executing a multi-variate sensitivity analysis as discussed in Section 5.3.2.

Furthermore, a similar limitation exists concerning the 'perception of future climate' and the subsequent delineation of flood risk zones. As discussed in Section 5.3.1, the limited amount of applied scenarios does not exclude the possibility that a *certain* urban planning strategy based on a different flood depth threshold and different delineation of the flood risk zones, does result in a significant increase in acquired resilience for urban planning based on the worst-case scenario over urban planning based on the optimistic scenario. A multi-variate sensitivity analysis can be applied to research the maximum impact that the perception of future climate can have on the resilience of the urban environment.

6.4.2 Future work

The several discussed limitations in Section 6.4.1 require future research. Evident future research directions considering the improvement and extension of the current thesis are (i) the execution of statistical validation of the land-use model, (ii) the execution of multi-variate sensitivity analyses on the varied parameters of urban planning and (iii) the construction of flood hazard maps based on runoff curve numbers that are derived from the land-use model.[2]

Furthermore, in-depth qualitative research on the varying response of land-use classes to urban planning is a promising future research direction. I.e. what makes people disobey urban planning policies in the MMR, and what could convince them to reallocate?

Moreover, in this thesis, forced evacuation of urban areas away from flood-prone regions is argued to result in the most resilient urban environment. However, forced evacuation of urban areas away from flood-prone regions appears infeasible since this is equivalent to the forced evacuation of vast parts of the urban environment away from prime central locations. In contrast, mediocre and weak urban planning, which mainly restrict urban growth in flood-prone areas, can be deemed more feasible. However, the MMR remains vulnerable to flood risk if mediocre or weak urban planning is applied. Hence, research should be conducted on approaches other than reallocation that establish flood-resilient communities. Qualitative research on this topic appears highly relevant.

[2]This would result in the modelling of another aspect of the flood-risk-land-use interaction.

Bibliography

Abadie, L. M., Jackson, L. P., Sainz de Murieta, E., Jevrejeva, S., and Galarraga, I. (2020). Comparing urban coastal flood risk in 136 cities under two alternative sea-level projections: Rcp 8.5 and an expert opinion-based high-end scenario. *Ocean Coastal Management*, 193:105249.

Aburas, M. M., Ho, Y. M., Ramli, M. F., and Ash'aari, Z. H. (2016). The simulation and prediction of spatio-temporal urban growth trends using cellular automata models: A review. *International Journal of Applied Earth Observation and Geoinformation*, 52:380–389.

Adnan, M. S. G., Abdullah, A. Y. M., Dewan, A., and Hall, J. W. (2020). The effects of changing land use and flood hazard on poverty in coastal bangladesh. *Land Use Policy*, 99:104868.

Alsalloum, A. (2018). Development in world heritage sites. *The Building Conservation Directory.*

Amponsah, O., Blija, D. K., Ayambire, R. A., Takyi, S. A., Mensah, H., and Braimah, I. (2022). Global urban sprawl containment strategies and their implications for rapidly urbanising cities in ghana. *Land Use Policy*, 114:105979.

Bhanage, V., Lee, H. S., and Gedam, S. (2021). Prediction of land use and land cover changes in mumbai city, india, using remote sensing data and a multilayer perceptron neural network-based markov chain model. *Sustainability*, 13:471.

Bruneau, M., Chang, S. E., Eguchi, R. T., Lee, G. C., O'Rourke, T. D., Reinhorn, A. M., Shinozuka, M., Tierney, K., Wallace, W. A., and Von Winterfeldt, D. (2003). A framework to quantitatively assess and enhance the seismic resilience of communities. *Earthquake spectra*, 19(4):733–752.

Butsch, C., Kraas, F., Namperumal, S., and Peters, G. (2016). Risk governance in the megacity mumbai/india – a complex adaptive system perspective. *Habitat International*, 54:100–111. Special Issue: Configuring knowledge in urban water-related risks and vulnerability: Varieties, institutional arrangements and outcomes.

Chakraborty, A., Wilson, B., and bin Kashem, S. (2015). The pitfalls of regional delineations in land use modeling: Implications for mumbai region and its planners. *Cities*, 45:91–103.

Chatterjee, A. and Chattopadhyay, R. (2020). Demographic and economic growth potentials of satellites of mmr and bmr. In *Satellite Towns in Neo-metropolitan Development in India*, pages 151–168. Springer.

Chatterjee, Badri Fernandes, S. (2019). Plastic waste flowing into sea major problem.

Chow, V. T., Maidment, D. R., and Larry, W. (1988). Mays. applied hydrology. *International edition, MacGraw-Hill, Inc*, 149.

Congalton, R. G. (1991). A review of assessing the accuracy of classifications of remotely sensed data. *Remote Sensing of Environment*, 37:35–46.

CSTEP (2022). District-level changes in climate: Historical climate and climate change projections for the western states of india.

Cumming, G. S., Cumming, D. H., and Redman, C. L. (2006). Scale mismatches in social-ecological systems: causes, consequences, and solutions. *Ecology and society*, 11(1).

Cushman, S. A. and McGarigal, K. (2008). *Landscape Metrics, Scales of Resolution*, pages 33–51. Springer Netherlands, Dordrecht.

Cutter, S. L., Barnes, L., Berry, M., Burton, C., Evans, E., Tate, E., and Webb, J. (2008). A place-based model for understanding community resilience to natural disasters. *Global Environmental Change*, 18(4):598–606. Local evidence on vulnerabilities and adaptations to global environmental change.

Das, D. N. and Bhusan, S. (2014). Magnetism in india's metros: A study on migrants' choice of destination. *Social Change*, 44(4):519–540.

De Bruijn, K. (2004). Resilience indicators for flood risk management systems of lowland rivers. *International Journal of River Basin Management*, 2(3):199–210.

de Moel, H. and Aerts, J. (2011). Effect of uncertainty in land use, damage models and inundation depth on flood damage estimates. *Natural Hazards*, 58(1):407–425.

Delden, H. v. and Vanhout, R. (2018). A short presentation of metronamica. In *Geomatic Approaches for Modeling Land Change Scenarios*, pages 511–519. Springer.

Doblas-Reyes, F. J., Hagedorn, R., and Palmer, T. (2005). The rationale behind the success of multi-model ensembles in seasonal forecasting—ii. calibration and combination. *Tellus A: Dynamic Meteorology and Oceanography*, 57(3):234–252.

Dou, W., Ren, Y., Wu, Q., Ruan, S., Chen, Y., Bloyet, D., and Constans, J.-M. (2007). Fuzzy kappa for the agreement measure of fuzzy classifications. *Neurocomputing*, 70(4):726–734. Advanced Neurocomputing Theory and Methodology.

Dyson, F. et al. (2004). A meeting with enrico fermi. *Nature*, 427(6972):297–297.

ExchangeRates.org (2022). Euro to indian rupee spot exhange rates for 2015: https://www.exchangerates.org.uk/eur-inr-spot-exchange-rates-history-2015.html.

Folke, C. (2003). Freshwater for resilience: a shift in thinking. *Philosophical Transactions of the Royal Society of London. Series B: Biological Sciences*, 358(1440):2027–2036.

Foudi, S. and Osés-Eraso, N. (2014). Flood risk management: assessment for prevention with hydro-economic approaches. In *Routledge handbook of the economics of climate change adaptation*, pages 331–348. Routledge.

Foudi, S., Osés-Eraso, N., and Tamayo, I. (2015). Integrated spatial flood risk assessment: The case of zaragoza. *Land Use Policy*, 42:278–292.

Gharaibeh, A., Shaamala, A., Obeidat, R., and Al-Kofahi, S. (2020). Improving land-use change modeling by integrating ann with cellular automata-markov chain model. *Heliyon*, 6(9):e05092.

Ghorpade, K. R. (2017). Mumbai: Economic restructuring by default. In *Public Problems-Private Solutions?*, pages 35–49. Routledge.

Gibson, C. C., Ostrom, E., and Ahn, T.-K. (2000). The concept of scale and the human dimensions of global change: a survey. *Ecological economics*, 32(2):217–239.

Gupta, K. (2007). Urban flood resilience planning and management and lessons for the future: a case study of mumbai, india. *Urban Water Journal*, 4(3):183–194.

Gupta, K. (2020). Challenges in developing urban flood resilience in india. *Philosophical Transactions of the Royal Society A: Mathematical, Physical and Engineering Sciences*, 378(2168). Cited by: 16; All Open Access, Bronze Open Access.

Hagen-Zanker, A. and Lajoie, G. (2008). Neutral models of landscape change as benchmarks in the assessment of model performance. *Landscape and Urban planning*, 86(3-4):284–296.

Hallegatte, S. (2009). Strategies to adapt to an uncertain climate change. *Global Environmental Change*, 19(2):240–247. Traditional Peoples and Climate Change.

Hallegatte, S., Ranger, N., Bhattacharya, S., Bachu, M., Priya, S., Dhore, K., Rafique, F., Mathur, P., Naville, N., Henriet, F., et al. (2010). Flood risks, climate change impacts and adaptation benefits in mumbai: an initial assessment of socio-economic consequences of present and climate change induced flood risks and of possible adaptation options.

Hammond, M. J., Chen, A. S., Djordjević, S., Butler, D., and Mark, O. (2015). Urban flood impact assessment: A state-of-the-art review. *Urban Water Journal*, 12(1):14–29.

Hansen, H. S. (2010). Modelling the future coastal zone urban development as implied by the ipcc sres and assessing the impact from sea level rise. *Landscape and Urban Planning*, 98(3):141–149. Climate Change and Spatial Planning.

Hazbavi, Z., Baartman, J. E., Nunes, J. P., Keesstra, S. D., and Sadeghi, S. H. (2018). Changeability of reliability, resilience and vulnerability indicators with respect to drought patterns. *Ecological Indicators*, 87:196–208.

Hempel, S., Frieler, K., Warszawski, L., Schewe, J., and Piontek, F. (2013). A trend-preserving bias correction ndash; the isi-mip approach. *Earth System Dynamics*, 4(2):219–236.

Hewitt, R., van Delden, H., and Escobar, F. (2014). Participatory land use modelling, pathways to an integrated approach. *Environmental Modelling Software*, 52:149–165.

Hollington, A., Salverda, T., Schwarz, T., and Tappe, O. (2015). Concepts of the global south.

Hoymann, J. and Goetzke, R. (2016). Simulation and evaluation of urban growth for germany including climate change mitigation and adaptation measures. *ISPRS International Journal of Geo-Information*, 5(7).

Hu, J., Wang, Y., Taubenböck, H., and Zhu, X. X. (2021). Land consumption in cities: A comparative study across the globe. *Cities*, 113:103163.

Huizinga, J., De Moel, H., and Szewczyk, W. (2017). Global flood depth-damage functions: Methodology and the database with guidelines. (KJ-NA-28552-EN-N).

IPCC (2007). Climate change 2007: Synthesis report. contribution of working groups i, ii and iii to the fourth assessment report of the intergovernmental panel on climate change.

IPCC (2014a). Climate change 2014: Impacts, adaptation, and vulnerability. part b: Regional aspects. contribution of working group ii to the fifth assessment report of the intergovernmental panel on climate change.

IPCC (2014b). Climate change 2014 synthesis report. *IPCC: Geneva, Szwitzerland*.

IPCC (2021). Climate change 2021: The physical science basis. contribution of working group i to the sixth assessment report of the intergovernmental panel on climate change.

IPCC (2022a). Health, wellbeing, and the changing structure of communities. in: Climate change 2022: Impacts, adaptation, and vulnerability. contribution of working group ii to the sixth assessment report of the intergovernmental panel on climate change.

IPCC (2022b). Summary for policymakers: Climate change 2022: Impacts, adaptation, and vulnerability. contribution of working group ii to the sixth assessment report of the intergovernmental panel on climate change. Technical report, IPCC.

Jafino, B. A., Haasnoot, M., and Kwakkel, J. H. (2019). What are the merits of endogenising land-use change dynamics into model-based climate adaptation planning? *Socio-Environmental Systems Modelling*, 1:16126.

Jongman, B. (2018). Effective adaptation to rising flood risk. *Nature communications*, 9(1):1–3.

Kim, D. (2012). *Modelling urban growth: Towards an agent based microeconomic approach to urban dynamics and spatial policy simulation*. PhD thesis, UCL (University College London).

Kim, Y. and Newman, G. (2020). Advancing scenario planning through integrating urban growth prediction with future flood risk models. *Computers Environment and Urban Systems*, 82:101498.

Koomen, E. and Stillwell, J. (2007). *Modelling Land-Use Change*, pages 1–22. Springer Netherlands, Dordrecht.

Koutsoyiannis, D. (2003). On the appropriateness of the gumbel distribution for modelling extreme rainfall. In *Proceedings of the ESF LESC Exploratory Workshop held at Bologna*, pages 24–25.

Kovacs, Y., Doussin, N., Gaussens, M., Pacoud, C. L., and Afd, O. (2017). Flood risk and cities in developing countries. *Technical Reports*, 35:1–104.

Kron, W. (2005). Flood risk= hazard• values• vulnerability. *Water international*, 30(1):58–68.

Krvavica, N. and Rubinić, J. (2020). Evaluation of design storms and critical rainfall durations for flood prediction in partially urbanized catchments. *Water*, 12(7):2044.

Lambert, S. J. and Boer, G. J. (2001). Cmip1 evaluation and intercomparison of coupled climate models. *Climate Dynamics*, 17(2):83–106.

Lantman, J., Verburg, P., Bregt, A., and Geertman, S. (2011). *Core Principles and Concepts in Land-Use Modelling: A Literature Review*, volume 101, pages 35–57.

Liao, K.-H. (2012). A theory on urban resilience to floods—a basis for alternative planning practices. *Ecology and society*, 17(4).

Liao, K.-H., Le, T. A., and Nguyen, K. V. (2016). Urban design principles for flood resilience: Learning from the ecological wisdom of living with floods in the vietnamese mekong delta. *Landscape and Urban Planning*, 155:69–78. Ecological Wisdom for Urban Sustainability: Doing real and permanent good in ecological practice.

Lin, W., Sun, Y., Nijhuis, S., and Wang, Z. (2020). Scenario-based flood risk assessment for urbanizing deltas using future land-use simulation (flus): Guangzhou metropolitan area as a case study. *Science of The Total Environment*, 739:139899.

Liu, Y., Feng, Y., and Pontius, R. G. (2014). Spatially-explicit simulation of urban growth through self-adaptive genetic algorithm and cellular automata modelling. *Land*, 3(3):719–738.

Maharashtra CZMA (2019). Approved czmp 2019.

Makandar, Suhel M and Naik, Saharsha A. (2020). The patterns of mobility and the socio-spatial environments created in and around the important multimodal nodes in a global city - a case of navi mumbai. *E3S Web Conf.*, 170:06002.

Malki, M. E. (2022). Exploring the impact of climate change on the long-term urban growth of the mumbai metropolitan region.

Masson-Delmotte, V., Zhai, P., Pirani, A., Connors, S. L., Péan, C., Berger, S., Caud, N., Chen, Y., Goldfarb, L., Gomis, M. I., Huang, M., Leitzell, K., Lonnoy, E., Matthews, J., Waterfield, T., Yelekçi, O., Yu, R., and Zhou, B. (2021). Ipcc, 2021: Summary for policymakers. *Cambridge University Press. In Press.*

MCGM (2016). Greater mumbai report on draft development plan 2016-2034.

MCGM Municipal Corporation of Greater Mumbai (2022). Mumbai climate action plan 2022.

Meerow, S., Newell, J. P., and Stults, M. (2016). Defining urban resilience: A review. *Landscape and Urban Planning*, 147:38–49.

Messner, F. (2007). Evaluating flood damages: guidance and recommendations on principles and methods. *T09-06-01*.

MIDC (2020). Midc industrial areas: https://midcland.com/midc-industrial-areas.html.

Ministry of Environment, Forest and Climate Change (2019). Coastal regulation zone notification. *The gazette of India: Extraordinary*.

Mishra, S. S., Sonal, G., Mahalaxmi, K., and Priyanka, C. (2016). Meteorological drought assessment in mumbai city using standardized precipitation index (spi). *International Journal of Environmental Sciences*, 6(6):1036–1046.

Mishra, V., Bhatia, U., and Tiwari, A. D. (2020). Bias-corrected climate projections for south asia from coupled model intercomparison project-6. *Scientific data*, 7(1):1–13.

MMR (1995). Draft mumbai metropolitan regional plan 1996-2011.

MMR (2002). Mumbai urban transport project -resettlement action plan-.

MMR (2016). Draft mumbai metropolitan regional plan 2016-2036.

MMRDA (2008). Draft development plan bhiwandhi surrounding notified area 2008-2028.

Murali, R. M., Riyas, M., Reshma, K., and Kumar, S. S. (2020). Climate change impact and vulnerability assessment of mumbai city, india. *Natural Hazards*, 102(2):575–589.

Nakamura, F., Ishiyama, N., Yamanaka, S., Higa, M., Akasaka, T., Kobayashi, Y., Ono, S., Fuke, N., Kitazawa, M., Morimoto, J., and Shoji, Y. (2020). Adaptation to climate change and conservation of biodiversity using green infrastructure. *River Research and Applications*, 36(6):921–933.

NASA (2022). Global precipitation mission imerg precipitation data [2000, 2020].

Nemiche, M., Sfa, F. E., and Pla-López, R. (2019). A generic model of reinforcement learning combined with macroscopic cellular automata to simulate land use change.

Newland, C. P. (2018). *Developing a (Semi) Automatic Calibration Procedure for Cellular Automata based Land-use Models*. PhD thesis, University of Adelaide.

Nijman, J. (2008). Against the odds: Slum rehabilitation in neoliberal mumbai. *Cities*, 25(2):73–85.

Nijman, J. (2012). India's urban challenge. *Eurasian Geography and Economics*, 53(1):7–20.

Nussbaumer, S., Schaub, Y., Huggel, C., and Walz, A. (2014). Risk estimation for future glacier lake outburst floods based on local land-use changes. *Natural Hazards and Earth System Sciences*, 14(6):1611–1624.

Odeh, L. E. et al. (2010). A comparative analysis of global north and global south economies. *Journal of Sustainable Development in Africa*, 12(3):338–348.

Olazabal, M., Chelleri, L., Waters, J. J., and Kunath, A. (2012). Urban resilience: towards an integrated approach. In *1st International Conference on Urban Sustainability & Resilience, London*.

OpenStreetMap (2017). OpenStreetMap data retrieved from: https://www.openstreetmap.org . `https://www.openstreetmap.org`.

Opperman, J. J., Galloway, G. E., Fargione, J., Mount, J. F., Richter, B. D., and Secchi, S. (2009). Sustainable floodplains through large-scale reconnection to rivers. *Science*, 326(5959):1487–1488.

Pathak, S., Liu, M., Jato-Espino, D., and Zevenbergen, C. (2020). Social, economic and environmental assessment of urban sub-catchment flood risks using a multi-criteria approach: A case study in mumbai city, india. *Journal of Hydrology*, 591:125216.

Patil, R. G. and Deo, M. (2020). Sea level rise and shoreline change under changing climate along the indian coastline. *Journal of Waterway, Port, Coastal and Ocean Engineering*, 146(5). Cited by: 3.

Penning-Rowsell, E., Johnson, C., Tunstall, S., Tapsell, S., Morris, J., Chatterton, J., and Green, C. (2005). The benefits of flood and coastal risk management: a handbook of assessment techniques. *ISBN 1904750516*.

Picciariello, A. (2021). The costs of climate change in india: a review of the climate-related risks facing india, and their economic and social costs.

Rahaman, S., Jahangir, S., Haque, M. S., Chen, R., and Kumar, P. (2021). Spatio-temporal changes of green spaces and their impact on urban environment of mumbai, india. *Environment, development and sustainability*, 23(4):6481–6501.

Rana, A., Bengtsson, L., Olsson, J., and Jothiprakash, V. (2013). Development of idf-curves for tropical india by random cascade modeling. *Hydrology and Earth System Sciences Discussions*, 10:4709–4738.

Rana, A., Bertacchi Uvo, C., Bengtsson, L., and Sarthi, P. (2012). Trend analysis for rainfall in delhi and mumbai, india. *Climate Dynamics*, 38(1-2):45–56.

Rana, A., Foster, K., Bosshard, T., Olsson, J., and Bengtsson, L. (2014). Impact of climate change on rainfall over mumbai using distribution-based scaling of global climate model projections. *Journal of Hydrology: Regional Studies*, 1:107–128.

Ranagalage, M., Morimoto, T., Simwanda, M., and Murayama, Y. (2021). Spatial analysis of urbanization patterns in four rapidly growing south asian cities using sentinel-2 data. *Remote Sensing*, 13(8).

Ranger, N., Hallegatte, S., Bhattacharya, S., Bachu, M., Priya, S., Dhore, K., Rafique, F., Mathur, P., Naville, N., Henriet, F., et al. (2011). An assessment of the potential impact of climate change on flood risk in mumbai. *Climatic change*, 104(1):139–167.

Rentschler, J., Salhab, M., and Jafino, B. A. (2022). Flood exposure and poverty in 188 countries. *Nature communications*, 13(1):1–11.

Riding, T. (2018). 'making bombay island': land reclamation and geographical conceptions of bombay, 1661–1728. *Journal of Historical Geography*, 59:27–39.

RIKS (2012). Metronamica documentation.

Roodposhti, M. S., Aryal, J., and Bryan, B. A. (2019). A novel algorithm for calculating transition potential in cellular automata models of land-use/cover change. *Environmental Modelling Software*, 112:70–81.

Sangameswaran, P. (2021). Dispersal and development: Two key moments in the growth of thane city. *South Asia: Journal of South Asian Studies*, 44(4):651–665.

Schipper, L. and Langston, L. (2015). A comparative overview of resilience measurement frameworks: analyzing indicators and approaches.

Schwalm, C. R., Glendon, S., and Duffy, P. B. (2020). Rcp8.5 tracks cumulative co₂ emissions. *Proceedings of the National Academy of Sciences*, 117(33):19656–19657.

Scripbox (2022). Online inflation calculator: https://scripbox.com/plan/inflation-calculator/.

Sekovski, I., Armaroli, C., Calabrese, L., Mancini, F., Stecchi, F., and Perini, L. (2015). Coupling scenarios of urban growth and flood hazards along the emilia-romagna coast (italy). *Natural Hazards and Earth System Sciences*, 15(10):2331–2346.

Shafizadeh Moghadam, H. and Helbich, M. (2013). Spatiotemporal urbanization processes in the megacity of mumbai, india: A markov chains-cellular automata urban growth model. *Applied Geography*, 40:140–149.

Shafizadeh-Moghadam, H. and Helbich, M. (2015). Spatiotemporal variability of urban growth factors: A global and local perspective on the megacity of mumbai. *International Journal of Applied Earth Observation and Geoinformation*, 35:187–198.

Shaji, C., Kar, S., and Vishal, T. (2014). Storm surge studies in the north indian ocean: A review.

Sharifi, A. and Yamagata, Y. (2016). *Urban Resilience Assessment: Multiple Dimensions, Criteria, and Indicators*, pages 259–276.

Shaw, A. (2004). *The Making of Navi Mumbai*. Orient Longman.

Shine, K. P., Derwent, R., Wuebbles, D. J., and Morcrette, J. (1990). Radiative forcing of climate. *Climate change: The IPCC scientific assessment*, pages 41–68.

Shira, D. (2019). Special economic zones and warehousing clusters in mumbai.

Smajgl, A., Toan, T. Q., Nhan, D. K., Ward, J., Trung, N. H., Tri, L., Tri, V., and Vu, P. (2015). Responding to rising sea levels in the mekong delta. *Nature Climate Change*, 5(2):167–174.

Song, J., Fu, X., Gu, Y., Deng, Y., and Peng, Z.-R. (2017). An examination of land use impacts of flooding induced by sea level rise. *Natural Hazards and Earth System Sciences*, 17(3):315–334.

Strauss, B. H., Kulp, S. A., Rasmussen, D. J., and Levermann, A. (2021). Unprecedented threats to cities from multi-century sea level rise. *Environmental Research Letters*, 16(11):114015.

Su, H.-T., Cheung, S. H., and Lo, E. Y.-M. (2018). Multi-objective optimal design for flood risk management with resilience objectives. *Stochastic environmental research and risk assessment*, 32(4):1147–1162.

Sun, H., Cheng, X., and Dai, M. (2016). Regional flood disaster resilience evaluation based on analytic network process: a case study of the chaohu lake basin, anhui province, china. *Natural Hazards*, 82.

Suzuki, Y. (2020). When will india reach china's levels? *Mitsui Co. Global Strategic Studies Institute Monthly Report*.

te Linde, A. H., Bubeck, P., Dekkers, J. E. C., de Moel, H., and Aerts, J. C. J. H. (2011). Future flood risk estimates along the river rhine. *Natural Hazards and Earth System Sciences*, 11(2):459–473.

Tebaldi, C. and Knutti, R. (2007). The use of the multi-model ensemble in probabilistic climate projections. *Philosophical transactions of the royal society A: mathematical, physical and engineering sciences*, 365(1857):2053–2075.

Thomson, A. M., Calvin, K. V., Smith, S. J., Kyle, G. P., Volke, A., Patel, P., Delgado-Arias, S., Bond-Lamberty, B., Wise, M. A., Clarke, L. E., et al. (2011). Rcp4. 5: a pathway for stabilization of radiative forcing by 2100. *Climatic change*, 109(1):77–94.

UDRI (2017). Loginmumbai. http://www.loginmumbai.org/.

United Nations (2018). World urbanization prospects: The 2018 revision, custom data acquired via website.

United Nations Office for Disaster Risk Reduction (UNDRR) (2020). Retrofitting terminology.

USDA (1986). Urban hydrology for small watersheds. *"Technical release number 55 (TR–55)*.

van Delden, H. and Hagen-Zanker, A. (2009). *New Ways of Supporting Decision Making: Linking Qualitative Storylines with Quantitative Modelling*, pages 347–367. Springer Netherlands, Dordrecht.

van den Berg, L., Drewett, R., Klaassen, L. H., Rossi, A., and Vijverberg, C. H. (1982). 3 - stages of urban development. In van den Berg, L., Drewett, R., Klaassen, L. H., Rossi, A., and Vijverberg, C. H., editors, *A Study of Growth and Decline*, pages 24–45. Pergamon.

Van der Veen, A., Vetere Arellano, A., and Nordvik, J.-P. (2003). In search of a common methodology on damage estimation. In *Joint NEDIES and University of Twente Workshop, Report EUR*, volume 20997.

Van Vliet, J. (2013). *Calibration and validation of land-use models*. Wageningen University and Research.

van Vliet, J., Bregt, A. K., and Hagen-Zanker, A. (2011). Revisiting kappa to account for change in the accuracy assessment of land-use change models. *Ecological Modelling*, 222(8):1367–1375.

van Vliet, J., Hagen-Zanker, A., Hurkens, J., and van Delden, H. (2013a). A fuzzy set approach to assess the predictive accuracy of land use simulations. *Ecological Modelling*, 261-262:32–42.

van Vliet, J., Naus, N., van Lammeren, R., Bregt, A., Hurkens, J., and van Delden, H. (2013b). Measuring the neighbourhood effect to calibrate land use models. *Computers, Environment and Urban Systems*, 41:55–64.

Verma, S., Mandal, S. N., Robinson, S., and Bajaj, D. (2020). Diffusion patterns and drivers of higher-rated green buildings in the mumbai region, india: a developing economy perspective. *Intelligent Buildings International*, 0(0):1–21.

Vinayak, B., Lee, H. S., and Gedem, S. (2021). Prediction of land use and land cover changes in mumbai city, india, using remote sensing data and a multilayer perceptron neural network-based markov chain model. *Sustainability*, 13(2).

Visser, H. and de Nijs, T. (2006). The map comparison kit. *Environmental Modelling Software*, 21(3):346–358.

Ward, P. J., Winsemius, H. C., Kuzma, S., Bierkens, M. F., Bouwman, A., De Moel, H., Loaiza, A. D., Eilander, D., Englhardt, J., Erkens, G., et al. (2020). Aqueduct floods methodology. *World Resources Institute*, pages 1–28.

Weedon, G. P., Gomes, S., Viterbo, P., Shuttleworth, W. J., Blyth, E., Österle, H., Adam, J. C., Bellouin, N., Boucher, O., and Best, M. (2011). Creation of the watch forcing data and its use to assess global and regional reference crop evaporation over land during the twentieth century. *Journal of Hydrometeorology*, 12(5):823 – 848.

Wickramasuriya, R. C., Bregt, A. K., van Delden, H., and Hagen-Zanker, A. (2009). The dynamics of shifting cultivation captured in an extended constrained cellular automata land use model. *Ecological Modelling*, 220(18):2302–2309.

Xu, W., Cong, J., Proverbs, D., and Zhang, L. (2021). An evaluation of urban resilience to flooding. *Water*, 13(15):2022.

Yazdani, S. and Dola, K. (2013). Sustainable city priorities in global north versus global south. *Journal of Sustainable Development*, 6(7):38.

Zevenbergen, C. and Gersonius, B. (2007). Challenges in urban flood management. In *Advances in urban flood management*, pages 13–24. CRC Press.

Zevenbergen, C., Gersonius, B., and Radhakrishan, M. (2020). Flood resilience.

Zhao, L., Song, J., and Peng, Z.-R. (2016). Modeling land use change and population relocation dynamics in response to different sea level rise scenarios: Case study in bay county, florida.

Appendices

Appendix A

Literature review

Paper	Approach	Time period	Scale and location	Type of flooding	Modelling method	Scenarios	Planning policies	Flood impact indicator
Sekovski et al. (2015)	1	2011 and 2050	Regional (Emilia-Romagna coast, Italy)	Coastal flooding due to sea-level rise	Cellular automata-based *SLEUTH* model	Three land-use scenarios overlaid with three flood hazard maps for three return-periods of 10, 100 and >100 year	X	Flooded built-up area (m^2)
de Moel and Aerts (2011)	1	2000	Regional (South bank Meuse River, The Netherlands)	Riverine flooding	GIS-based *Land Use Scanner* Model	Five land-use maps overlaid with one combined flood hazard map for an extreme scenario	X	Absolute damage change (10^9 Euro/10 cm inundation depth), Proportional damage change (% of base damage/10 cm inundation depth)
Zhao et al. (2016)	1	2030 and 2080	Regional (Bay County, Florida, USA)	Coastal flooding due to sea-level rise	Multinomial logit location choice cellular automata-based model	one land-use scenario overlaid with three flood hazard maps for three climate scenarios	X	Flooded built-up area (m^2)
te Linde et al. (2011)	1	2000 and 2030	Regional (Rhine Basin, The Netherlands and Germany)	Riverine flooding	GIS-based *Land Use Scanner* Model	Two land-use scenarios overlaid with flood hazard maps for two climate scenarios	X	Potential flood damage (Euro), Expected annual damage (Euro/year)

Paper	Approach	Time period	Scale and location	Type of flooding	Modelling method	Scenarios	Planning policies	Flood impact indicator
Lin et al. (2020)	1	2015, 2030, and 2050	Regional (Guangzhou Metropolitan Area, China)	Coastal flooding due to sea-level rise	deep learning, neural networks, cellular automata-based model	one land-use scenario overlaid with two flood hazard maps for two climate scenarios	X	Flooded built-up area (m^2)
Adnan et al. (2020)	1	2005, 2010, 2019, and 2030	Regional (5 districts in the south western coastal area, Bangladesh)	Riverine flooding	logistic regression, markov chain, cellular automata-based model	One land-use scenario overlaid with flood hazard maps for seven return-periods of [1,100] year	X	Potential flood damage (Euro), Expected annual damage (Euro/year)
Nussbaumer et al. (2014)	1	1985, 1997, 2009, and 2045	local (Naters, Valais, Switzerland)	Glacier lake flooding	Extrapolation, scenario-based model	Three land-use scenarios overlaid with two flood hazard maps for two outburst scenarios	X	Flooded built-up area for 4 risk categories (m^2)
Hoymann and Goetzke (2016)	2	2010, 2030	National (Germany)	Flooding	GIS-based *Land-use Scanner* Model	One land-use scenario for one flood hazard map of a 100 year return-period	Comparison of a no-policy scenario with one planning policy scenario that applies restrictive spatial planning in flood-prone areas.	X

Paper	Approach	Time period	Scale and location	Type of flooding	Modelling method	Scenarios	Planning policies	Flood impact assessment
Song et al. (2017)	1 and 2	2030 and 2080	Regional (Bay County, Florida, USA)	Coastal flooding due to sea-level rise	cellular automata-based *SLEUTH* model	Three land-use scenarios times four flood policies overlaid with three flood hazard maps based on three climate scenarios.	Comparison of a no-policy scenario with three planning policies that apply restrictive spatial planning in flood-prone areas.	Flooded built-up area (m^2)
Hansen (2010)	1 and 2	2008 and 2040	Regional (Northern Jutland, Denmark)	Coastal flooding due to sea-level rise and storm surge	cellular automata-based *LUCIA* model	Three land-use scenarios times two flood response scenario overlaid with two flood hazard maps based on a sea-level rise scenario and a sea-level rise plus storm surge scenario.	Comparison of a no-policy scenario with a planning policy scenario that applies restrictive spatial planning and additional insurance costs.	Flooded built-up area (m^2)
Kim and Newman (2020)	1 and 2	2011 and 2040	Regional, municipal and local (Tampa, Florida, USA)	Coastal flooding due to sea-level rise	GIS-based artificial neural network *Land Transformation* model	One land-use scenario times three flood policies overlaid with three flood hazard maps for three climate scenarios	Comparison of a no-policy scenario with two planning policy scenarios that apply restrictive spatial planning in flood-prone areas.	Flooded built-up area (m^2)

Table A.1: *A table of the analysed papers that have linked flood and land-use models. Concerning the types: type 1 indicates that land-use maps were overlaid with flood hazard maps. Type 2 indicates that flood hazard maps were incorporated in the land-use model as a policy layer. Type 3 indicates that land-use, derived from a land-use model, was taken into account during flood modelling. Also note that an X in the policies column, indicates that no policies were implemented in the model. Note that this list is not exhaustive.*

Appendix B

General MMR

B.1 MMR regions

Figure B.1: *Regions of the MMR (MMR, 2016)*

B.2 Land-use maps

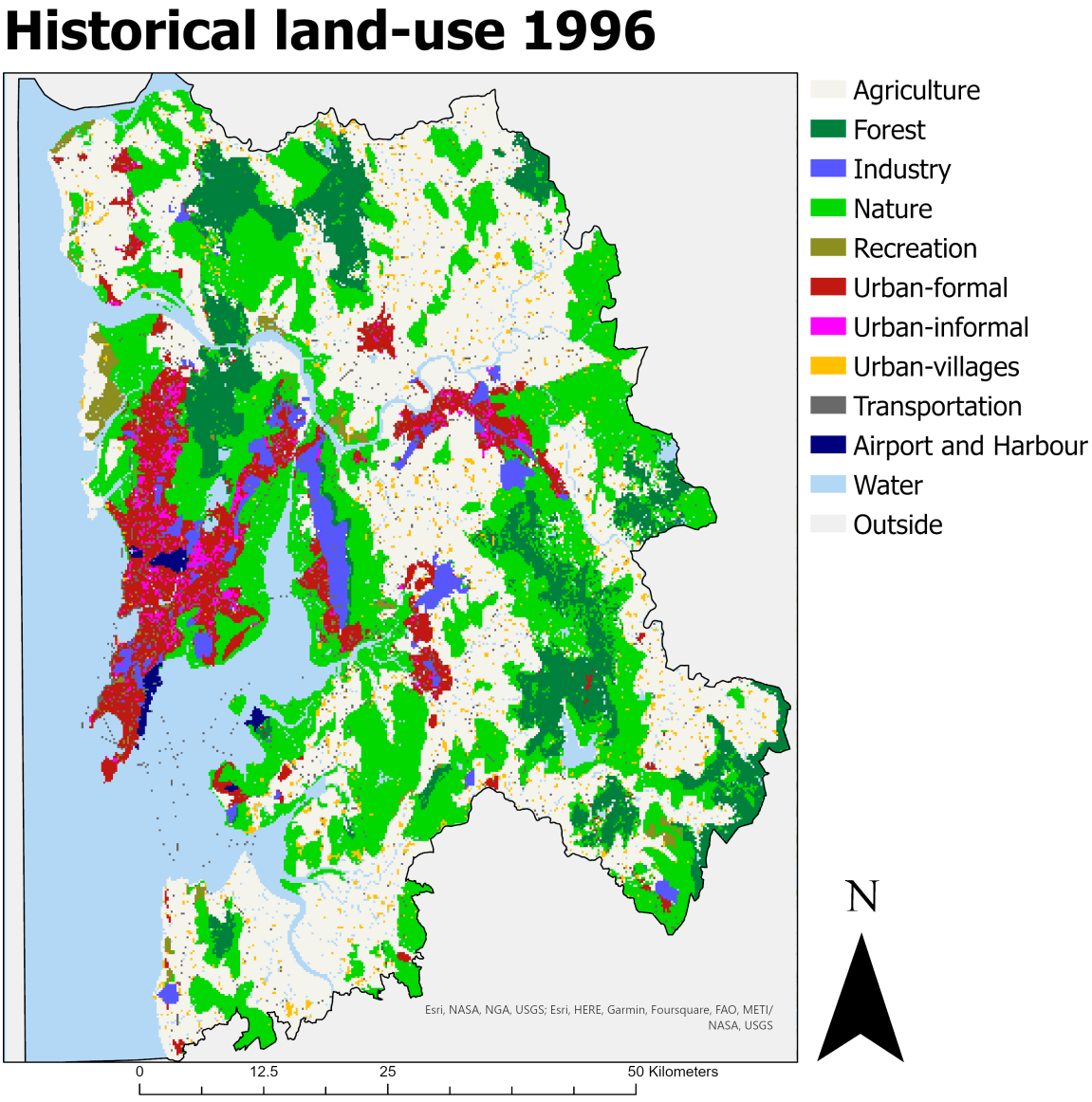

Figure B.2: *A historical land-use map for 1996, constructed by Malki (2022), based on the sources mentioned in Table 4.1.*

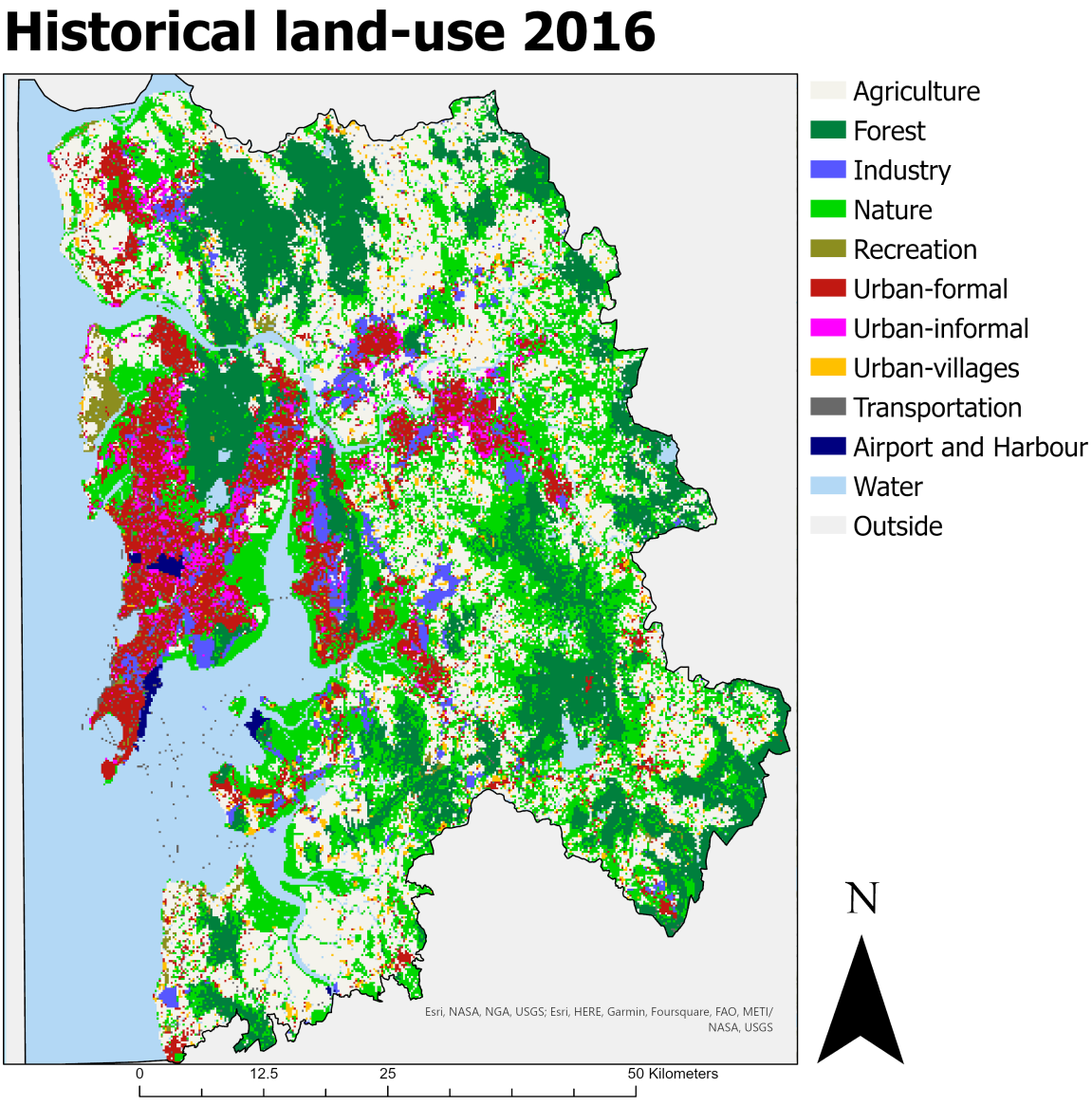

Figure B.3: *A historical land-use map for 2016, constructed by Malki (2022), based on the sources mentioned in Table 4.1.*

Appendix C

Land-Use Model

C.1 Neighbourhood interactions

C.1.1 Calculation of the neighbourhood interactions

Throughout this section, the historical land-use map of timestep 1 (1996) will be referred to as land-use map 1 and the historical land-use map of timestep 2 (2016) is referred to as land-use map 2. The inertia and conversion points were derived from the contingency table. A contingency table exhibits the number of cells that changed from class i in land-use map A to class j in land-use map B. A standard contingency table format is visualised in Figure C.1. The contingency table for this study can be found in Appendix C.1.2.

		$\widehat{X}_a$			
		A_1	A_2	$\cdots$	A_n
$\widehat{X}_0$	A_1	$\eta_{1,1}$	$\eta_{1,2}$	$\cdots$	$\eta_{1,n}$
	A_2	$\eta_{2,1}$	$\eta_{2,2}$	$\cdots$	$\eta_{2,n}$
	$\vdots$	$\vdots$	$\vdots$	$\ddots$	$\vdots$
	A_n	$\eta_{n,1}$	$\eta_{n,2}$	$\cdots$	$\eta_{n,n}$

Figure C.1: *A standard contingency table format (Newland, 2018).*

In Figure C.1, $\widehat{X}_0$ is land-use map 1 and $\widehat{X}_A$ land-use map 2. While $\eta_{i,i}$ is the total number of cells that remained class i from land-use map $\widehat{X}_0$ to land-use map $\widehat{X}_A$ and $\eta_{i,j}$ the total number of cells that changed from class i to class j from land-use map $\widehat{X}_0$ to land-use map $\widehat{X}_a$. For a more elaborate explanation of the contingency table, we refer to Congalton (1991); Newland (2018).

The inertia points, which describe the tendency of a land-use class to persist, can be derived from the contingency table according to the following equation:

$$IR_i = \frac{\eta_{i,i}}{\sum_{m=1}^{n} \eta_{i,m}} \tag{C.1}$$

where, IR_i is the inertia rate of land-use class i, $\eta_{i,i}$ the number of cells of class i in land-use map 2 and $\sum_{m=1}^{n} \eta_{i,m}$ the number of cells of class i in land-use map 1.

The conversion points, which indicate the tendency of a land-use class to transition to another land-use class, can be derived from the contingency table according to the following equation:

$$CR_{i,j} = \frac{\eta_{i,j}}{\left(\sum_{m=1}^{n} \eta_{m,j}\right) - \eta_{j,j}} \tag{C.2}$$

where, $CR_{i,j}$ is the conversion rate of class i to class j, $\eta_{i,j}$ the number of cells of class i that changed to class j, $\left(\sum_{m=1}^{n} \eta_{m,j}\right) - \eta_{j,j}$ the number of cells that changed to class j.

Self-influence tails indicate the gravitational pull of a land-use class on itself, i.e. the tendency of a land-use class to be present in the vicinity of itself. In contrast, cross-influence tails indicate the gravitational pull of a land-use class on another land-use class, i.e. the tendency of a land-use class to be present in the vicinity of another land-use class. Both can be derived from the enrichment curves according to the following equation:

$$EF_{i,j,d} = \log_{10}\left(\frac{\bar{R}_{i,j,d}}{\frac{n_j}{n}}\right) \tag{C.3}$$

where $EF_{i,j,d}$ is the enrichment factor for the presence of class j at a distance d in the neighbourhood of cells that converted to class i, and $\bar{R}_{i,j,d}$ is the average presence of class j at a distance d in the neighbourhood of cells that converted to class i. Furthermore, $\frac{n_j}{n}$ is the fraction of class j cells over the total amount of cells in land-use map 1. Hence the enrichment factor expresses the overrepresentation [1] of land-use class j at a certain distance of cells that changed to class i, relative to the representation of class j in the entire landscape (van Vliet et al., 2013b). In the case of $i = j$ self-influence tails are calculated, while in the case of $i \neq j$ cross-influence tails are calculated. We refer to Van Vliet (2013); Newland (2018) for an elaborate discussion on the enrichment curves.

C.1.2 Contingency table

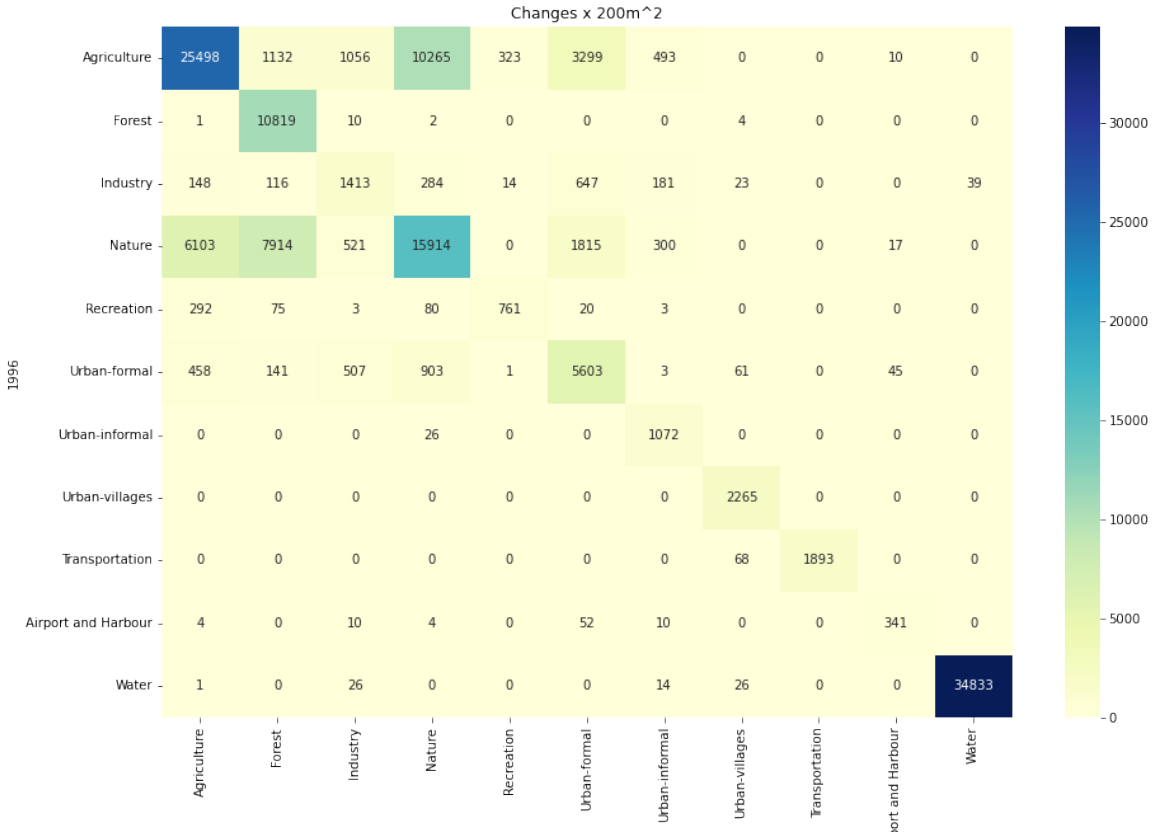

Figure C.2: *A contingency table derived from the available land-use maps.*

[1] The enrichment curves can also exhibit under-representation. We, however, do not include this in our analysis.

C.2 Future Demand

Exact details on the reasoning behind the estimates for future demand are discussed per land-use class in this Section.

C.2.1 Built-up land

In literature, no detailed future growth estimates were found for Urban-Formal, Urban-Informal and Urban-Villages. However, built-up land has been discussed in some detail by (MMR, 2016). Therefore built-up land is used as a proxy for Urban-Formal, Urban-Informal and Urban-Villages.

Built-up land is projected to increase from $\approx$ 697.01 km^2 to 992.92 km^2 (an increase of 42.3%) for the period [2016,2036] MMR (2016). This estimate is adopted here.

Concerning Urban-Informal the following logic was applied. According to (MMR, 2016), there is governmental ambition to reduce the amount of households living in slums (from $\approx$ 27%to $\approx$ 6%) by increasing the availability of affordable formal settlements. However, although this ambition has been expressed several times in the past, change has failed to happen. Indicative of this is the nearly constant fraction (52%) of the population living in slums in Greater Mumbai during the period [2001,2011] (Nijman, 2008, 2012). The projected growth of MMR population from 24.3 million in 2016 to $\approx$ 30.5 million in 2036 (MMR, 2016), will also trouble achieving the set target. However, governmental ambition seems to have increased relative to the past (MMR, 2016, 1995). Therefore the fraction of built-up land, used by Urban-Informal is reduced by 10% for the period [2016, 2036].

For the [1996, 2016] period, Urban-Villages was modelled to be stable. For the future we assume the same stability. This assumption was deemed valid based on the expert interviews discussed in Section 3.1.5. Through these interviews was confirmed that urban villages have a high inertia and show significant resilience to infrastructural development. An assumption was also necessary, since no data was available.

Precise estimates for Urban-Formal were not found. The future demand for Urban-Formal was based on (i) the fact that informal settlements will decrease in relative size to be replaced by formal settlements and (ii) the fact that built-up land will increase by $\approx$ 43% for the period [2016, 2036]. In line with this, we implement that Urban-Formal will compensate for the reduced presence of informal land-use and will increase by $\approx$ 48% for the period [2016, 2036].

C.2.2 Industry

According to MMR (2016), Industry will increase from $\approx$ 88 km^2 to $\approx$ 215 km^2 during the time period [2016, 2036]. Hence, an increase of $\approx$ 144% is estimated. This relative increase is adopted by us and implemented for the period [2016, 2036].

C.2.3 Forest

According to MMR (2016), forest will increase from $\approx$ 833 km^2 to $\approx$ 1071 km^2 during the period [2016, 2036]. Hence, an increase of $\approx$ 29% is estimated. This relative increase is adopted by us and implemented for the period [2016, 2036].

C.2.4 Nature

The nature classification in our model diverges from the definitions of the green zones G1 and G2 described in MMR (1995, 2016). In our model nature considers all green space, excluding agriculture and protected forests. To calculate nature for 2050, the growth-rate for all green space, including agriculture and excluding protected forests, was calculated from MMR (2016). This was subsequently combined with the area delineated as agriculture and nature for our land-use model to arrive at the green space for our model for 2036. Thereafter the fraction of nature for our model is used to derive the demand for nature in 2050.

C.2.5 Recreation

Zones devoted to recreation and tourism for the period [2016, 2036] were not specified by MMR (2016). Further statistics on future recreational land-use were not found for the MMR; hence an estimation was needed.

The demand for recreational areas for the MMR, has previously been correlated with a growth in population and income by MMR (1995). This correlation is used to project the future demand for recreational areas. Since there are no readily-available GDP projections for the MMR, solely population growth will be used.

The projected growth of MMR population from 24.3 million in 2016 to $\approx$ 30.5 million in 2036, corresponds with an increase of $\approx$ 26% (MMR, 2016). Therefore, recreational area will be estimated to equally grow by 26%.

Appendix D

Flood-depth Damage Functions

The flood depth damage function derivation was fully based on Huizinga et al. (2017). Hence all equations and used parameter values should be ascribed to Huizinga et al. (2017), unless specifically mentioned.

D.1 Urban-Formal, Urban-Informal, Urban-Villages and Industry

To arrive at the flood-depth damage functions, the normalised damage function and the maximum flood damage need to be determined. This is done in a similar manner for the land-use classes: *Urban-Formal*, *Urban-Informal*, *Urban-Villages*, and *Industry*.

D.1.1 Normalised damage functions

The normalised damage functions were constructed by normalising and taking the average of various damage functions for the Asian continent found in literature by Huizinga et al. (2017). As an example, the damage functions for the land-use class *Industry* are visualised in Figure D.1. For the normalised damage function of the residential land-use class for Asia, on which the Urban-Informal, Urban-Formal and Urban-Villages are based, we refer to Huizinga et al. (2017).

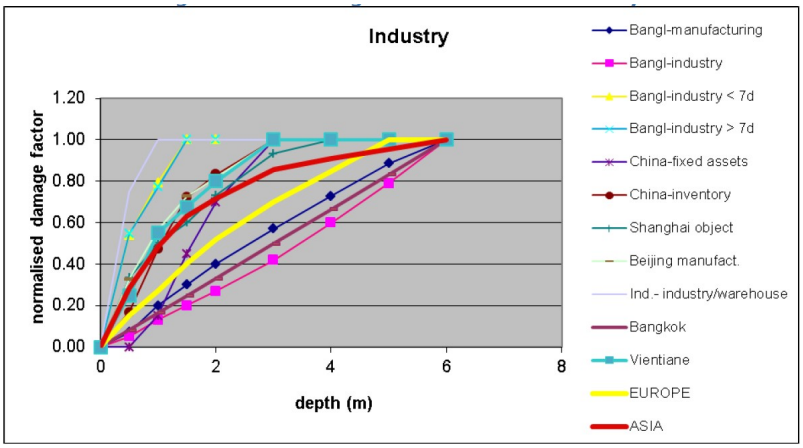

Figure D.1: *On the horizontal axis, the water depth is visualised and on the vertical axis the normalised damage factor. The deduced normalised averaged damage function for the Asian continent is visualised in red and the various, from literature derived, damage functions for the land-use class Industry are visualised in other colours.This figure was extracted from Huizinga et al. (2017).*

D.1.2 Maximum flood damage

Maximum flood damage was derived through a variety of steps. First, a correlation between GDP per capita (2010 US$) and construction cost (Euro/m^2) was found, using a regression analysis ($R^2 = 0.704$). This enables the usage of GDP per capita as a starting point. After the derivation of construction cost from GDP per capita, the maximal structure damage is derived using equation D.1 (Huizinga et al., 2017):

$$Max_{structure} = cost_{construction} \cdot depreciation_{fraction} \cdot (1 - undamageable_{fraction}) \cdot material_{worth} \quad \text{(D.1)}$$

where, $Max_{structure}$ is the maximal damage to a structure in Euro/m^2, $cost_{construction}$ is the construction cost (Euro/m^2), $depreciation_{fraction}$ indicates the depreciation of the construction cost, $undamageable_{fraction}$ is the fraction of a construction that is regarded never to be damaged, $material_worth$ is an indication of the materials used, ranging from 0 for not expensive to 1 for

expensive. From the derived maximal structure damage can subsequently the maximal content damage be derived, using equation D.2:

$$Max_{content} = Max_{structure} \cdot content_{factor} \tag{D.2}$$

where $Max_{content}$ is the maximal damage to the content of a structure in [Euro/m^2]and the $content_{factor}$ is a factor that indicates the value the content has in relation to the value of the structure.

After the addition of equation D.1 and D.2, the combined maximal damage Max_{comb} is derived. To ensure the applicability of the combined maximal damage to our land-use model, equation D.3 is used:

$$Max_{land-use} = Max_{comb} \cdot footprint_{fraction} \tag{D.3}$$

where $footprint_{fraction}$ indicates the fraction of land covered by buildings.

The variables used for the various land-use classes are shown in Table D.1. The values are based on the analysis done by Huizinga et al. (2017), the uncertainties were added here to also account for uncertainties in the abstract parameters, which are no universal constant and hence should not be treated as such. Including a relative uncertainty for these parameters in the uncertainty assessment, will result in more realistic uncertainty bounds for the flood-depth damage functions.

LUC	$depreciation_{fraction}$	$undamageable_{fraction}$	$material_{worth}$	$content_{factor}$	$footprint_{fraction}$
Urban-Formal	$0.6 \pm 5\%$	$0.4 \pm 5\%$	$1 \pm 5\%$	$0.5 \pm 5\%$	$0.2 \pm 5\%$
Urban-Informal	$0.6 \pm 5\%$	$0.0 \pm 5\%$	$0.125 \pm 5\%$	$0.5 \pm 5\%$	$0.6 \pm 5\%$
Urban-Villages	$0.6 \pm 5\%$	$0.0 \pm 5\%$	$0.33 \pm 5\%$	$0.5 \pm 5\%$	$0.2 \pm 5\%$
industry	$0.6 \pm 5\%$	$0.4 \pm 5\%$	$1 \pm 5\%$	$1.5 \pm 5\%$	$0.3 \pm 5\%$

Table D.1: *A table on the variables used for the various land-use classes.*

The derived values for $Max_{land-use}$ that follow from the implementation of Table D.2, can be found in Table D.2. The included uncertainties are derived based on the uncertainties associated with the variables from Table D.1, and the uncertainties associated with the regression analysis and construction costs, as given by Huizinga et al. (2017).

LUC	$Max_{land-use}$ Euro/m^2
Urban-Formal	$68.1^{+50.8}_{-33.8}$
Urban-Informal	$42.6^{+31.8}_{-21.1}$
Urban-Villages	$37.5^{+28.0}_{-18.6}$
Industry	$130.7^{+99.3}_{-69.3}$

Table D.2: *A table of the derived maximum damage numbers in terms of land-use for the various land-use classes.*

D.1.3 Flood-depth damage functions

The flood-depth damage functions can be constructed by combining the, from literature derived, normalised damage functions with the land-use class specific maximum flood damage estimates. To ensure direct applicability to the constructed land-use model, $Max_{land-use}$ is used as the maximum flood damage estimate. Note that the normalised damage function is no smooth function but a concatenation of points. These points will be used to construct a smooth fit for the flood-depth damage functions that enables the estimation of flood damage for continuous flood depth. This is done using a power-law fit of the form $y = a * x^b$. The resulting fits are visualised in Figures 4.8,4.9,4.10, and 4.11 in orange, together with the points, as estimated by the above analysis, their uncertainties and a power-law fit for the upper and lower bounds in respectively black and yellow. The included uncertainties are derived based on the uncertainties associated with the variables from Table D.2 and the uncertainties associated with the normalised damage functions and the construction costs, as given by Huizinga et al. (2017). All fits have R^2 values higher than 0.96.

D.2 Transportation

Also for the flood-depth damage function of Transportation, the normalised damage function and the maximum flood damage need to be determined. The normalised damage function for the land-use class *Transportation* is derived in the same manner as the earlier described normalised damage functions for the land-use classes *Urban-Formal*, *Urban-Informal*, *Urban-Villages*, and *Industry*. The maximum flood damage is determined in a different way, hence a separate section is devoted to *Transportation*.

D.2.1 Maximum flood damage

To determine the maximum flood damage for transportation, Equation D.4 is applied. The equation calculates the maximum flood damage by:

$$max\_flood\_damage(city) = \frac{continental\_average\_max\_flood\_damage \cdot GDP(city)}{GDP(continental\_average)} \tag{D.4}$$

where, max flood_damage(city) is the derived maximum flood damage for a specific city, continental_average_max_flood_damage is the maximum flood damage for the continent on which the city is located, GDP(city) is the Gross Domestic Product of the city and GDP(continental average) is the average Gross Domestic Product for the continent on which the city is located.

By filling in the statistics on continental average max flood damage for Asia and the average GDP of Asia, made available by Huizinga et al. (2017), and the GDP estimate for the MMR of Suzuki (2020), we arrive at 354.21 as the max flood damage for the MMR.

D.2.2 Flood-depth damage function

The flood-depth damage function for Transportation is now, similar to the other land-use classes, constructed by combining the normalised damage function with the maximum flood damage estimate. In this case, smooth flood-depth damage functions for the estimates, lower-bounds and upper-bounds are created using a polynomial fit of the form $y = a \cdot log(x)^2 + b \cdot log(x) + c$. Solely

in this case, this resulted in higher R^2 values. The resulting fits, in combination with the data and the estimations for uncertainty are visualised in Figure D.2. The included uncertainties are derived based on the uncertainties associated with the maximum flood damage and the uncertainties associated with the flood-depth damage function, as given by Huizinga et al. (2017). All fits have R^2 values higher than 0.95.

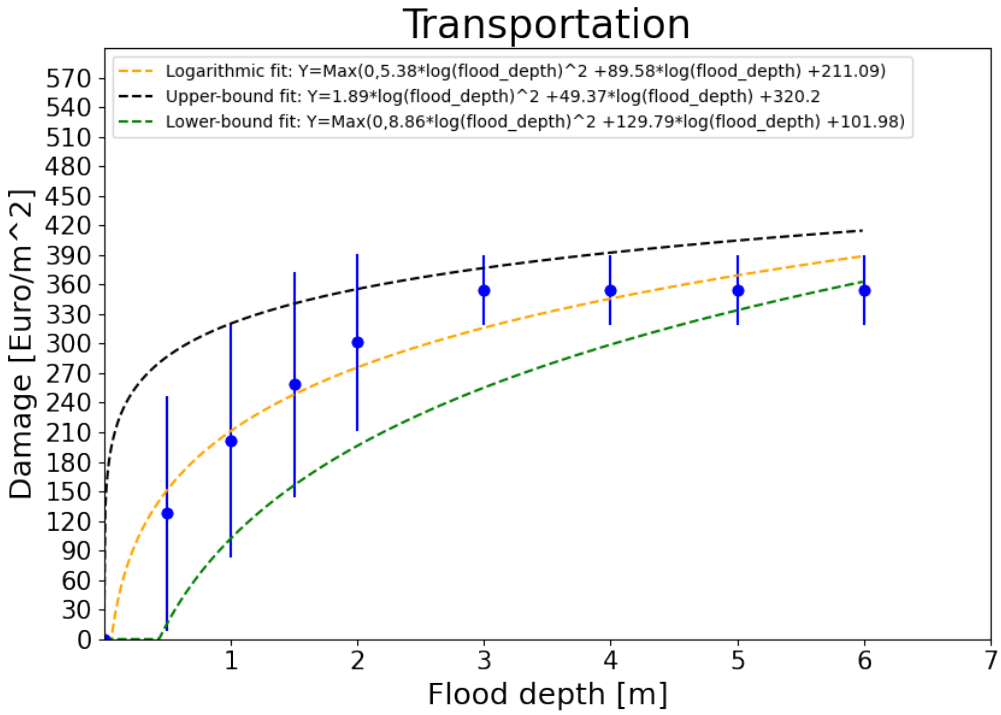

Figure D.2: *In this figure, the smooth FDDF (orange), the 90% upper-bound fit (black) and the 90% lower-bound fit (yellow) for transport, are visualised together with the data points. The power-fits have the following* R^2 *values:* $R^2_{FDDF} = 0.965, R^2_{upperbound} = 0.963, R^2_{lowerbound} = 0.950$.

D.3 Agriculture

Also for the flood-depth damage function of Agriculture, the normalised damage function and the maximum flood damage were determined. The normalised damage function for the land-use class *Agriculture* is derived in the same manner as the earlier described normalised damage functions for the land-use classes *Urban-Formal*, *Urban-Informal*, *Urban-Villages*, *Industry*, *Transportation*. The maximum flood damage is determined in a different way, hence a separate section is devoted to *Agriculture*.

D.3.1 Maximum flood damage

To determine the maximum flood damage for agricultural lands, the loss in output of these lands due to floods are considered. These can be derived from the value added per hectare of Agricultural land. Agricultural buildings, infrastructure and machinery are thus not considered.

Huizinga et al. (2017) arrived at a value added per hectare of $\approx$ 0.12Euro/m^2 for agriculture for India in general. MMR specific data could not be found. Uncertainty for this flood damage estimate was taken into account by including an uncertainty of 0.12 Euro/m^2 $\pm$5%.

D.3.2 Flood-depth damage function

The flood-depth damage function for Agriculture is now, similar to the other land-use classes, constructed by combining the normalised damage function with the maximum flood damage estimate. Again, a smooth flood-depth damage function, a function for the upper-bound and a function for the lower bound were constructed using a power-law fit of the form $y = a * x^b$. The resulting fits, in combination with the data and the estimations for uncertainty are visualised in Figure D.3. The included uncertainties are derived based on the uncertainties associated with the maximum flood damage and the uncertainties associated with the flood-depth damage function, as given by Huizinga et al. (2017). All fits have R^2 values higher than 0.84.

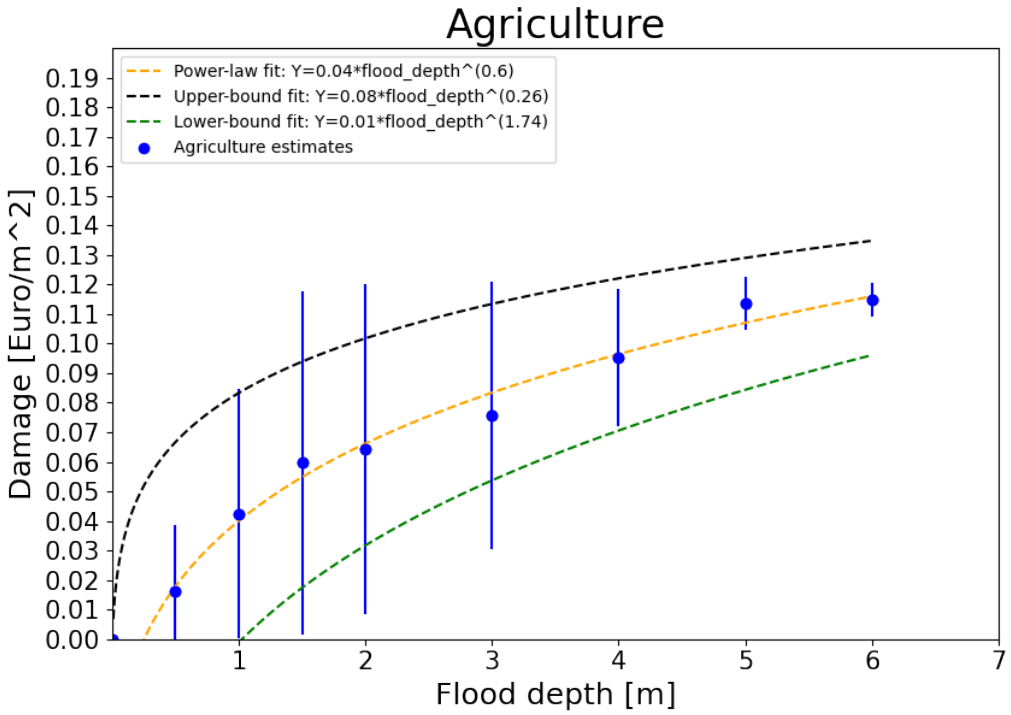

Figure D.3: *In this figure, the smooth FDDF (orange), the 90% upper-bound fit (black) and the 90% lower-bound fit (yellow) for Agriculture, are visualised together with the data points. The power-fits have the following* R^2 *values:* $R^2_{FDDF} = 0.99, R^2_{upperbound} = 0.88, R^2_{lowerbound} = 0.84$.

Appendix E

Results

E.1 Inter-model differences

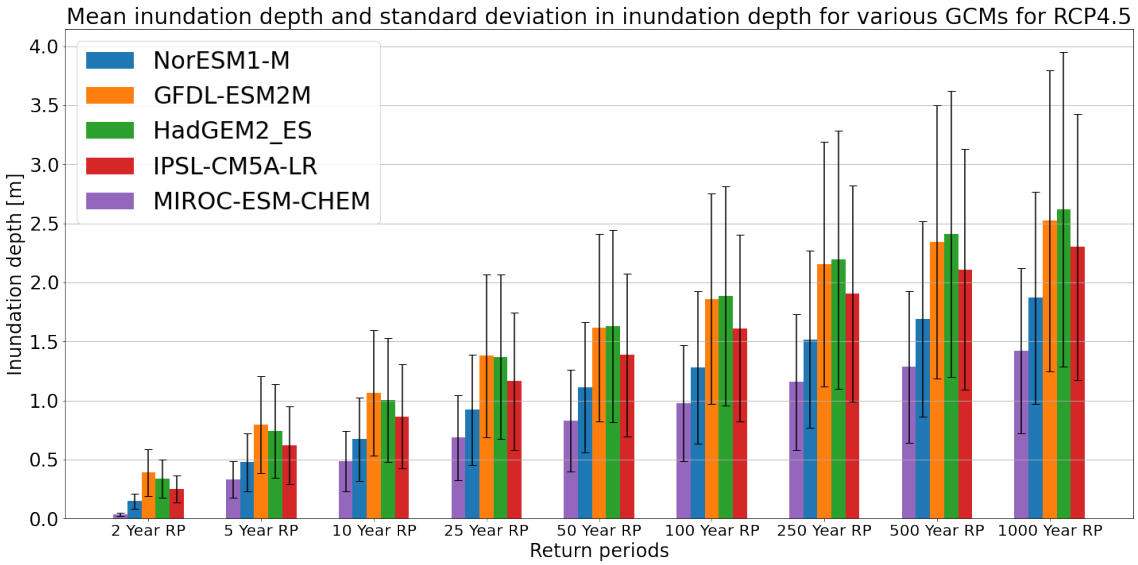

Figure E.1: *A histogram concerning the average inundation depth and the standard deviation in inundation depth for the 5 evaluated GCMs for RCP4.5.*

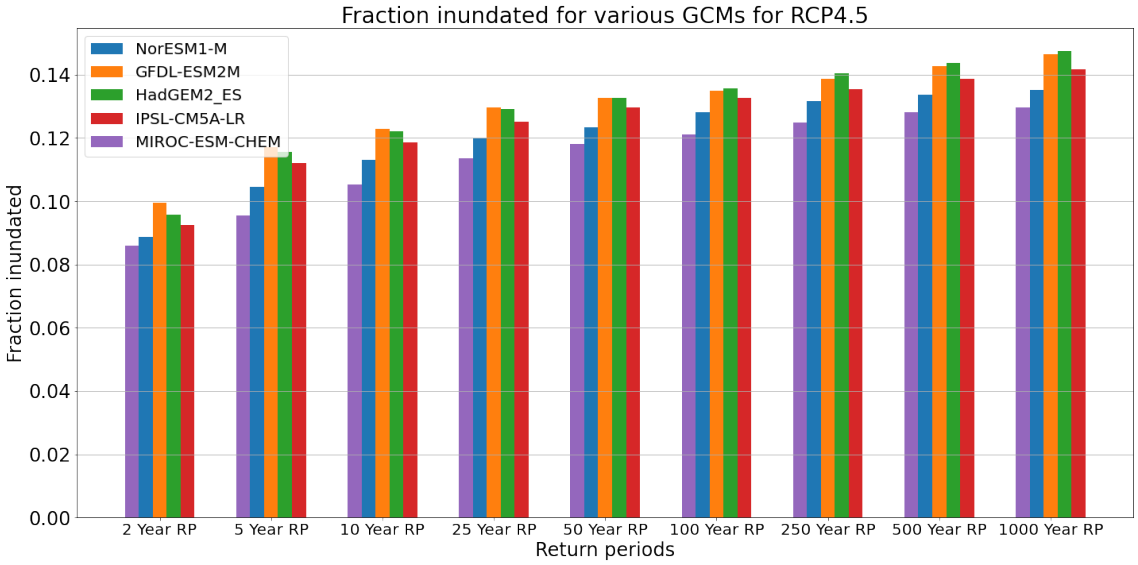

Figure E.2: *A histogram concerning the fraction of surface inundated. This is calculated by dividing the total inundated area by the total evaluated area.*

E.2 PAIL informal settlements 2010

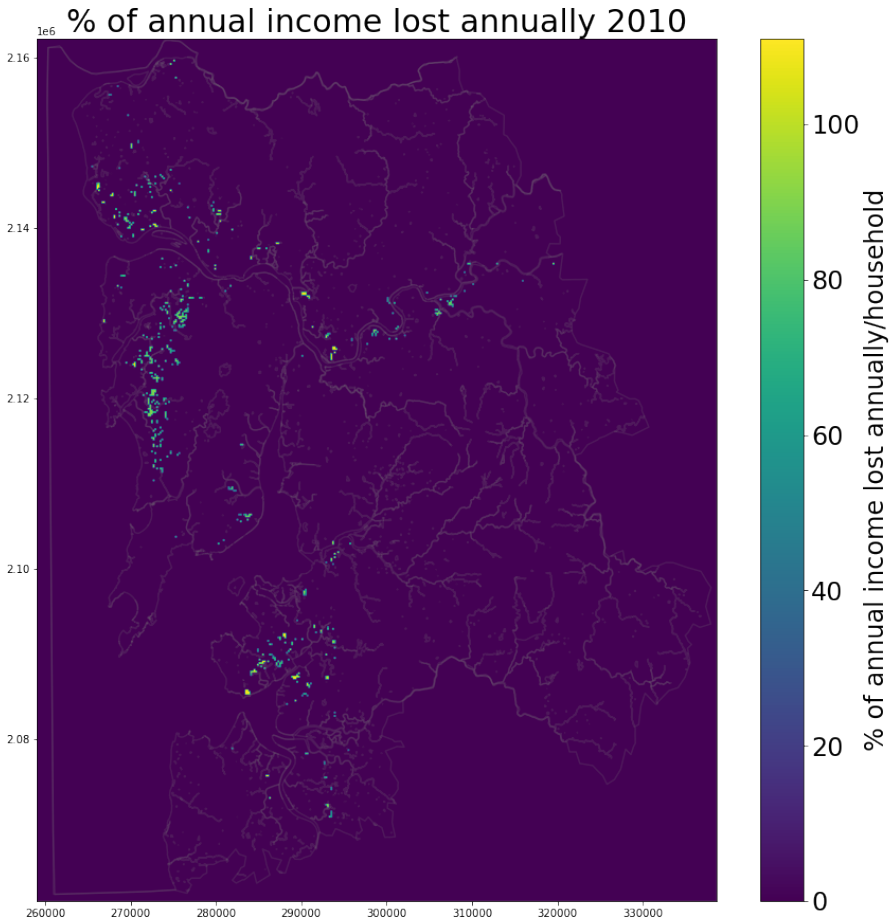

Figure E.3: *PAIL for informal settlements in 2010.*

E.3 PAIL URBAN VILLAGES 2050 BAU

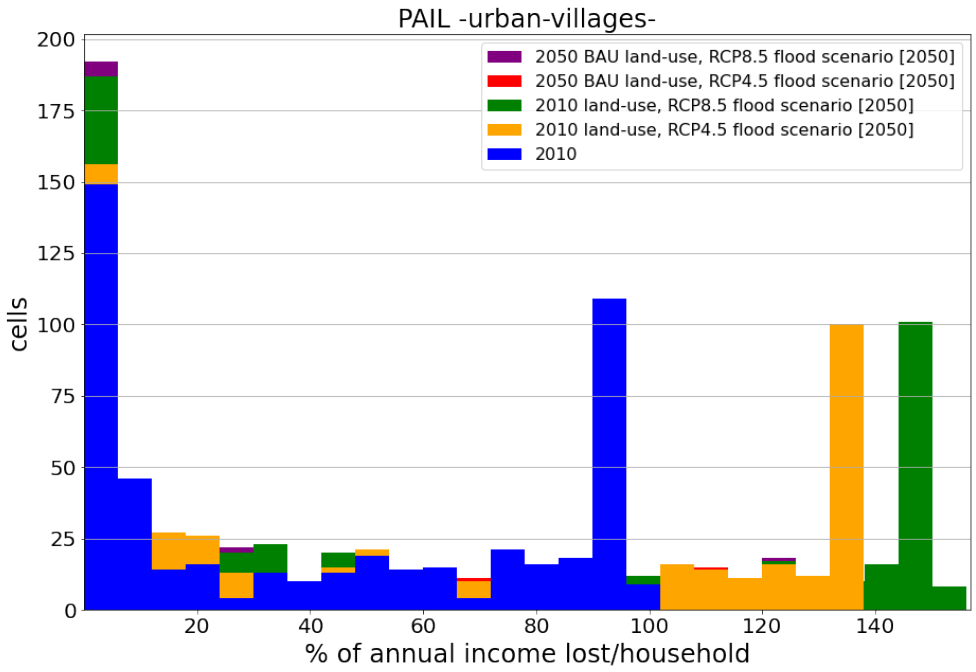

Figure E.4: *Histograms of the percentage of annual income lost for the affected cells of urban-villages land-use class. The scenarios (i) '2010 land-use, 2010 flood scenario', (ii) '2010 land-use, RCP4.5 flood scenario', (iii) '2010 land-use, RCP8.5 flood scenario', (iv)'2050 BAU land-use, RCP4.5 flood scenario', (v) '2050 BAU land-use, RCP8.5 flood scenario', are compared. Due to hardly no land-use change for Urban-Villages, scenario (ii) is equal to (iv) and scenario (iii) is equal to (v), resulting in solely (ii) and (iii) being visible.*

E.4 Spatially Explicit EAMD and EAPA RCP4.5

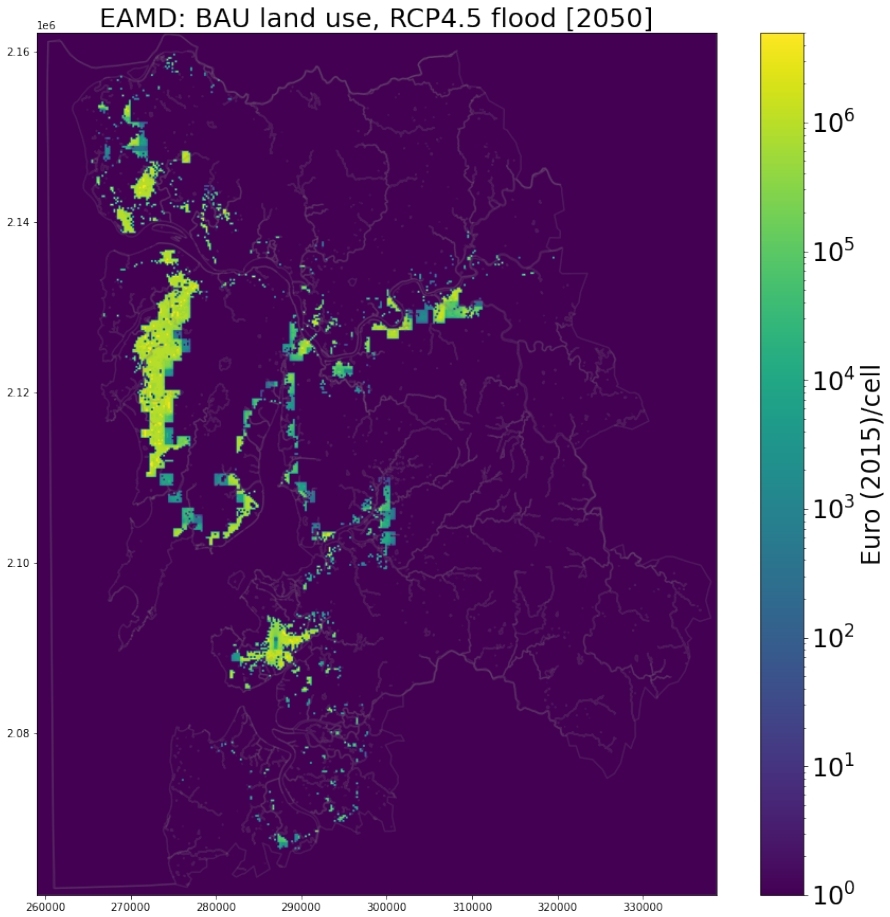

Figure E.5: *A figure visualising the spatial distribution of EAMD, in case of BAU growth and RCP4.5 flood hazard for 2050.*

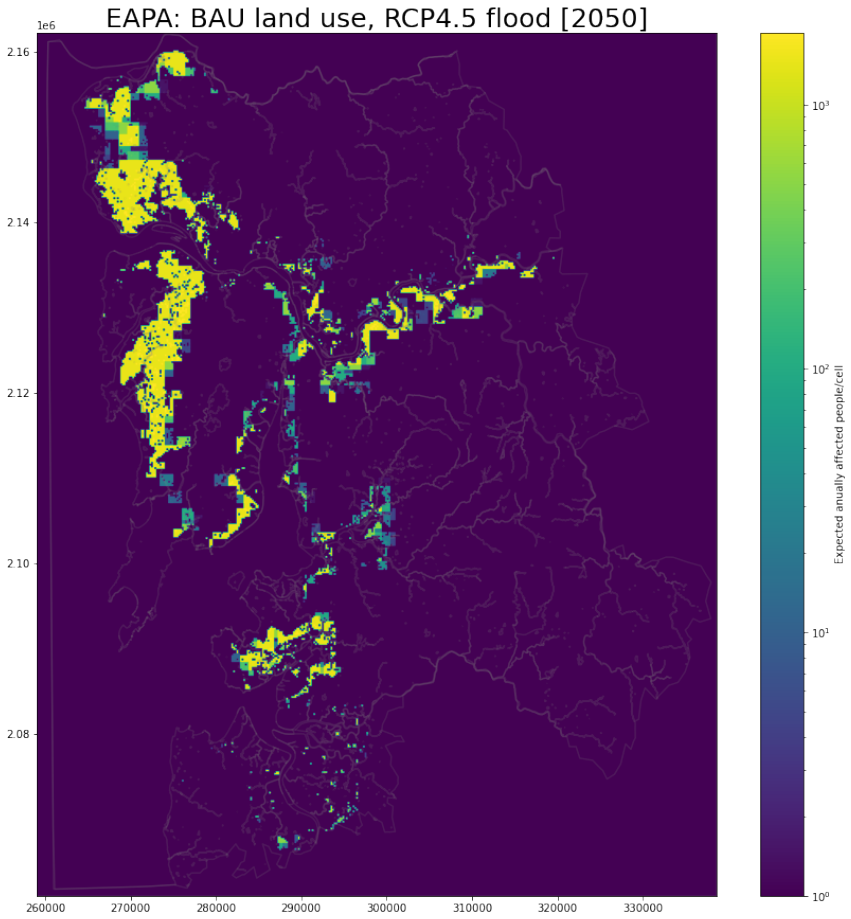

Figure E.6: *A figure visualising the spatial distribution of EAPA, in case of BAU growth and RCP4.5 flood hazard for 2050.*

E.5 PAIL individual histograms

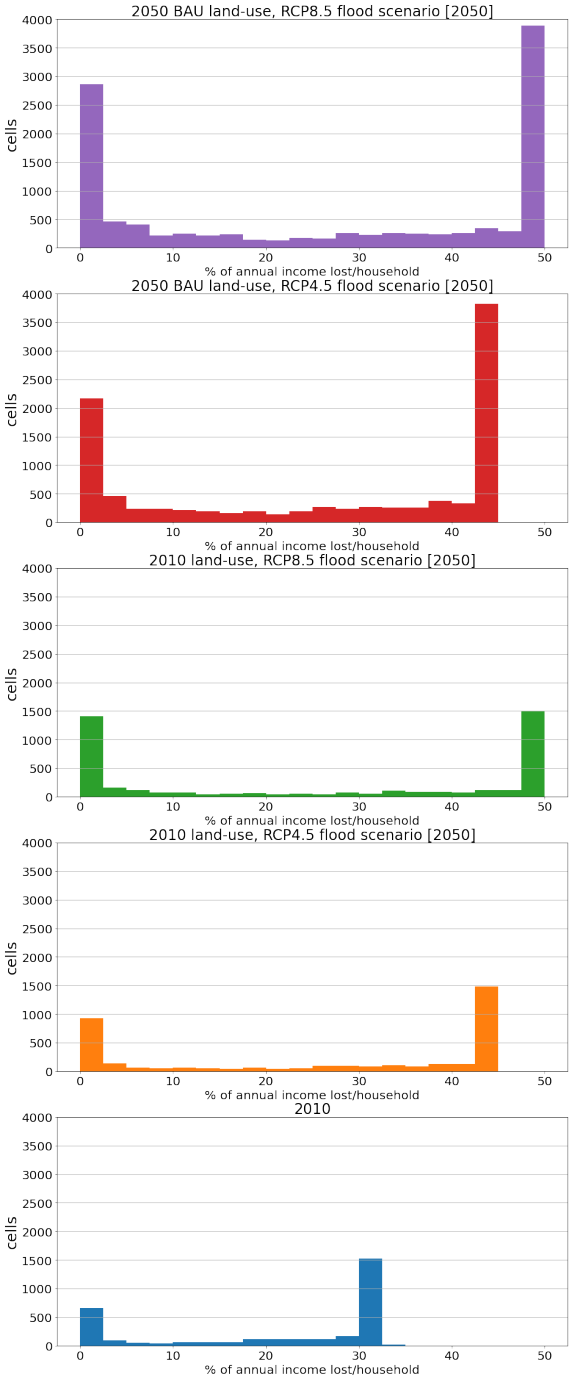

Figure E.7: *Histograms of the percentage of annual income lost concerning the urban-formal land-use class for various BAU and 2010 land-use scenarios.*

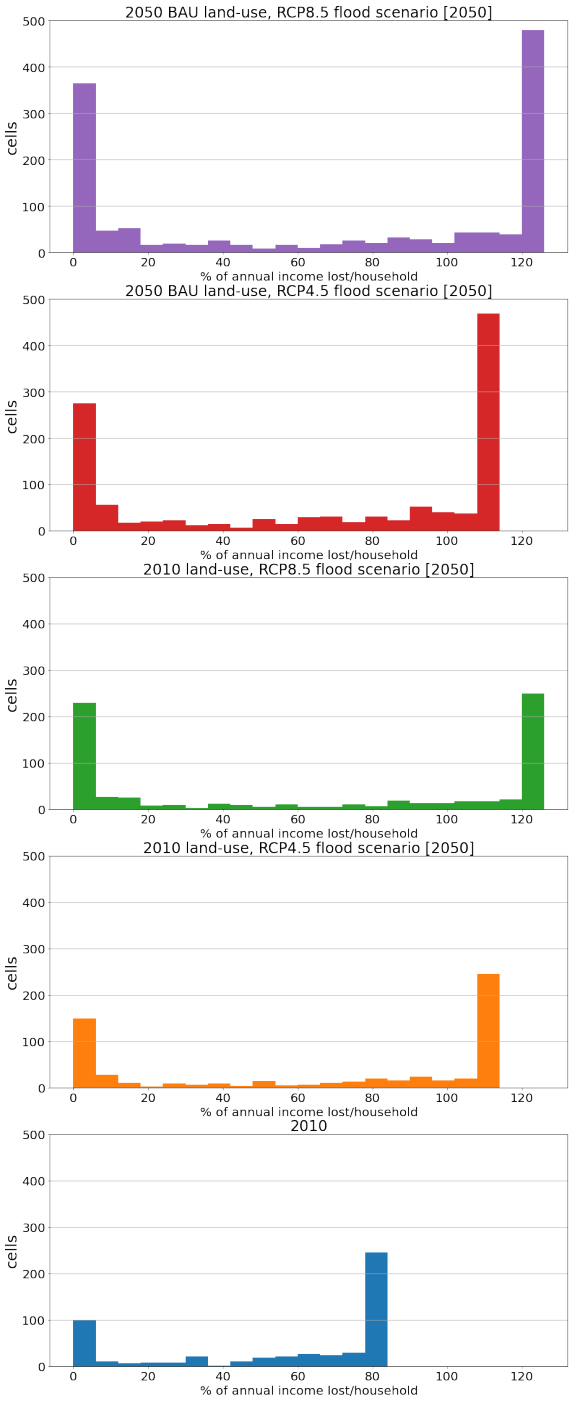

Figure E.8: *Histograms of the percentage of annual income lost concerning the urban-informal land-use class for various BAU and 2010 land-use scenarios.*

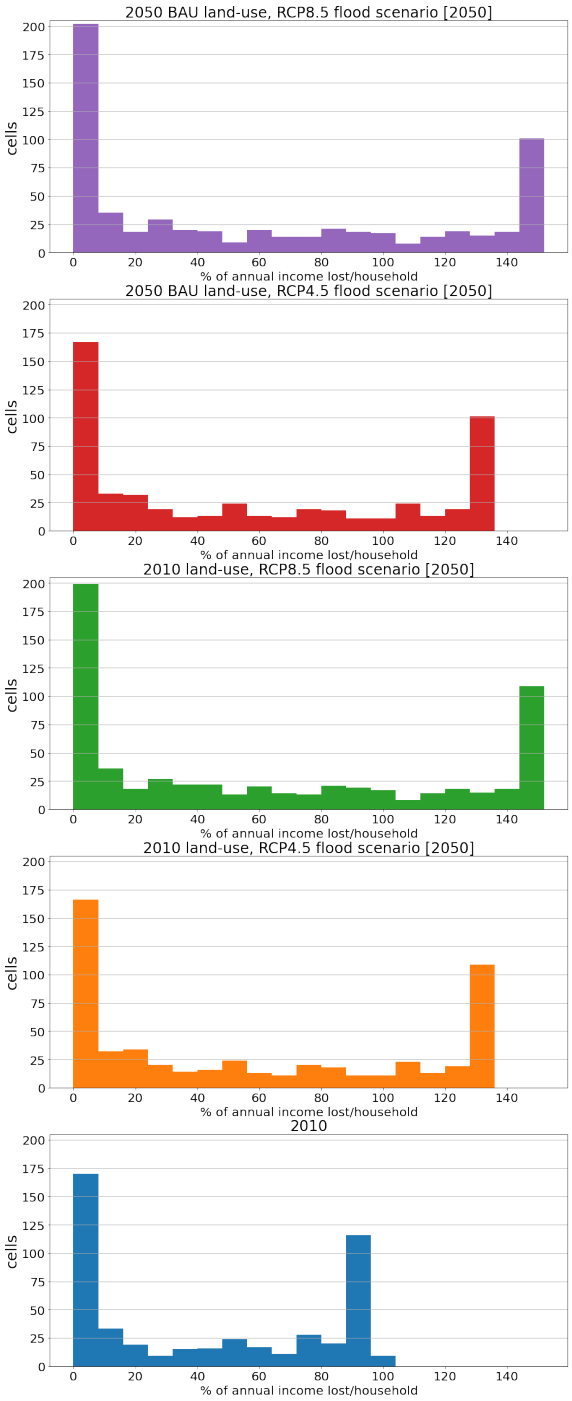

Figure E.9: *Histograms of the percentage of annual income lost concerning the urban-villages land-use class for various BAU and 2010 land-use scenarios.*

E.6 Urban planning EAPA

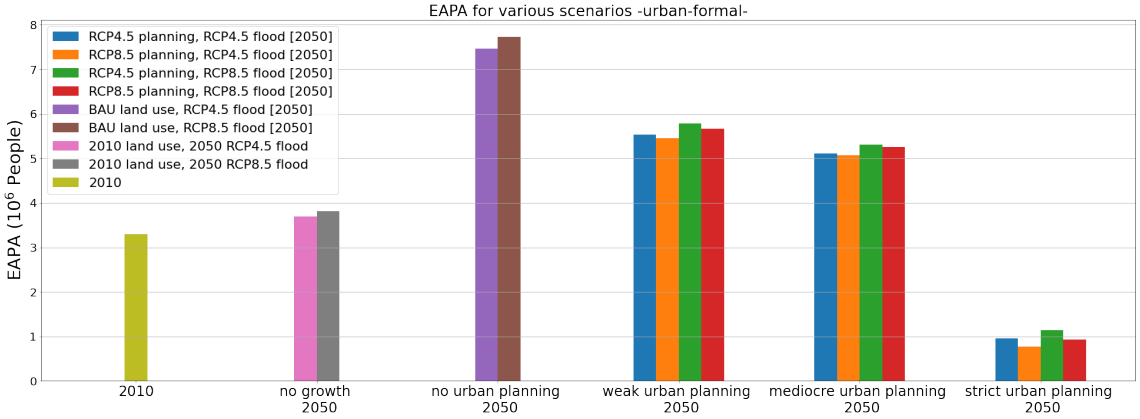

Figure E.10: *Figures on the EAPA for the urban-formal land-use class for various scenarios. Concerning the included scenarios, the naming goes as follows. RCP4.5 planning indicates that urban planning was based on RCP4.5. RCP4.5 flood indicates that the flood hazard maps that were laid on top of the land-use map were coherent with RCP4.5. If '2050' is in square brackets at the end of the scenario name, it indicates that both land use and flood hazard were derived for 2050.*

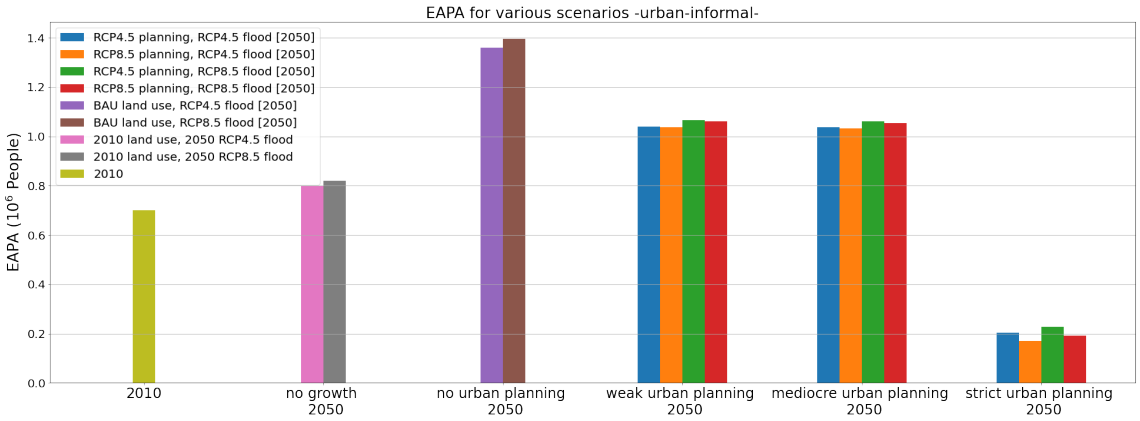

Figure E.11: *Figures on the EAPA for the urban-informal land-use class for various scenarios. Concerning the included scenarios, the naming goes as follows. RCP4.5 planning indicates that urban planning was based on RCP4.5. RCP4.5 flood indicates that the flood hazard maps that were laid on top of the land-use map were coherent with RCP4.5. If '2050' is in square brackets at the end of the scenario name, it indicates that both land use and flood hazard were derived for 2050.*

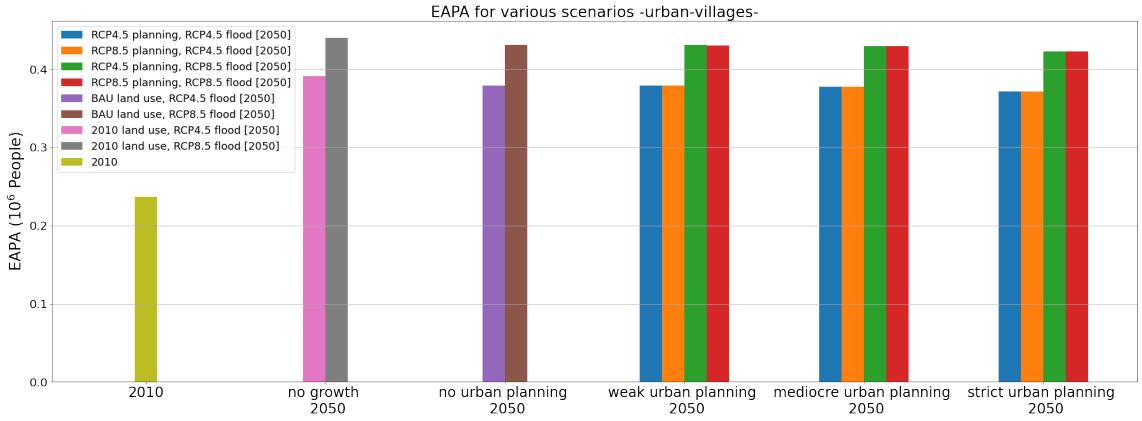

Figure E.12: *Figures on the EAPA for the urban-villages land-use class for various scenarios. Concerning the included scenarios, the naming goes as follows. RCP4.5 planning indicates that urban planning was based on RCP4.5. RCP4.5 flood indicates that the flood hazard maps that were laid on top of the land-use map were coherent with RCP4.5. If '2050' is in square brackets at the end of the scenario name, it indicates that both land use and flood hazard were derived for 2050.*